1

Manufacturing and internal geometry of textiles

S LOMOV, I VERPOEST, Katholieke Universiteit Leuren, Belgium and
F ROBITAILLE, University of Ottawa, Canada

1.1 Hierarchy of textile materials

Textiles technologies have evolved over millennia and the term 'textile' now has a very broad meaning. Originally reserved for woven fabrics, the term now applies to fibres, filaments and yarns, natural or synthetic, and most products derived from them. This includes threads, cords, ropes and braids; woven, knitted and non-woven fabrics; hosiery, knitwear and garments; household textiles, textile furnishing and upholstery; carpets and other fibre-based floor coverings; industrial textiles, geotextiles and medical textiles.

This definition introduces three important notions. First, it states that textiles are **fibrous** materials. A fibre is defined as textile raw material, generally characterised by flexibility, fineness and high ratio of length to thickness; this is usually greater than 100. The diameter of fibres used in textile reinforcements for composites (glass, carbon, aramid, polypropylene, flax, etc.) varies from 5 μm to 50 μm. Continuous fibres are called *filaments*. Fibres of finite length are called *short*, *discontinuous*, *staple* or *chopped* with lengths from a few millimetres to a few centimetres.

Fibres are assembled into *yarns* and fibrous plies, and then into textiles. The second important feature of textiles is their **hierarchical** nature. One can distinguish three hierarchical levels and associated scales: (1) fibres at the *microscopic* scale; (2) yarns, repeating unit cells and plies at the *mesoscopic* scale; and (3) fabrics at the *macroscopic* scale. Each scale is characterised by a characteristic length, say 0.01 mm for fibre diameters, 0.5–10 mm for yarn diameters and repeating unit cells, and 1–10 m and above for textiles and textile structures. Each level is also characterised by dimensionality where fibres and yarns are mostly one-dimensional while fabrics are two- or three-dimensional, and by structural organisation where fibres are twisted into yarns, yarns are woven into textiles, etc.

Textiles are **structured** materials. On a given hierarchical level one can think of a textile object as an entity and make abstraction of its internal structure: a yarn may be represented as a flexible rod, or a woven fabric as

a membrane. This approach is useful but the internal structure must be considered if one wishes to assess basic features and behaviour of textile objects such as the transverse compression of yarns or shear behaviour of fabrics. The diversity of textile technologies results in a large variety of available textile structures. Figure 1.1 depicts textile structures that are widely used as reinforcements for composites; these are discussed in this chapter.

The properties of a fabric are the properties of fibres transformed by the textile structure. The latter is introduced deliberately during manufacturing. Modern fibres turn millennium-old textile technologies into powerful tools for creating materials designed for specific purposes, where fibre positions are optimised for each application. Textile manufacturing methods and internal structure are two important topics that are addressed in this chapter.

1.2 Textile yarns

1.2.1 Classification

The term yarn embraces a wide range of 1D fibrous objects. A yarn has substantial length and relatively small cross-section and is made of fibres and/or filaments, with or without twist. Yarns containing only one fibre are *monofilaments*. Untwisted, thick yarns are termed *tows*. Flat tows are called *rovings* in composite parlance; in textile technology this word designates an intermediate product in spinning. *Sizing* holds the fibres together and facilitates the processing of tows; it also promotes adhesion of fibres to resin in composites. In *twisted yarns*, fibres are consolidated by the friction resulting from twist. A twist is introduced to a *continuous filament* yarn by *twisting*. For a *twisted yarn made of staple fibres* the process is called *spinning* and involves a long chain of preparatory operations. There are different *yarn spinning* processes (*ring spinning, open-end spinning, friction spinning*) leading to yarns with different internal distributions of fibres. Note that these are distinct from fibre spinning processes such as wet spinning, melt spinning or gel spinning, which are used to make individual fibres, most often from various polymers.

Fibres of different types are easily mixed when yarn spun, producing a *blend*; thermoplastic matrix fibres can be introduced among load-carrying fibres in this way. Finally, several strand yarns can be twisted together, forming a *ply* yarn.

1.2.2 Linear density, twist, dimensions and fibrous structure of yarns

The *linear density* is the mass of a yarn per unit length; the inverse quantity is called *yarn count* or *number*. Common units for linear density are given in Table 1.1. Linear density, the most important parameter of a yarn, is normalised

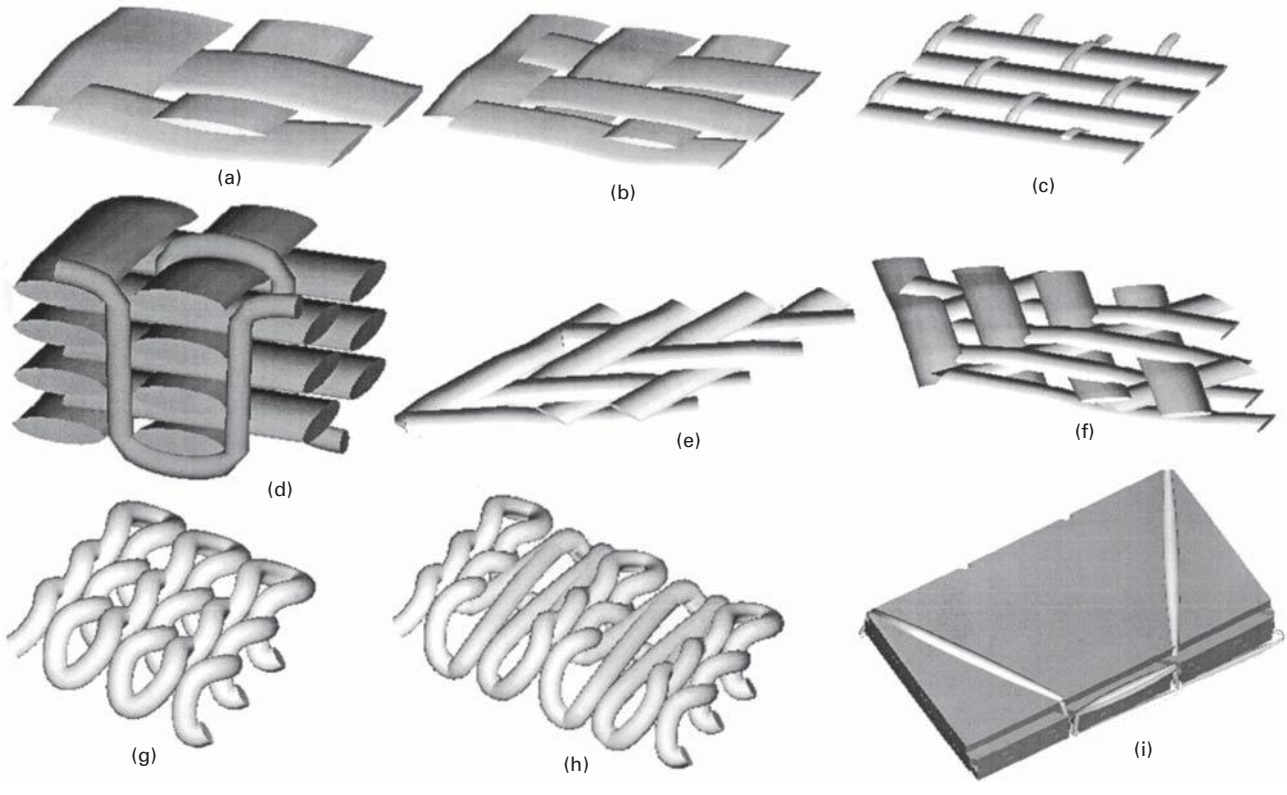

1.1 Textile structures: (a–c) 2D woven fabrics; (d) 3D woven fabrics; (e, f) 2D braided fabrics; (g, h) weft-knitted fabrics; (i) multiaxial multiply warp-knitted fabric.

Table 1.1 Units of linear density and yarn count

Unit	Definition
Tex (SI)	1 tex = 1 g/km
Denier	1 den = 1 g/9 km
Metric number	1 Nm = 1 km/kg
Glass (UK and US)	N_G = 1 pound/1 yard

by specifications and controlled in manufacturing. The *unevenness*, or coefficient of variation of linear density, is normally below 5% for continuous filament yarns while for spun yarns special measures in manufacturing keep it within a specified range. For yarns made of short and stiff fibres such as flax the unevenness can be as high as 15–20%.

The *twist K* of a yarn is a number of turns per unit length. Values of twist for yarns used in composite reinforcements are normally below 100 m^{-1}. The *twist angle* is the inclination of fibres on the surface of the yarn due to twist (Fig. 1.2). If d is the yarn diameter and $h = 1/K$ is the length of the period of twist, the twist angle is calculated as:

$$\tan \beta = \frac{\pi d}{h} = \pi d K \qquad 1.1$$

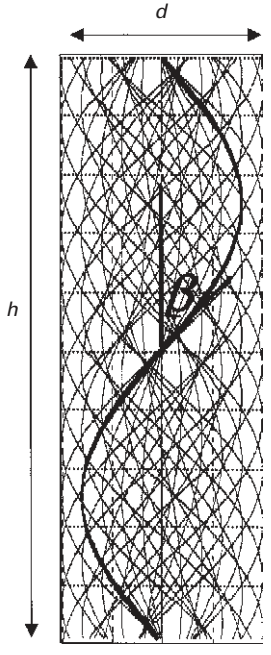

1.2 Calculation of twist angle.

The twist angle is indicative of the intensity of frictional interaction between fibres inside a yarn, and of the tensile resistance of a staple yarn. It provides an estimation of the deviation of the orientation of fibres from the yarn axis and ideal load direction in the case of textile reinforcements for composites; the effective modulus of an impregnated yarn can be estimated as proportional to $\cos^4\beta$. For example, a yarn of diameter $d = 0.5$ mm and twist $K = 100$ m^{-1} would lead to $\beta = 9°$ and $\cos^4\beta = 0.95$, resulting in a decrease in stiffness of 5% for the impregnated yarn.

Fibrous yarns do not have precise boundaries; their dimensions are arbitrary. Considering a circular yarn with similar dimensions along all radii, the diameter of a cylinder having the same average density as that yarn is:

$$d = \sqrt{\frac{4T}{\pi\rho_f V_f}} \qquad 1.2$$

where T is the linear density of the yarn, ρ_f is the fibre density and V_f is the fibre volume fraction in the yarn (which is generally unknown). In practice, eqn 1.2 is rewritten:

$$d = C\sqrt{T} \qquad 1.3$$

where an empirical coefficient C applies to each yarn type. Typical values of C correspond to $V_f = 0.4$ to 0.6. Measuring d presents difficulties with values depending on the pressure applied to the yarn and on image processing of yarn cross-sections. These can be avoided by extrapolating the results of transverse yarn compression tests to zero load. Remarkably, values of C obtained empirically for very different yarns (cotton, wool, polyester, aramid, glass, etc.) all lie in the range 0.03–0.04 (d in mm and T in tex), which is useful for first estimations.

Rovings and tows used in composites are normally sized, leading to better-defined surfaces without loose fibres. Roving cross-sections can be approximated by elliptical, lenticular or various other shapes with a width-to-thickness ratio of 3 to 10. Actual dimensions depend on manufacture-induced spreading; however, relationships exist between linear density and section dimensions (Fig. 1.3). Fibres are positioned randomly within cross-sections. Clusters separated by random voids are formed, and these remain present upon compaction. Fibres do not align in theoretically ideal hexagonal arrays because of fibre crimp[1].

1.2.3 Mechanical properties of yarns

During textile manufacture, yarns are subjected to different loads and constraints that define their final configuration in the textile. The behaviour of yarns under load is non-linear and non-reversible owing to their fibrous nature and inter-fibre friction. The most important yarn deformation modes in determining

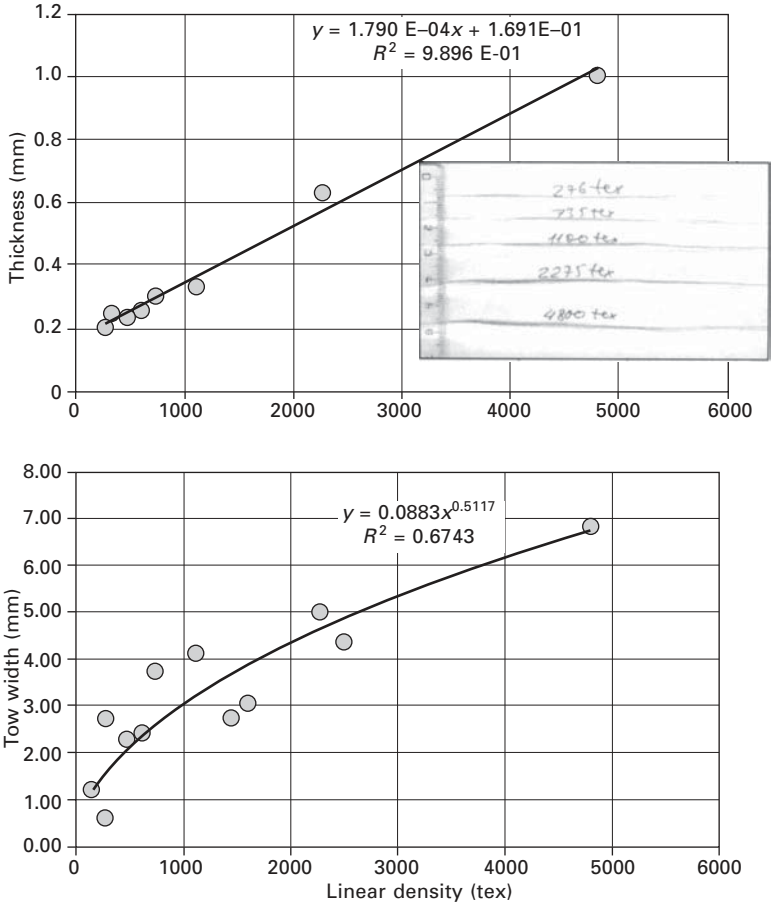

1.3 Thickness and width of glass rovings (from different manufacturers).

the internal geometry of a fabric are bending, which allows interlacing of yarns and generates yarn interaction forces in the fabric, and transverse compression which results from these interactive forces and defines the shape of yarns in the fabric. Tension and torsion are generally unimportant for unloaded fabrics.

Bending of textile yarns

Yarn bending is characterised by a bending diagram $M(\kappa)$ where M is the bending moment and κ is the curvature, with $\kappa = 1/R$ where R is the radius of curvature. Typical bending diagrams registered on the Kawabata (KES-F) bending tester[2] appear in Fig. 1.4 for a sized carbon tow; the lower cycle was

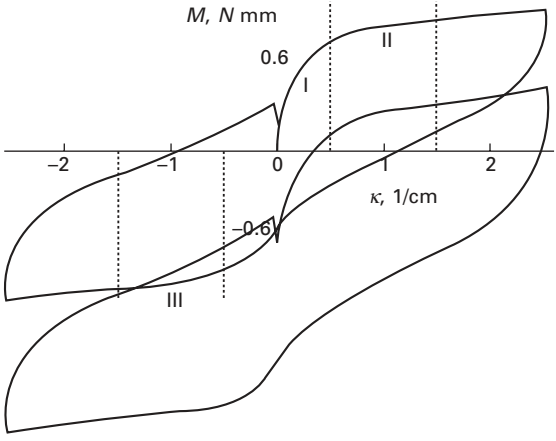

1.4 Bending diagrams for carbon roving (3.2 ktex).

shifted vertically for clarity. The initial stage of bending (stage I – κ lower than 0.2 cm^{-1}, R higher than 5 cm) features high stiffness values associated to fibres linked by sizing and friction[3]; the yarn acts as a solid rod. Curvature radii in fabrics are of the order of a few millimetres. hence stage I is not relevant to their internal structure: standard practice stipulates that bending rigidity should be determined between $\kappa = 0.5$ and $\kappa = 1.5$ cm^{-1}. The slope over stages II and III is averaged and bending rigidity is calculated as:

$$B = \frac{\Delta M}{\Delta \kappa} \qquad 1.4$$

The bending diagram also provides information on the hysteresis, typically defined as the difference between values of the bending moment at $\kappa = 1$ cm^{-1} upon loading and unloading; this is rarely used in practice but helps in understanding the physics of the phenomenon: clearly the behaviour is not elastic. There are many simple test methods for determining B using the deformation of the yarn under its own weight[4,5]. These are easier to use but their application to thick, rigid tows used in composites is limited as small deformations lead to large errors.

The bending rigidity of a yarn can be estimated from the bending rigidity of single fibres. Each fibre in a yarn containing N_f circular fibres of diameter d_f and modulus E_f has a bending rigidity of:

$$B_f = \frac{E_f d_f^4}{64} \qquad 1.5$$

Fibres in a yarn are held together by friction and/or bonding. In one extreme the yarn can be regarded as a solid rod, while in the other extreme each fibre bends independently. Lower and upper estimates of the yarn bending

rigidity can be derived as $N_f B_f \leq B \leq N_f^2 B_f$; the difference between these two extremes is great as N_f is counted in hundreds or thousands. Experiments show that for rovings typical of composite reinforcements the lower estimation is valid:

$$B \approx N_f B_f \qquad 1.6$$

Figure 1.5 shows measured bending rigidity values for glass and carbon rovings and estimates from eqn 1.6. The trend for glass rovings is not linear as fibre diameters differ (13 to 21 μm) for different yarns. The carbon tows are all made of fibres with a diameter of 6 μm. The difference in the fibre diameters explains why bending rigidity of the glass rovings is higher. The outlier point in Fig. 1.5, located below the trend line, results from internal fibre crimp in an extremely thick (80K) tow.

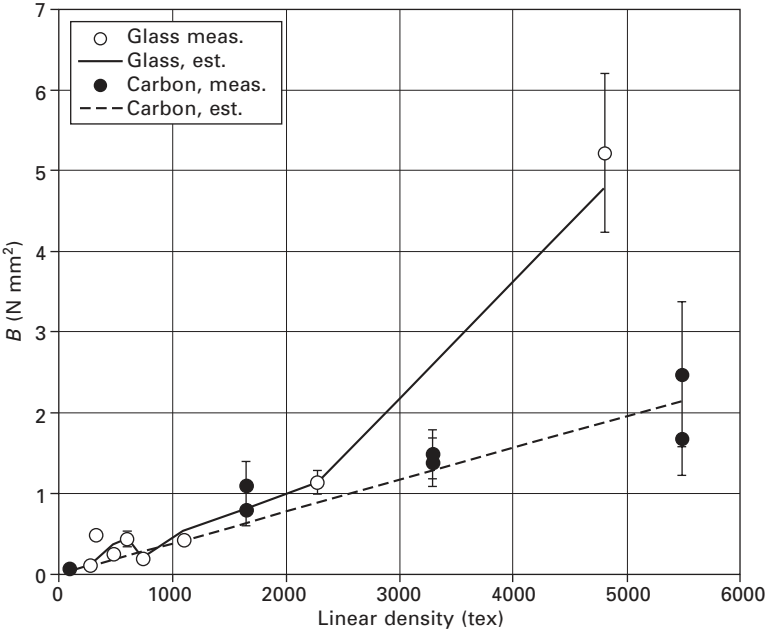

1.5 Bending rigidity of glass and carbon rovings.

Compression of textile yarns

When compressed a textile yarn becomes thinner in the direction of the force and wider in the other direction, Fig. 1.6. Changes in yarn dimensions can be expressed using coefficients of compression η:

$$\eta_1(Q) = \frac{d_1(Q)}{d_{1,0}}, \quad \eta_2(Q) = \frac{d_2(Q)}{d_{2,0}} \qquad 1.7$$

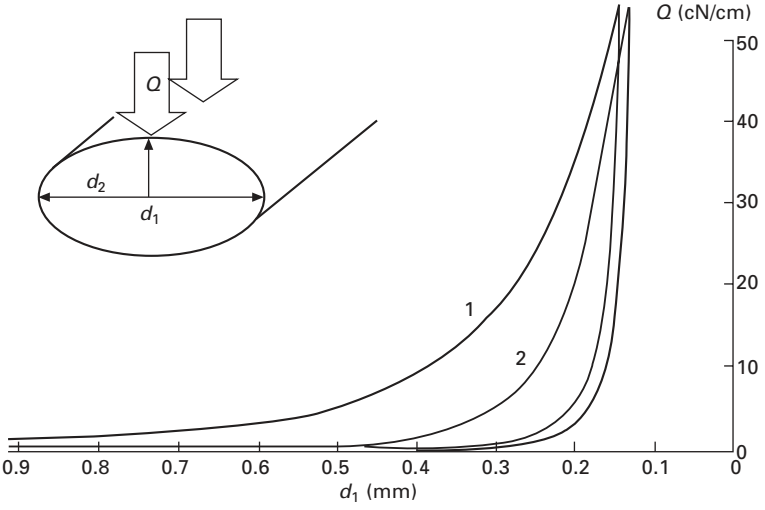

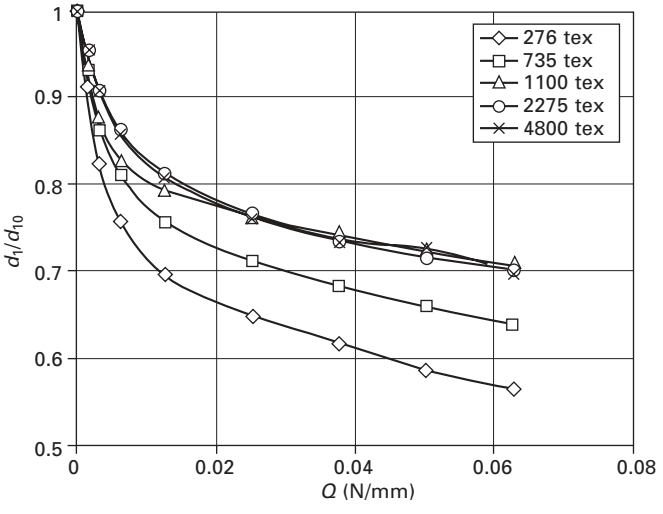

1.6 Compression of textile yarns. Top: schematic of test configuration and typical KES-F curves (two loading cycles). Bottom: compressibility of glass rovings.

where d_1 and d_2 are the yarn dimensions, Q is the load, $\eta_1 < 1$, $\eta_2 > 1$ and subscript 0 refers to the shape at $Q = 0$. The load Q is defined as a force per unit length, which is simpler to use than a pressure because of changes in yarn dimensions.

Measuring η_1 is straightforward. The Kawabata compression tester[2] is the standard tool for doing this. As shown in Fig. 1.6 the first and second compression cycles differ substantially but subsequent cycles are similar to

the second. The first cycle measures forces associated to factors such as the imperfect flatness of relaxed rovings, which disappear in subsequent cycles. Latter cycles should be regarded as characteristic of yarn behaviour. Figure 1.6 also shows compression curves for glass rovings of different linear density, to be compared with zero-load thickness data in Fig. 1.3. Non-linearity is evident from Fig. 1.6. The curves may be approximated by a power law:

$$\frac{1 - \eta_1(Q)}{\eta_1(Q) - \eta_{1\min}} = \left(\frac{Q}{Q^*}\right)^{\alpha} \qquad 1.8$$

where $\eta_{1\min}$ is the maximum compressibility of the yarn ($Q \to \infty$). The curve for the 276 tex glass roving can be approximated with $\eta_{1\min} = 0.398$, $Q^* = 0.014$ N/mm and $\alpha = 0.612$. Measuring η_2 is a different issue for which no standard procedure exists. Published techniques[6–8] involve observing the dimensions of a yarn compressed between two transparent plates. Experimental results show that:

$$\eta_2 \approx \eta_1^{-a},\ a = 0.2 \text{ to } 0.3 \qquad 1.9$$

1.3 Woven fabrics

1.3.1 Parameters and manufacturing of woven fabric

A woven fabric is produced by interlacing *warp* and *weft* yarns, identified as *ends* and *picks*. It is characterised by linear densities of warp and weft yarns, a weave pattern, a number of warp yarns per unit width P_{Wa} (ends count, inverse to warp pitch or centre-line spacing p_{Wa}), a number of weft yarns per unit length P_{We} (picks count, inverse to weft spacing p_{We}), warp and weft yarn crimp, and surface density.

Figure 1.7 represents a weaving loom. Warp yarns are wound on the warp beam, rolling off it parallel to one another under regulated tension. Each warp yarn is linked to a *harness*, a frame positioned across the loom with a set of *heddles* mounted on it. The heddle is a wire or thin plate with an eye through which a warp yarn goes. When a harness goes up or down, the warp yarns connected to it go up (warp 2) or down (warp 1). A *shed* is formed, which is a gap between warp yarns where a weft yarn may be inserted using a weft insertion device such as a shuttle, projectile, air/water jet or rapier. The weft yarn is positioned by battening from a *reed*, a grid of steel plates between which warp yarns extend. The reed is mounted on a slay which moves back and forth; the backward motion opens space for weft insertion while the forward motion battens the weft. Once a weft yarn is in position the harnesses move in opposite directions, closing the shed and locking the weft in the fabric. The fabric is moved forward by the cloth beam and the process is repeated (Fig. 1.7). In the final fabric roll the warp ends extend

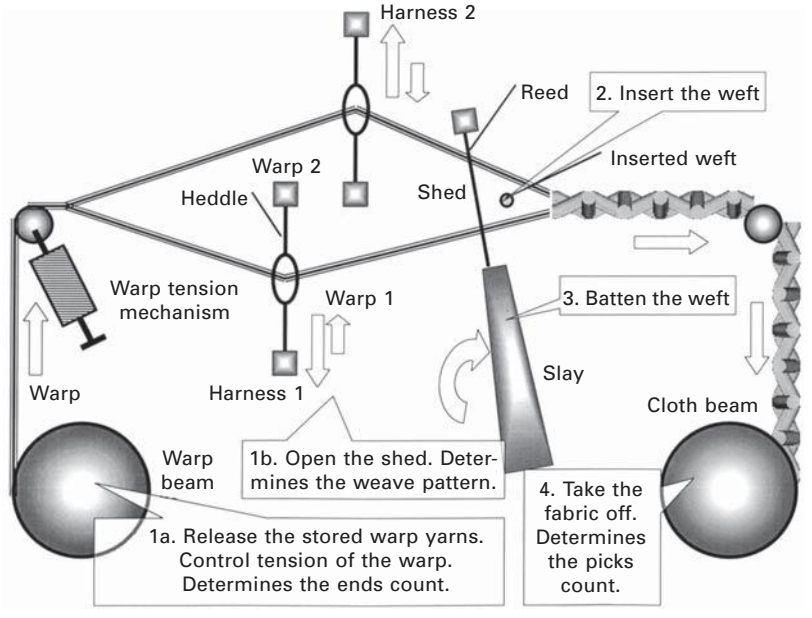

1.7 Schematic diagram of a weaving loom.

along the roll direction while the weft picks extend parallel to the roll axis. Lateral extremities are sometimes referred to as the selvedge.

The ends count, picks count and weave pattern are respectively determined by the total number of warp yarns on the beam and the fabric width, by the rotation speed of the cloth beam, and by the sequence of connection between warp yarns and harnesses and the harness motions. All motions happen within one rotation of the main shaft. The rotation speed of this shaft determines the number of weft yarns inserted per minute. Modern looms rotate at 150 to 1000 rpm. The loom speed determines the productivity A, the area of fabric produced in a given time:

$$A = \frac{nb}{P_{We}} \qquad 1.10$$

where n and b are the loom speed and fabric width. Typical values for a composite reinforcement produced on a loom with a projectile weft insertion are $n = 300\ \text{min}^{-1}$, $P_{We} = 4.0\ \text{cm}^{-1}$, $b = 1.5$ m. Productivity here is then 67.5 m^2/h or, assuming a surface density of 300 g/m^2, 20 kg/h.

Weft insertion

Weaving looms are classified according to weft insertion devices: shuttle, projectile ('shuttleless'), rapier, air or water jet. Air jet insertion is unsuitable

for thick glass and carbon tows. Weft insertion speeds are typically between 7 and 35 m/s, depending on the insertion technique employed. These relate to the productivity of different looms. If weft insertion takes a fraction α of the weaving cycle (typically $\alpha = 1/4$ to $1/3$), loom speed can be estimated as:

$$n = \frac{\alpha v}{b} \tag{1.11}$$

where v is the average velocity of the weft insertion.

A *shuttle* is a device shut from side to side of the loom. It carries a spool with a weft thread that is unwound during insertion. Automatic looms work on the same principle as shuttle hand looms. In order to carry enough weft yarn, the shuttle must be large. The shed must open wide with considerable warp tension to prevent it from tearing. Shuttles with masses of about 500 g prevent velocities above 10 m/s. Noisy shuttle looms consume much energy but can insert any type of weft yarn with ease, including heavy tows. They are widely used to produce composite reinforcements.

Shuttleless looms use a projectile instead of a shuttle. The projectile does not carry a spool and can be much lighter, about 50 g. A weft yarn is fixed to the projectile and unwound from the bobbin during insertion. The projectile is kept on target by a grid fixed to a reed, preventing contact with warp yarns. This allows smaller shed opening, while the lighter projectile leads to high insertion speeds (up to 20 m/s). Shuttleless looms can carry heavy yarns up to a certain limit.

Air looms use an air jet as the weft carrier. A length of weft yarn is cut off and fed into an air nozzle. An air jet carries the yarn across the loom in a tunnel attached to a reed. The tunnel helps maintaining the jet speed. On wide looms (above 1 m) additional nozzles accelerate the jet along the weft yarn path. High velocity of insertion (up to 35 m/s) ensures maximum production speed but weft linear densities are limited to 100 tex, restricting usage of these looms for composite reinforcements.

Water looms use a water jet for weft yarn insertion. This allows handling of heavier yarns, including thick tows for composite reinforcements, but excludes moisture-sensitive fibres such as aramids.

Rapier looms insert weft yarns using mechanical carriers. Yarns are stored on a bobbin and connected to the left rapier, which moves to the centre. The right rapier does the same from the other side. When they meet, the yarn is transferred mechanically from one rapier to the other and cut off before a new weaving cycle is started. Rapier looms are relatively slow (~ 7 m/s) but have no restrictions in weft thickness, and consume less energy than shuttle or projectile looms.

Shedding mechanisms

Shedding mechanisms lift and bring down warp yarns in a prescribed order, creating sheds. Groups of warp yarns are lifted and lowered by harnesses; their number determines weave complexity, with the maximum usually being 8 or 16 but sometimes as many as 32. The motion of harnesses can be effected by cams or dobby. Alternatively the motion of each warp yarn can be controlled separately, allowing any weave pattern. Such shedding mechanisms are called Jacquards.

Consider a shedding mechanism with harnesses. Figure 1.8 illustrates the way to weave a desired pattern. The pattern shows crossovers of warp (columns) and weft (rows) yarns. In the *paper-point diagram*, squares corresponding to crossovers where the warp is on top of the weft appear in black, otherwise they are white. *Top* (face) and *bottom* (back) refer to fabric on the loom. Circles in the *loom up order* diagram indicate which harness controls which warp yarns, and crosses in the shedding diagram indicate the lifting sequence of the harnesses.

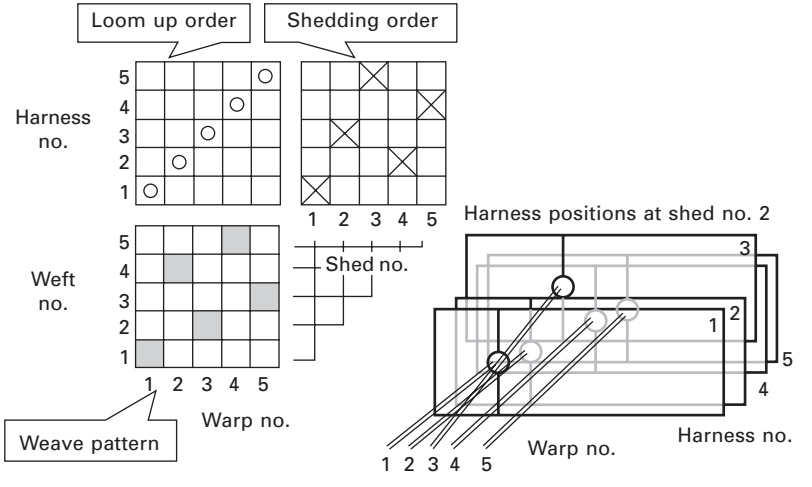

1.8 Weave design and movement of harness.

In *cam shedding mechanisms*, each cam controls the motion of one harness. To change a weave pattern one must change the cams. *Dobby shedding mechanisms* control harnesses through more complex electronic programs. They are used when the number of cams on a loom, usually eight, is insufficient for a chosen weave pattern. *Jacquard machines* control the motions of warp yarns independently. Warp yarns go through the heddles which are connected with the Jacquard machine by harness cords, lifting and lowering the heddles according to a program. Such machines are used to make 3D reinforcements.

1.3.2 Weave patterns

Figure 1.9 depicts elements of a woven pattern used for weave classification. The pattern is represented with a paper-point diagram, with black squares corresponding to crossovers where the warp yarn is on top. The minimum repetitive element of the pattern is called a *repeat*. The repeat can have a different number of warp (N_{Wa}) and weft (N_{We}) yarns.

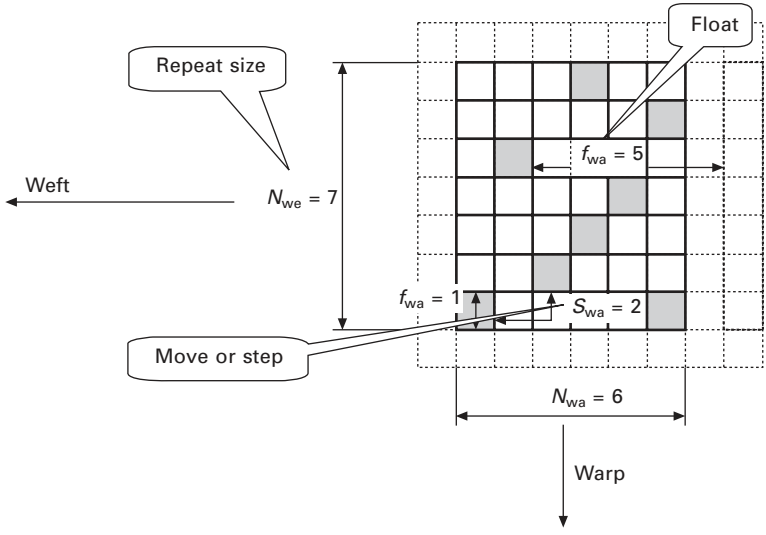

1.9 Elements of a typical weave.

The length of a weft yarn on the face of the fabric, measured in number of intersections, is called *weft float* (f_{We}). For common weaves it is equal to the number of white squares between black squares on any weft yarn. The *warp float* (f_{Wa}) is defined similarly. Consider two adjacent weft yarns and two neighbouring warp intersections on them. The distance between them, measured in number of squares, is called *move* or *step* (s). This characterises the shift of the weaving pattern between two weft insertions. Different yarns in the pattern shown in Fig. 1.9 have different floats and steps. In common weaves these parameters take uniform and regular values, as described below.

Fundamental weaves

The family of weaves having the most regular structures and used as basis for other weaves is called *fundamental weaves*. They are characterised by a square repeat with $N_{Wa} = N_{We} = N$. Each warp/weft yarn has only one weft/warp crossing with $f = 1$ for warp/weft, and the pattern of adjacent yarns is regularly shifted with s being a constant.

The *plain weave*, Fig. 1.10, is the simplest fundamental weave with repeat size $N = 2$ and step $s = 1$. Each weft yarn interlaces with each warp yarn. *Twill weaves*, Fig. 1.11, are characterised by $N > 2$ and $s = \pm 1$. Constant shift by one position creates typical diagonals on the fabric face. If the step is positive, diagonals go from the lower left to the upper right of the pattern and a *right* or *Z-twill* is formed. If the step is negative, the twill is called *left* or *S-twill*. Different twill patterns are designated as f_{Wa}/f_{We} where f_{Wa} is the number of warp intersections on a yarn (warp float) and f_{We} is the number of weft intersections on a yarn (weft float). If there are more warp intersections than weft ones on the fabric face, the twill is a *warp twill*. The term *weft twill*

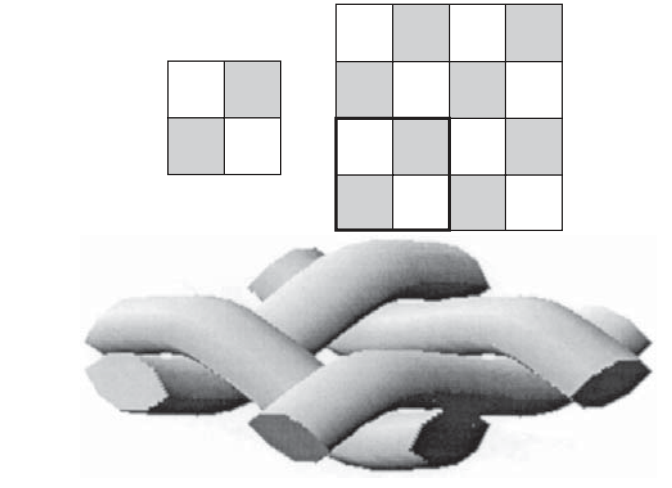

1.10 Plain weave.

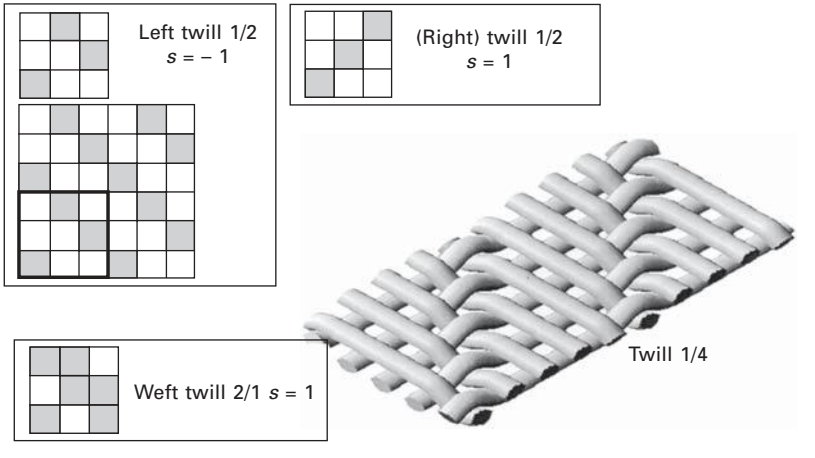

1.11 Twill weaves.

for the opposite case is normally omitted. A full designation for a twill weave reads (*right*)|*left* or *warp*|(*weft*) *twill* f_{Wa}/f_{We} where terms in brackets can be omitted and vertical lines mean 'or'. Twill weaves are often characterised by a propensity to accommodate in-plane shear, resulting in good drape capability (see section 2.2).

Satin weaves, Fig. 1.12, are characterised by $N > 5$ and $| s | > 1$. Sparse positioning of the interlacing creates weaves in which the binding places are arranged with a view to producing a smooth fabric surface devoid of twill lines, or diagonal configurations of crossovers. The terms *warp satin*, or simply satin, and *weft satin*, or sateen, are defined similarly as for twills. *N* and *s* cannot have common denominators, otherwise some warp yarns would not interlace with weft yarns, which is impossible (Fig. 1.12). The most common satins (5/2 and 8/3) are called *5-harness* and *8-harness*. In composites literature the terms *3-harness* and *4-harness* (or *crowfoot*) can be found. Such satins are actually twills (Fig. 1.12). Satins are designated as *N/s*; a full designation of a satin weave reads *warp*|(*weft*) *satin N/s,* or *N harness* and *s step satin*|*sateen*. Rigorously, each warp yarn interlaces with each weft yarn only once, each weft yarn interlaces with each warp yarn only once, interlacing positions must be regularly spaced, and interlacing positions can never be adjacent – both along the warp and weft.

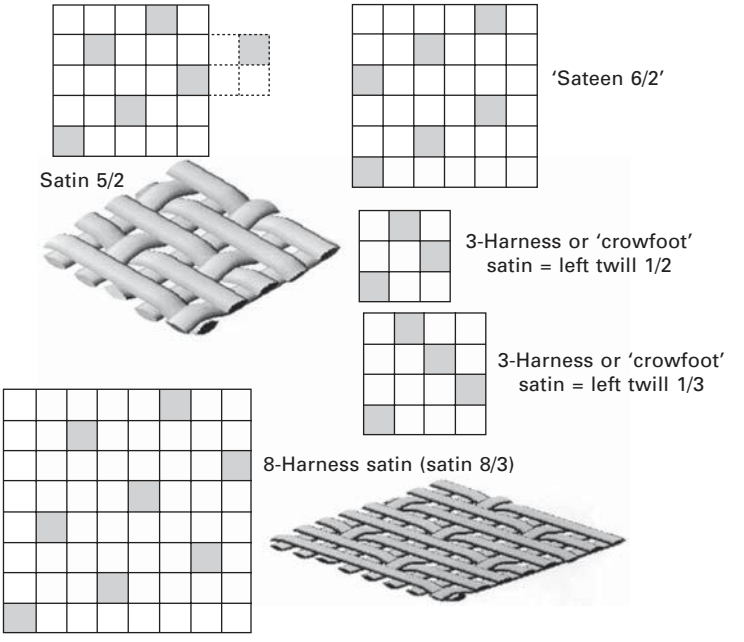

1.12 Satin weaves.

Modified and complex weaves

Fundamental weaves can serve as a starting point for creating complex patterns, to create some design effect or ensure certain mechanical properties for the fabric. Figure 1.13 shows modified weaves created by doubling warp intersections in plain (resulting in *rib* and *basket* weaves) and twill patterns. Such weaves are identified by a fraction f_{Wa}/f_{We}, where f_{Wa} is the number of warp intersections on a warp yarn and f_{We} is the number of weft intersections on a yarn (Fig. 1.13a–c). Complex twills can have diagonals of different width identified by a sequence $f_{Wa1}/f_{We1}, \ldots f_{WaK}/f_{WeK}$, (Fig. 1.13d). A twill pattern can also be broken by changing diagonal directions (sign of s), creating a *herringbone* weave (Fig. 1.13e). If an effect of apparent random interlacing is desired the repeat can be disguised (*crepe* weave) by combining different weaves in one pattern (Fig. 1.13f).

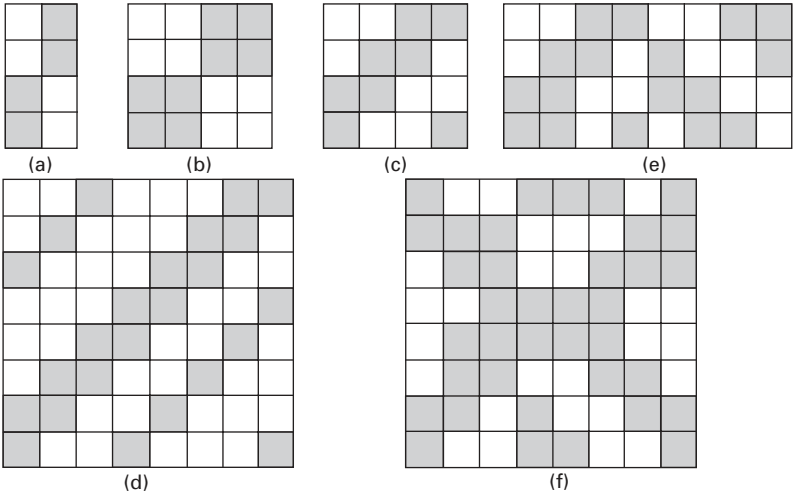

1.13 Modified and complex weaves: (a) warp rib 2/2; (b) basket 2/2; (c) twill 2/2; (d) twill 2/3/1/2; (e) herringbone; (f) crepe (satin 8/3 + twill 2/2).

Tightness of a 2D weave

The *weave tightness* or *connectivity* is determined by the weave pattern and quantifies the freedom of yarns to move. This is not to be confused with fabric tightness, which is the ratio of yarn spacing to their dimensions. The weave tightness characterises the weave pattern, providing an indication on fabric properties as a function of weave type. Two simple ways to characterise weave tightness follow:

$$\text{Tightness} = \frac{N_{\text{liaison}}}{2N_{\text{Wa}}N_{\text{We}}} \qquad 1.12$$

where $N_{liaison}$ is the number of transitions of warp/weft yarns from one side of the fabric to another and the denominator is multiplied by 2 so as to have a value of 1 for plain weaves, and:

$$\text{Tightness} = \frac{2}{f_{Wa} + f_{We}} \qquad 1.13$$

Equation 1.12 will be used in the remainder of the chapter. Lower weave tightness values indicate less fixation of the yarns in a fabric, less fabric stability and better fabric drapability. As the fabric is less stable it tends to be distorted easily as shown by differences in fabric resistance to needle penetration (Fig. 1.14a). Higher tightness means also higher crimp, which deteriorates fabric strength (Fig. 1.14b).

Multilayered weaves

Conventional weaving looms allow the production of multilayered weaves used for heavy apparel and footwear. Multilayer integrally woven reinforcements are often called *3D* or *warp-interlaced 3D* weaves. A multilayer weave is shown in Fig. 1.15. The weave is called *1.5-layered satin* as the pattern is similar to satin on the fabric face and the fabric has two weft layers and one warp layer – 1.5 being an average. The weave pattern is more complex. Positions where warp yarns appear at the fabric face above the upper weft layer (Arabic figures) are black. Positions between the upper and the weft layers lower (Roman figures) appear as crosses and positions at the back of the fabric appear in white.

The weaving pattern does not reveal the weave structure clearly. The spatial positioning of yarns is created by stopping the fabric upon insertion of a lower weft and only resuming after insertion of an upper weft, hence inserting two wefts at the same lengthwise position in the fabric. The spatial weave structure is better revealed by a section in the warp direction, (Fig. 1.15b). A fabric with L weft layers can have warps occupying $L + 1$ levels, level 0 being the fabric face and level L being the back. Each warp is coded as a sequence of level codes and the entire weave is coded as a matrix.

In composite reinforcements warps are often layered as shown in Fig. 1.16. Warp paths are coded as *warp zones*, identifying sets of warp yarns layered over each other. The 1.5-layered satin of Fig. 1.15 has four warp zones, each occupied by one yarn. Yarns going through the thickness of a fabric are called *Z-yarns*. Multilayered composite reinforcements are termed *orthogonal* when Z-yarns go through the whole fabric between only two columns of weft yarns (Fig. 1.16a), *through-thickness angle interlock* when Z-yarns go through the whole fabric across more than two columns of weft yarns (Fig. 1.16b) or *angle interlock* when Z-yarns connect separate layers of the fabric (Fig. 1.16c).

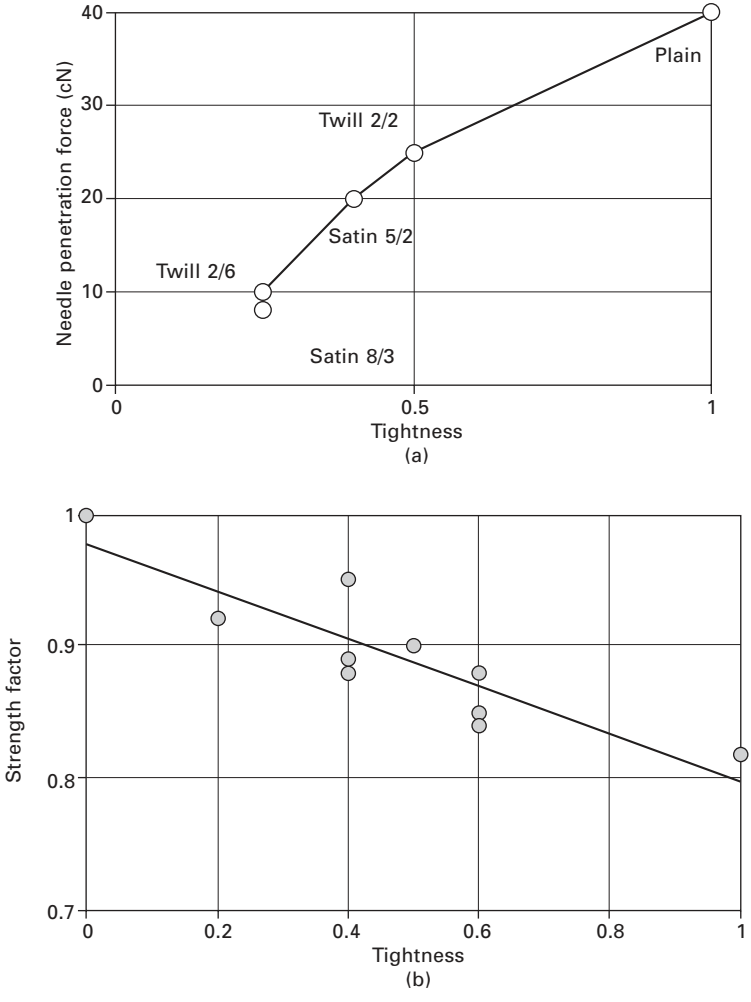

1.14 Influence of fabric tightness on the fabric properties: (a) resistance of cotton fabrics (warp/weft 34/50 tex, 24/28 yarns/cm) to needle penetration; (b) strength factor of yarns in aramid fabrics (ratio of the strength of the fabric per yarn to the strength of the yarn).

Matrix coding of weaves allows the analysis of their topology. Consider for example the front warp yarn in Fig. 1.16b with level codes $\{w_i\} = \{0, 2, 4, 2\}$. This coding means that the yarn path goes from the top of the fabric (level 0) on the left, to beneath the second weft (level 2), to the bottom of the fabric (level 4), then back to level 2 before the pattern repeats. Consider *crimp intervals*, which are yarn segments extending between two crossovers. Over the first crimp interval the yarn interacts with weft yarns in layers

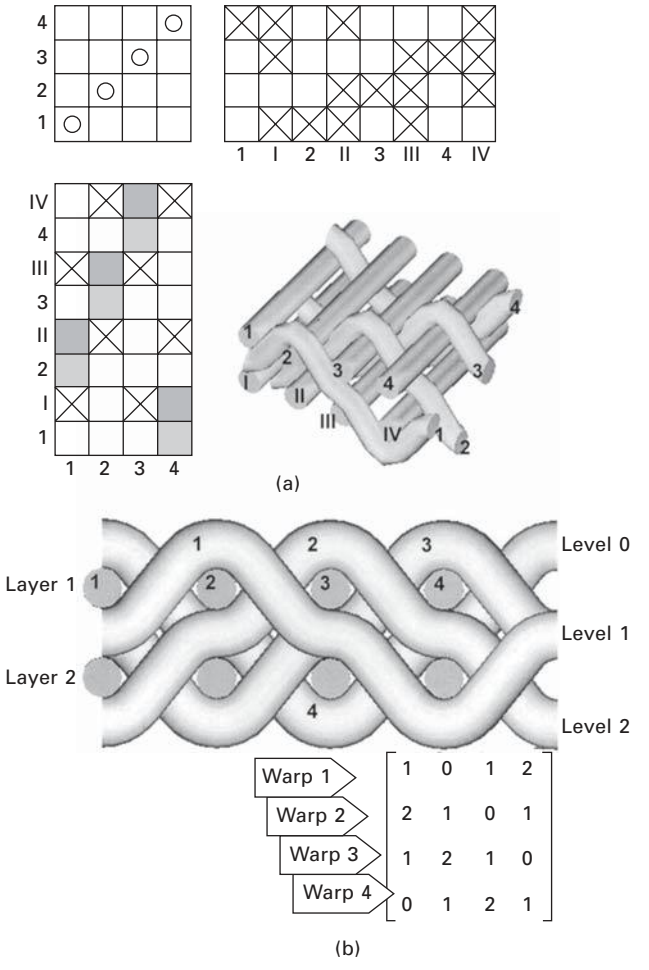

1.15 1.5-Layered satin: (a) weaving plan and structure; (b) coding.

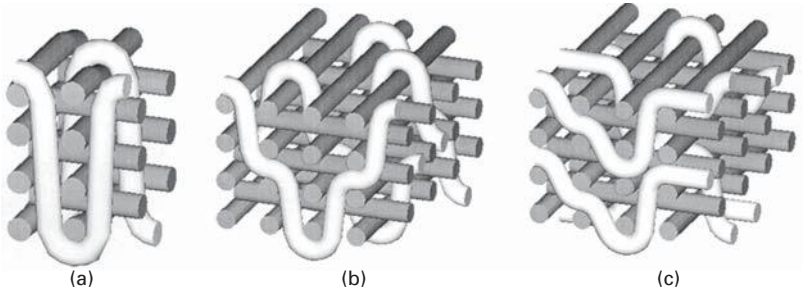

1.16 Types of multilayered weaves: (a) orthogonal; (b) through-the-thickness angle interlock; (c) angle interlock.

$l_1^1 = 1$ and $l_1^2 = 2$, where the subscript and superscript identify the crimp interval and each of its ends. The yarn is above its supporting weft at the left end (1) of the crimp interval $(P_1^1 = 1)$ and below its supporting weft at the right (2) end $(P_1^2 = -1)$. For all the crimp intervals of this yarn:

$$\begin{aligned} &l_1^1 = 1, l_1^2 = 2, P_1^1 = +1, P_1^2 = -1 \\ &l_2^1 = 3, l_2^2 = 4, P_2^1 = +1, P_2^2 = -1 \\ &l_3^1 = 4, l_1^2 = 3, P_1^1 = -1, P_1^2 = +1 \\ &l_4^1 = 2, l_1^2 = 1, P_1^1 = -1, P_1^2 = +1 \end{aligned} \tag{1.14}$$

These values can be obtained from the intersection codes $\{w_i\}$, using the following algorithm:

$$\begin{aligned} &w_i = w_{i+1} \Rightarrow l_i^1 = l_i^2 = \min(w_i + 1, L), P_i^1 = P_i^2 = \begin{cases} +1, w_i < L \\ -1, w_i = L \end{cases} \\ &w_i < w_{i+1} \Rightarrow l_i^1 = w_i, l_i^2 = w_{i+1} + 1, P_i^1 = +1, P_i^2 = -1 \\ &w_i > w_{i+1} \Rightarrow l_i^1 = w_i + 1, l_i^2 = w_{i+1}, P_i^1 = -1, P_i^2 = +1 \end{aligned} \tag{1.15}$$

Similar descriptions of weft yarns are obtained from intersection codes and crimp interval parameters for warp yarns. For a weft yarn i at layer l, the first warp yarn with $l_i^1 = l$ or $l_i^2 = l$ (supported by weft yarn i at layer l) is found from the crimp interval parameters list; this is the left end of the first crimp interval on the weft yarn. The support warp number is thus found, with a weft position sign inverse to that of the warp. Then the next warp yarn supported by weft (i, l) is found; this is the right end of the first weft crimp interval and the left end of the second. This is then continued for all crimp intervals.

1.3.3 Geometry of yarn crimp

The topology and waviness of interlacing yarns are set by the weave pattern. The waviness is called *crimp*. The term also characterises the ratio of the length of a yarn to its projected length in the fabric:

$$c = \frac{l_{\text{yarn}}}{l_{\text{yarn}} - l_{\text{fabric}}} \tag{1.16}$$

Crimp is caused primarily by out-of-plane waviness; reinforcements do not feature significant in-plane waviness because of the flat nature of their rovings. Typical crimp values range from less than 1% for woven rovings to values of well over 100% for warp-interlaced multilayered fabrics. The wavy shape of a yarn in a weave may be divided in intervals of crimp, say between intersections A and B; Fig. 1.17. Considering a warp yarn, let p and h be distances

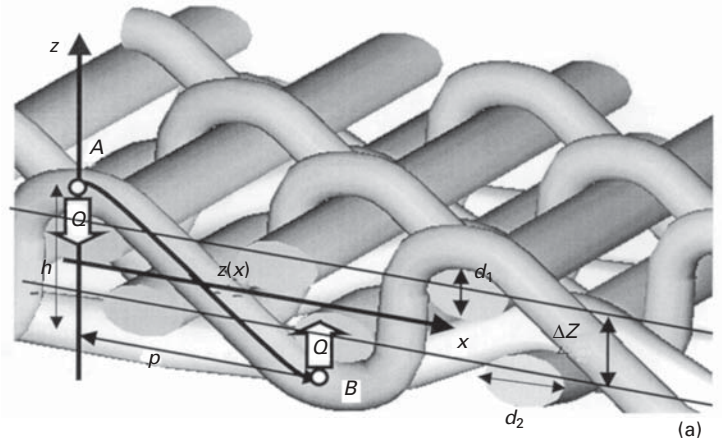

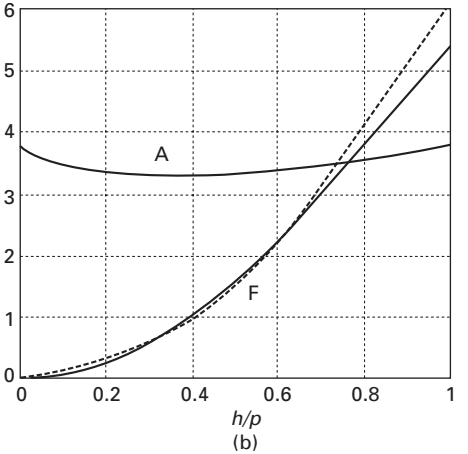

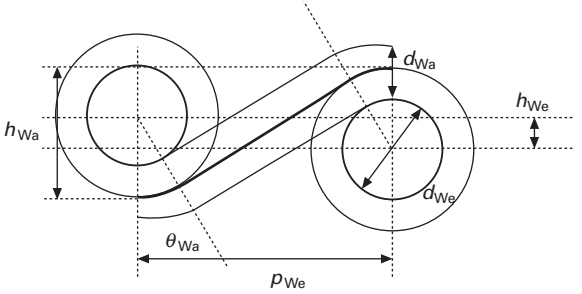

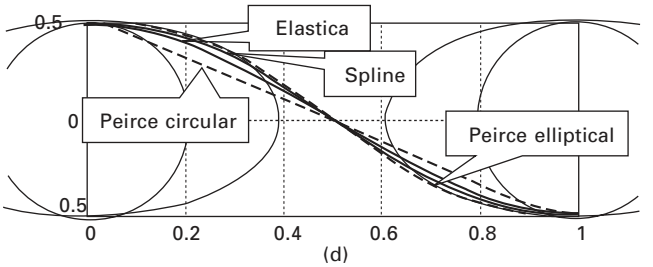

1.17 Elementary crimp interval: (a) scheme; (b) characteristic functions; (c) Peirce's model; (d) comparison between various models.

between points A and B along the warp direction x and thickness z, with p defined as the yarn spacing. The distance h is called the crimp height. If this is known one may wish to describe the middle line of the yarn over the crimp interval:

$$z(x) : z(0) = h/2;\ z'(0) = 0;\ z(p) = -h/2;\ z'(p) = 0 \qquad 1.17$$

The actual shapes of warp and weft yarn cross-sections can be very complex, even if dimensions d_1 and d_2 known are known (subscripts 'Wa' and 'We', Fig. 1.17c). Two simplified cases will be considered here. In the first, cross-section shapes are defined by the curved shape of interlacing yarns. This is acceptable when fibres move easily in the yarns, for example with untwisted continuous fibres. In the second case cross-section shapes are fixed and define the curved shape of interlacing yarn. This is representative of monofilaments or consolidated yarns with high twist and heavy sizing.

Elastica model

In the first approach one can consider yarn crimp in isolation, find an elastic line satisfying boundaries represented by eqn 1.17 and minimise the bending energy:

$$W = \frac{1}{2}\int_0^p B(\kappa)\frac{(z'')^2}{(1+(z')^2)^{5/2}}\,\mathrm{d}x \rightarrow \min \qquad 1.18$$

where $B(\kappa)$ is the yarn bending rigidity which depends on local curvature. A further simplification using an average bending rigidity leads to the well-known problem of the elastica[9] for which a solution can be written using elliptical integrals. Calculations are made easier with an approximation of the exact solution:

$$\frac{z}{h} = \underline{\frac{1}{2}(4\bar{x}^3 - 6\bar{x}^2 + 1)} - A\left(\frac{h}{p}\right)\bar{x}^2(\bar{x}-1)^2\left(\bar{x}-\frac{1}{2}\right),\ \bar{x} = \frac{x}{p} \qquad 1.19$$

where function $A(h/p)$ is shown in Fig. 1.17b; the value $A = 3.5$ provides a good approximation in the range $0 < h/p < 1$. The first, underlined term of eqn 1.19 is the solution to the linear problem. This cubic spline very closely approximates the yarn line.

As the yarn shape defined by eqn 1.19 is parameterised with the dimensionless parameter h/p, all properties associated with the bent yarn centreline can be written as a function of this parameter only. This allows the introduction of a *characteristic function* F for the crimp interval, used to define the bending energy of the yarn W, transversal forces at the ends of the interval Q and average curvature κ, (Fig. 1.17b):

$$W = \frac{1}{2}B(\kappa)\int_0^p \frac{(z'')^2}{[1+(z')^2]^{5/2}}\,\mathrm{d}x = \frac{B(\kappa)}{p}F\left(\frac{h}{p}\right) \qquad 1.20$$

$$Q = \frac{2W}{h} = \frac{2B(\kappa)}{ph} F\left(\frac{h}{p}\right) \tag{1.21}$$

$$\overline{\kappa} = \sqrt{\frac{1}{p}\int_0^p \frac{(z'')^2}{[1+(z')^2]^{5/2}}\,\mathrm{d}x} = \frac{1}{p} F\left(\frac{h}{p}\right) \tag{1.22}$$

If a spline approximation of eqn 1.19 and linear approximation of eqn 1.20 are used,

$$W = \frac{1}{2} B(\kappa) \int_0^p (z'')^2\,\mathrm{d}x = 6B(\kappa)\frac{h^2}{p^3} \tag{1.23}$$

and $F \approx 6(h/p)^2$ (dotted line, Fig. 1.17b). The difference with the exact $F(h/p)$ is negligible.

Peirce type models

In the second approach, yarn cross-sections take set shapes. The simplest model for this case, proposed by Peirce[10] and still widely used, is based on two assumptions: weft cross-sections are regarded as circular when considering crimp intervals for warp yarns, and warp yarns are straight when not in contact with the weft (Fig. 1.17c). The vertical distance between centres of the weft yarns is the weft crimp height h_{We}. As the warp and weft yarns are in contact the following geometric constraint holds:

$$h_{Wa} + h_{We} = d_{Wa} + d_{We} = D \tag{1.24}$$

The yarn spacing p, yarn length l and contact angle θ must satisfy the following relations:

$$\begin{aligned} p_{We} &= (l_{Wa} - D\theta_{Wa})\cos\theta_{Wa} + D\sin\theta_{Wa} \\ h_{Wa} &= (l_{Wa} - D\theta_{Wa})\sin\theta_{Wa} + D(1-\cos\theta_{Wa}) \end{aligned} \tag{1.25}$$

The same equations may be written for weft yarns:

$$\begin{aligned} p_{We} &= (l_{We} - D\theta_{We})\cos\theta_{We} + D\sin\theta_{We} \\ h_{We} &= (l_{We} - D\theta_{We})\sin\theta_{We} + D(1-\cos\theta_{We}) \end{aligned} \tag{1.26}$$

The system 1.24–1.26 providess five equations for six unknowns h_{Wa}, h_{We}, l_{Wa}, l_{We}, θ_{Wa} and θ_{We}. If one of the crimp heights is given or some relation between them is assumed then all parameters can be determined. Peirce's model can represent non-circular cross-sections in a similar manner.

Mixed model

The two above models have their advantages and limitations. Figure 1.17(d) compares yarn mid-line shapes obtained from the different models. Differences

are small, justifying a mixed model where average characteristics of crimp intervals are obtained from (1.20–1.22), taking advantage of the single parameter h/p involved in these equations, while yarn shapes over crimp intervals are defined by Peirce-type models for an assumed cross-section shape. This approach is taken in the following section.

1.3.4 Balancing yarn crimp

Plain weave, incompressible yarns

Consider a plain weave fabric made of incompressible yarns. Yarn spacing p, bending rigidity B and vertical dimensions d are given. Crimp height h is needed to derive a full description of the yarn geometry from the previous equations. This can be calculated by minimising bending energy of all yarns in the repeat:

$$W_\Sigma = \frac{B_{\mathrm{Wa}}}{p_{\mathrm{We}}} F\left(\frac{h_{\mathrm{Wa}}}{p_{\mathrm{We}}}\right) + \frac{B_{\mathrm{We}}}{p_{\mathrm{Wa}}} F\left(\frac{h_{\mathrm{We}}}{p_{\mathrm{Wa}}}\right) \rightarrow \min \qquad 1.27$$

Using the approximation from eqn 1.23 this is easily solved:

$$h_{\mathrm{Wa}} = D\frac{B_{\mathrm{We}} p_{\mathrm{We}}^3}{B_{\mathrm{Wa}} p_{\mathrm{Wa}}^3 + B_{\mathrm{We}} p_{\mathrm{We}}^3}, h_{\mathrm{We}} = D\frac{B_{\mathrm{Wa}} p_{\mathrm{Wa}}^3}{B_{\mathrm{Wa}} p_{\mathrm{Wa}}^3 + B_{\mathrm{We}} p_{\mathrm{We}}^3} \qquad 1.28$$

A few special cases are illustrated in Fig. 1.18(b). If $B_{\mathrm{Wa}} = B_{\mathrm{We}}$ and $p_{\mathrm{Wa}} = p_{\mathrm{We}}$ then $h_{\mathrm{Wa}} = h_{\mathrm{We}} = D/2$, which is typical of a balanced fabric. If $B_{\mathrm{Wa}} >> B_{\mathrm{We}}$ and $p_{\mathrm{Wa}} = p_{\mathrm{We}}$ then $h_{\mathrm{Wa}} = 0$ and $h_{\mathrm{We}} = D$. Rigid warp yarns stay straight and compliant weft yarns wrap around them, which is typical of quasi-unidirectional woven fabrics. If $p_{\mathrm{Wa}} >> p_{\mathrm{We}}$ and $B_{\mathrm{Wa}} = B_{\mathrm{We}}$ then again $h_{\mathrm{Wa}} = 0$ and $h_{\mathrm{We}} = D$. Long segments of weft yarn extending between crossovers are easier to bend than short segments of warp yarns.

Plain weave, compressible yarns

Consider the same problem with compressible yarns. Compressibility of warp and weft yarns is given by experimental diagrams. Subscripts 0, 1 and 2 respectively designate the relaxed state, yarn dimension in the vertical direction and in-plane dimensions; q is a compression force per unit length.

$$d_1^{\mathrm{Wa}} = d_{10}^{\mathrm{Wa}} \eta_1^{\mathrm{Wa}}(q), d_2^{\mathrm{Wa}} = d_{20}^{\mathrm{Wa}} \eta_2^{\mathrm{Wa}}(q) \qquad 1.29a$$

$$d_1^{\mathrm{We}} = d_{10}^{\mathrm{We}} \eta_1^{\mathrm{We}}(q), d_2^{\mathrm{We}} = d_{20}^{\mathrm{We}} \eta_2^{\mathrm{We}}(q) \qquad 1.29b$$

Equation 1.27 applies with constraint including dimensions depending on yarn interaction forces:

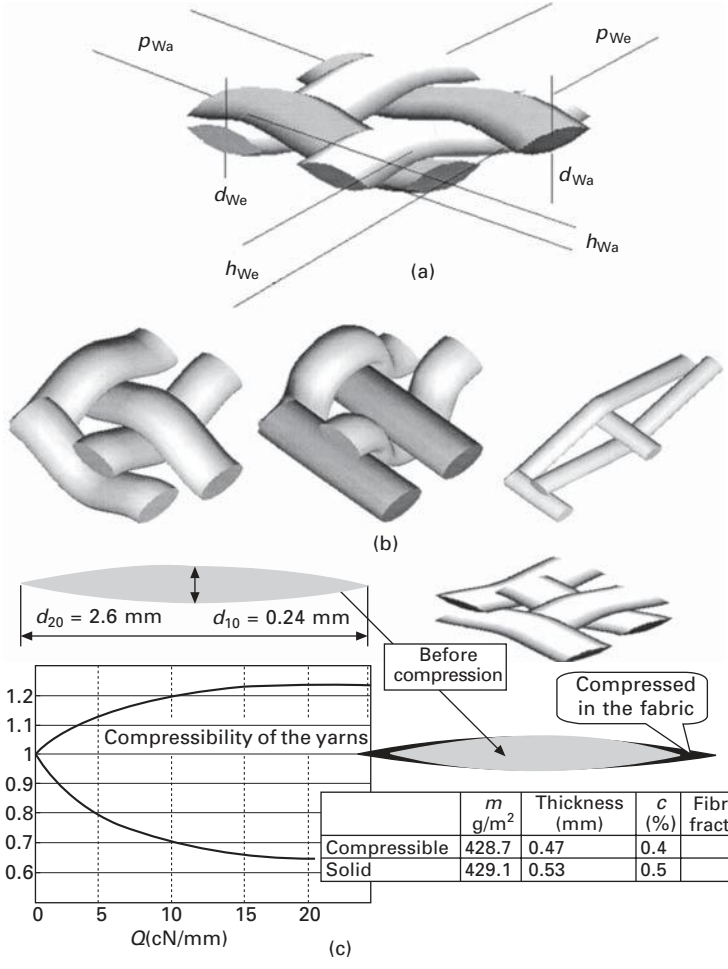

	m g/m^2	Thickness (mm)	c (%)	Fibre volume fraction, V_f (%)
Compressible	428.7	0.47	0.4	36
Solid	429.1	0.53	0.5	32

1.18 Balance of crimp in plain weave: (a) scheme; (b) three special cases; (c) change in yarn dimensions for typical fabric with compressible yarns.

$$h_{Wa} + h_{We} = d_{10}^{Wa}\eta_1^{Wa}\left(\frac{Q}{d_2^{Wa}}\right) + d_{10}^{We}\eta_1^{We}\left(\frac{Q}{d_2^{We}}\right) \qquad 1.30$$

where the transversal forces Q are calculated from eqn 1.21, giving:

$$Q = \frac{B_{Wa}}{p_{We}h_{Wa}}F\left(\frac{h_{Wa}}{p_{We}}\right) + \frac{B_{We}}{p_{Wa}h_{We}}F\left(\frac{h_{We}}{p_{Wa}}\right) \qquad 1.31$$

Equation 1.30 assumes that the zone over which Q acts has dimensions equal to in-plane yarn dimensions; a better description of the yarn contact zone would improve the model. The non-linear system (eqn 1.29–1.31) can be solved iteratively by setting:

$$d_1^{Wa} = d_{10}^{Wa},\ d_2^{Wa} = d_{20}^{Wa},\ d_1^{We} = d_{10}^{We},\ d_2^{We} = d_{20}^{We},\ h_{We} = h_{Wa}$$

$$= (d_1^{Wa} + d_1^{We})/2 \qquad 1.32$$

Transversal forces are computed from eqn 1.31, yarn dimensions are obtained from eqn 1.29 and the minimum problem of eqn 1.27 is solved for h_{Wa} and h_{We}. Then convergence is checked by comparing with values from eqn 1.32 and the above steps are repeated as necessary.

Figure 1.18(c) shows an example of changes in yarn dimensions for a glass plain weave with tow linear density of 600 tex, tow bending rigidity of 0.44 N mm^2 and ends/picks count 36/34 yarns/cm. The compression diagram in Fig. 1.18(c) was measured using the KES-F tester. Results show that the yarns are compressed considerably, changing the fabric thickness by 8%.

1.4 Braided fabrics

1.4.1 Parameters and manufacturing of a 2D braided fabric

In braiding, three or more threads interlace with one another in a diagonal formation, producing flat, tubular or solid constructions. Such fabrics can often be used directly as net-shape preforms for liquid moulding processes such as resin transfer moulding (RTM). This section discusses 2D flat or tubular braids.

Braiding process

The principle of braiding is explained in Figs 1.19 and 1.20 for a maypole machine. Carriers move spools in opposite directions along a circular path. Yarn ends are fixed on a mandrel and interlace as shown in Fig. 1.19. Interlaced yarns move through the convergence zone of the machine, towards the mandrel which takes the fabric up the loom. The yarns follow helical paths on the mandrel and interlace each time spools meet. Producing a thin, tight braided lace or a circular tube does not require a mandrel. On the other hand, 2D braids produced on shaped mandrels can be used as reinforcements for composite parts. Braiding over shaped mandrels allows the introduction of curvature, section changes, holes or inserts in the reinforcement without need to cut the yarns, as shown in the photograph in Fig. 1.19.

In the process described above spools must travel to and from the inner and outer sides of the circular path to create interlacing. Fig. 1.20 shows the necessary spool motions for a part of the path. Carriers with odd and even numbers move from left to right (clockwise) and from right to left (counter-clockwise) respectively. The notched discs are located on the circumference

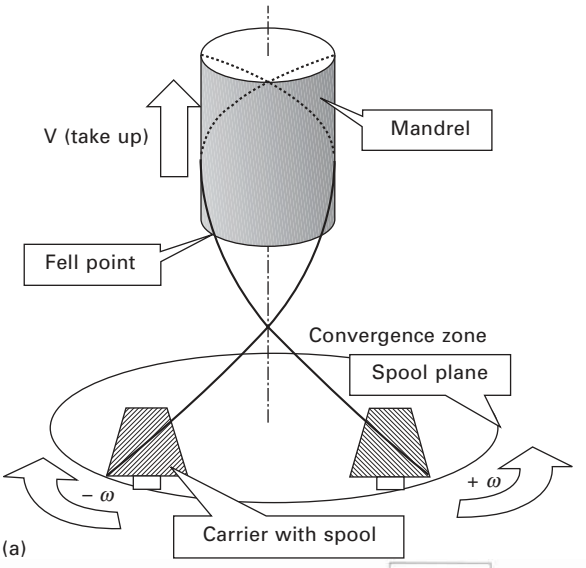

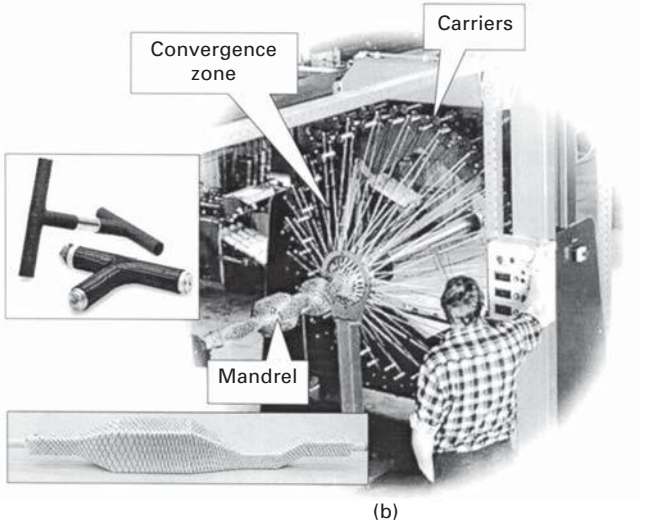

1.19 Scheme and photograph of a maypole braider: diagonal interlacing of the yarns, where only two carriers are shown. Insets: non-axisymmetric mandrel and braided products with holes and inserts.

of the machine, spool carrier axles are located in these notches and adjacent disks rotate in opposite directions. Consider carrier 1; once taken by a disk to a position where notches superpose with those of the neighbouring disk the carrier is transferred to that disk by centrifugal force and a rotating guide. Because of the difference in rotation directions, spool 1 is taken toward the

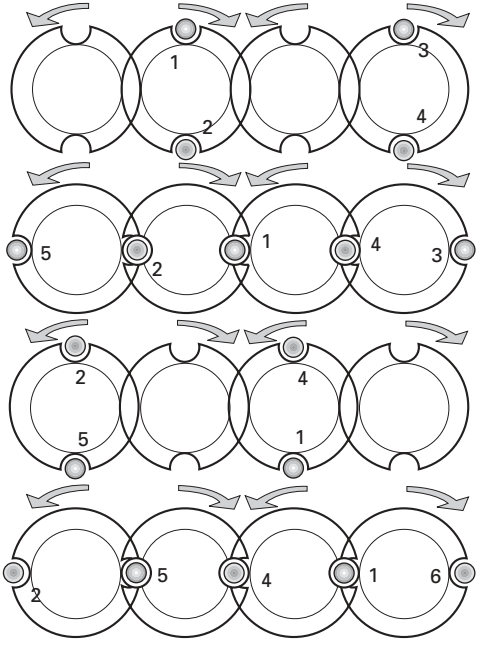

1.20 Horn gears and movements of the yarn carriers.

outside of the machine by the second disk. The same happens to its counterpart 2 carried by the notched disks in the opposite direction. Hence carriers 1 and 2 cross each other and change sides, creating interlacing. Figure 1.21(a) shows carrier paths producing a tubular braid. If the sequence of disks is interrupted, the carriers create a flat braid as shown in Fig. 1.21(b). In modern braiders notched disks are replaced by horn gears and carrier feet are directed along slots in a steel plate covering the gears.

Additional yarns extending along the braid axis can be incorporated, producing what are commonly described as triaxial braids. They do not travel on carriers but are fed from stationary guides situated at the centres of horn gears, Fig. 1.21(c). Such *inlays* or *warp yarns* are supported by the braided yarns and are almost devoid of crimp. They are common in reinforcements.

Braid patterns and braiding angle

Patterns created by braiding are similar to weaves and can be described in these terms (Fig. 1.22). Braids are identified in the same way as twills, by floats lengths for the two interlacing yarn systems. Three patterns have special names: *diamond* (1/1), *regular* or *plain* (2/2) and *hercules* (3/3) braids. A *plain* weave and a *plain* braid correspond to different patterns.

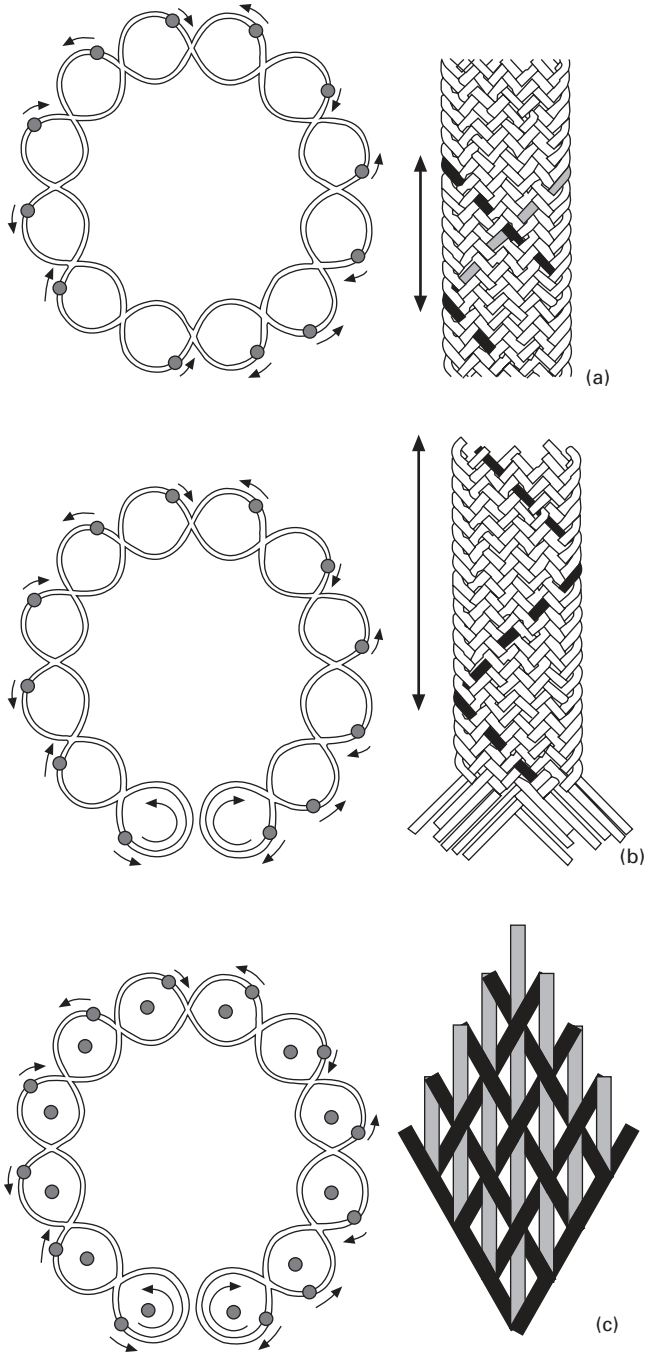

1.21 Carrier paths and braided patterns: (a) circular braid; (b) flat braid; (c) braid with inlays (triaxial braid).

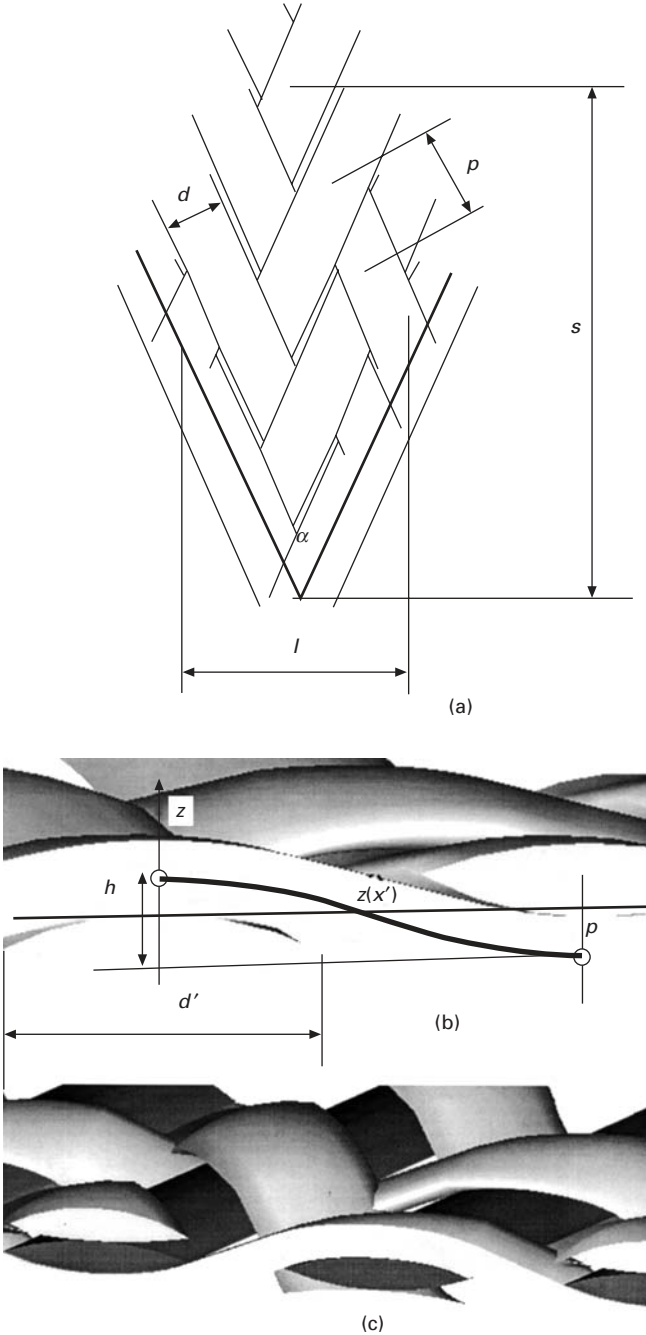

1.22 Geometry of a braid unit cell: (a) dimensions of the unit cell; (b) geometry of crimp; (c) yarn crimp in a braid with inlays (darker yarns).

The repeat of a braid is defined as the number of intersections required for a yarn to leave at a given point and to return to the equivalent position further along the braid (arrows, Fig. 1.21). This measure is called *plait*, *stitch* or *pick* and equals the total number of yarns in a flat braid or half their number in tubular braids. The definition differs from that of repeat in weaves; to avoid confusion the term *unit cell* is used to identify the basic repetitive unit of a pattern. The most important parameter of a braid is the *braiding angle* between interlaced yarns (Fig. 1.22), calculated from the machine speed and mandrel diameter D_m:

$$\alpha = 2 \arctan \frac{\pi D_m n}{v} \tag{1.33}$$

where n and v are the rotational speed (s^{-1}) and take-off speed. The angle depends on the mandrel diameter; if a complex mandrel is used the take-up speed must be constantly adjusted to achieve a uniform angle. By varying the take-up speed variable angles can be induced, allowing stiffness variations for the composite part. The practical range of braiding angles is between 20° and 160°.

Equation 1.33 implies that the mandrel is circular (or at least axisymmetric), but as shown in Fig. 1.19 this is not a requirement for the process. An average braid angle for a non-axisymmetric mandrel can be obtained by replacing the term πD_m in eqn 1.33 with the local perimeter of the mandrel. However, it has been observed that the braid angle changes significantly with position around any section of a complex mandrel. Models have been proposed recently to predict this behaviour[11,12].

A braider can be set vertically or horizontally. The former is common for the production of lace or general tubular braids, and the latter for braiding over long mandrels. Typical carrier numbers are up to 144. Rotation and take-up speeds can reach 70 rpm (depending on carrier numbers) and 100 m/min respectively. Productivity as mass of fabric per unit time can be estimated by the equation:

$$A = \frac{TvN}{\cos^2 \frac{\alpha}{2}} = \frac{2\pi D_m TNn}{\sin \alpha} \tag{1.34}$$

where T and N are the yarn linear density and number of carriers. The productivity can reach several hundreds of kilograms per hour; braiding is more productive than weaving by an order of magnitude.

1.4.2 Internal geometry of 2D braids

The internal geometry of braids is governed by the same phenomenon mentioned for woven fabrics namely yarn crimp. The non-orthogonal interlacing of the yarns results in certain peculiarities. Consider a braided unit cell. Let

n be a float in the braid pattern identified as n/n; $n = 2$ in Fig. 1.22. Unit cell dimensions are given by the braiding angle, stitch length per unit cell s and line length per unit cell l:

$$l = s \tan \frac{\alpha}{2} \qquad 1.35$$

The shape of yarn centrelines can be modelled in a similar way as for woven fabrics (Fig. 1.22b). On a section of the fabric including the centre of a yarn (axis x'), spacing p and dimensions d' of support cross-sections are given by:

$$p = \frac{s}{4n \sin \frac{\alpha}{2}} = \frac{l}{4n \cos \frac{\alpha}{2}}, d' = \frac{d}{\sin \frac{\alpha}{2}} \qquad 1.36$$

where d is the yarn width. A function $z(x')$ is constructed for a given crimp height h using an elastica or Peirce-type model and crimp balance is computed using the algorithm previously formulated. Observation of triaxial braids reveals mostly straight and crimp-free inlays extending along the machine direction. This is expected for balanced braids, while unbalanced braids are quite rare in practice. The presence of inlays changes the crimp height of interlacing yarns but the algorithms for the calculation of the mid-line shape and crimp balance remain unchanged, (Fig. 1.22c).

When the braided yarns are not perpendicular the yarn paths will be twisted, so that yarn cross-sections appear rotated. This also applies to woven fabrics subjected to shear deformation (for example during fabric draping).

1.4.3 3D braided fabrics

3D braiding presents some similarities with 2D braiding. In 2D maypole braiding only two sets of carriers rotate around the braiding axis in opposite directions, creating a single textile layer. In contrast, 3D braids can be regarded as multiple layers of interlaced yarns which are connected more or less extensively by individual yarns extending through the thickness. It is possible to braid preforms where the level of interlacing between different layers is such that it becomes impossible to discern the distinct layers in the final preform. Carrier paths may be defined over concentric circles or Cartesian arrays, which are square or rectangular.

Two examples of 3D braiding processes are described by Byun and Chou[13], known as the four-step and two-step processes. The four-step process (Fig. 1.23a) uses a framework of yarn carriers in a rectangular or circular array. As the name suggests, the process consists of four steps, each involving alternate movements of the rows and columns of yarn carriers. Between cycles the yarns are 'beaten up' into the structure and the braid is hauled off by one pitch length. The two-step process (Fig. 1.23b) involves a large number of axial yarns arranged in the required preform geometry, with a smaller number

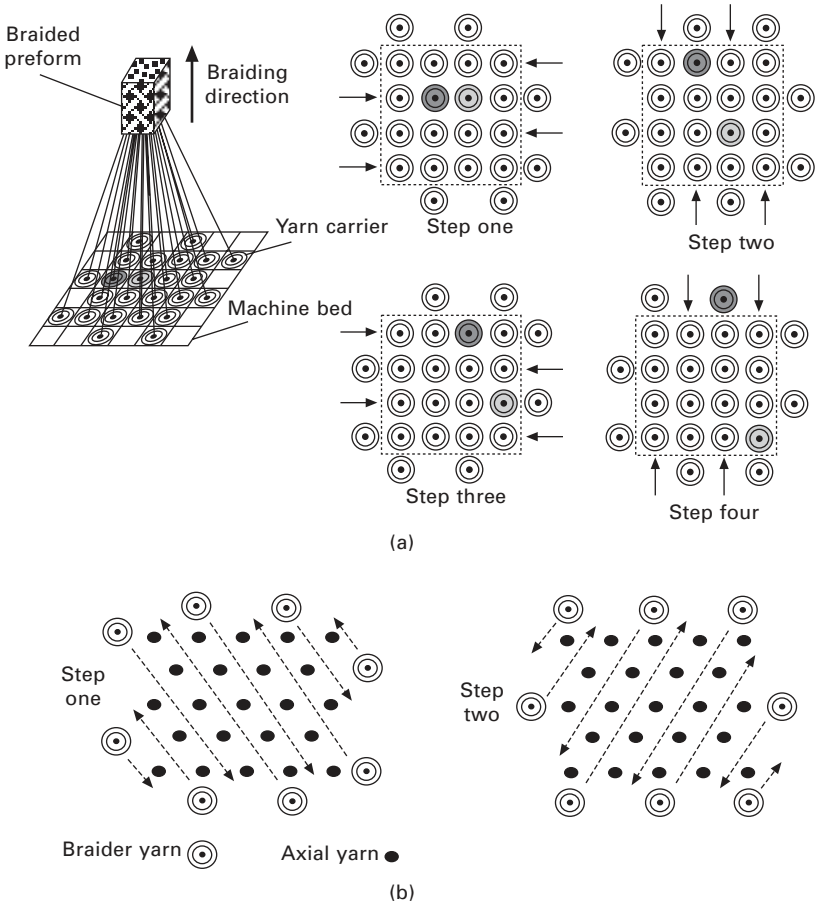

1.23 Schematic illustration of the (a) four-step and (b) two-step 3D braiding processes.

of yarn carriers arranged around them. The carriers are moved through the array of axial yarns in two alternate directions.

Such processes can be used to produce preforms featuring yarns that extend along many directions. Yarn directions are not limited to a plane, and this constitutes the main advantage of the process. However, any increase in out-of-plane properties is achieved at the expense of in-plane properties. 3D braids generally feature axial yarns. Preforms of various shapes can be produced, for composite parts of which the geometry is very different to the shells associated to parts based on 2D textiles such as weaves or non-crimp fabrics. Such applications are still relatively rare; rocket engines constitute a classic example while biomedical engineering is one area of emergence.

1.5 Multiaxial multiply non-crimp fabrics

The above textile reinforcements offer economical advantages while being easier to process than prepregs. However, compromises are made on the performance of the composite because of crimp that causes fibre misalignments. Non-crimp fabrics combine unidirectional crimp-free fibre layers by assembling them together by stitching – sewing or knitting – and/or bonding by chemical agents.

1.5.1 Terminology and classification

European standard EN 13473 defines a multiaxial multiply fabric as

> A textile structure constructed out of one or more laid parallel non-crimped not-woven thread plies with the possibility of different orientations, different thread densities of single thread plies and possible integration of fibre fleeces, films, foams or other materials, fixed by loop systems or chemical binding systems. Threads can be oriented parallel or alternating crosswise. These products can be made on machines with insertion devices (parallel-weft or cross-weft) and warp knitting machines or chemical binding systems.

The definition stresses that fibrous plies are laid up with threads. Stitching the plies together by warp-knitting can be achieved in such a way that the stitches pierce the plies between the laid yarns, resulting in an open preform architecture; Fig. 1.24a. On the other hand wide threads (flat tows) laid close together form continuous fibrous plies bound by warp-knitting with piercing sites positioned according to the needle spacing, without any connection to tow positioning. Needles pierce the fibrous plies and distort them locally; Fig. 1.24b. Such a preform construction is close to ideal unidirectional uniform plies. The latter case is the most common, and is the subject of this section.

A fabric is characterised by the nature of the fibres (E/G/C/A glass, carbon or aramid), surface density of each ply (g/m^2), fibre direction in each ply given as an angle with respect to the machine direction in the range [–90°, 90°], type of binding agent, nature of the binding agent (polyamide/poly(ethylene)/poly(ether sulphone)/poly(ethylene terephthalate/polypropylene; PA/PE/PES/PET/PP, chemical binder) and surface density of the binding agent. For example the designation stipulated by the standard for a 3-ply +45°/–45°/0° glass fabric stitched by a polyester yarn is:

[G, 235, +45° // G, 235, –45° // G, 425, 0°][PES, 12, L]

with a total surface density of 907 g/m^2. Ply weight depends on yarn weight and placement density. In general yarn weight is characterised by a number

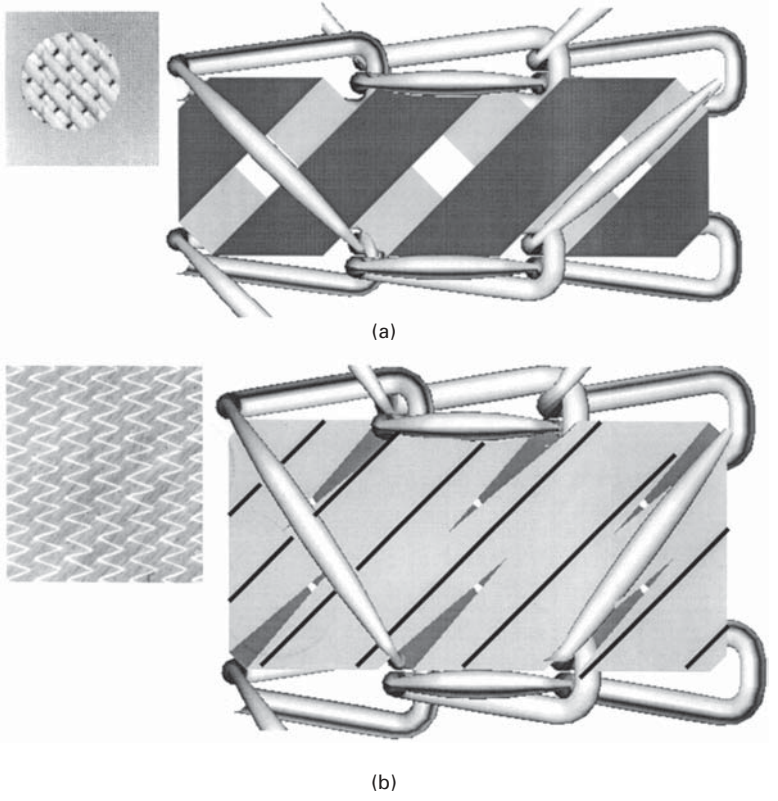

1.24 Multiaxial multiply warp knitted fabrics: (a) open structure, with stitching sites in between the tows; (b) continuous plies, with stitching penetrating the tows forming 'cracks' in the plies.

of filaments ranging from 3K to 80K for carbon tows. Surface densities usually range from 100 g/m^2 upwards. Higher yarn weights normally translate into higher ply surface density values for a closely covered surface. Low surface density values may be reached with thick tows by spreading, using a special unit. Yarns with higher fibre count present the economical advantages of cheaper raw material and faster production. Low ply surface weights are desirable as lighter fabrics have better drapability. Current technology achieves 150 g/m^2 with 12K yarns in the weft or 24K in 0° layers.

1.5.2 Manufacturing

Producing a multiaxial multiply fabric involves laying plies or *weft insertion*, and stitching or *knitting* them together. Hence the machine has two main parts, a weft insertion device and a knitting unit.

Weft insertion

Weft insertion carriages travelling across the machine lay several tows simultaneously at a desired angle across the fabric. The tows are fixed to the needles of the moving chains. The length of the weft insertion part of a typical machine is about 10 m and allows up to three layers with angles from 20° to 90° or –20° to –90°. The speeds of weft insertion carriages dictate the fibre angles. Measurements show that the orientation of oblique fibres can deviate from the prescribed value by several degrees.

Weft inserted tows together with optional 0° plies are stitched by a warp-knitting device. A powder binder (e.g. epoxy) can be added beforehand to facilitate composite processing. A foil or non-woven ply may be added below the plies. A warp-knitting device as described below stitches the plies by an action of needles, which are collected in a needle bed and move upwards, piercing the plies.

Walking needle

Stitching of ply construction by warp-knitting is optimised to decrease misalignment and disturbance of the weft yarns by the knitting needles. In older knitting units needles move in one direction only, standing at a certain angle to the plies. The needles move linearly upwards to catch the warp knitting yarn and then down to pull the yarn through the ply, building a stitching mesh. Plies move constantly forward. The relative movement of plies and needles in the horizontal direction causes misalignment during penetration, the extent of which depends on the stitching length and other parameters. This limitation was reduced drastically by the development of the *walking needle* device, introducing a new needle movement where the needle is placed at 90° to the textile and moves in the vertical direction as well as in the direction of ply movement during penetration. The relative horizontal motion between the textile and needle is minimal. The needle head is designed to penetrate the ply construction by pushing away the filaments of reinforcing yarns, minimising the damage.

Warp knitting

The principle of warp knitting is illustrated in Fig. 1.25. An actual warp knitted fabric or a knitted web, whereby warp knitting is used to stitch unidirectional fibrous plies, is an assembly of loops formed by the interaction of needles and guides. Yarns are fed through all guides and all needles are fixed on a needle bar, moving simultaneously and forming a loop around every needle in every cycle.

Consider a warp yarn about to be looped, going thorough the guide at the beginning of the knitting cycle (Fig. 1.25a). Knitting needles are in their

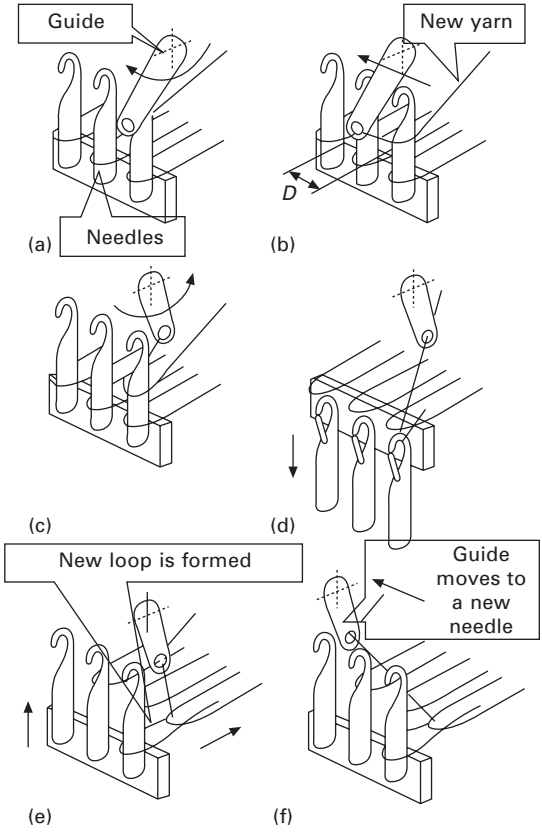

1.25 Principle of warp knitting, showing interaction of the knitting needles and guides.

upper position. Loops forming the edge of the fabric are on the stems of the needles. The guide carries the new yarn around a needle, forming a new loop (Fig. 1.25b,c). The needle moves down, connecting the new loop with the old one sitting on its stem (Fig. 1.25d,e); in the case of ply stitching the loop is pulled through the plies. The textile is pulled and a new cycle starts. The knitting action creates loop connections in the machine (*course*) direction. Movements of the guides across the needle bed create connections in the cross (*wale*) direction, forming a warp-knit pattern; Fig. 1.26. The positions of the gaps between the needles, where guides pass in subsequent knitting cycles, can be used to code the pattern by the so-called Leicester notation. Consider a diagram of the guides' movement, called a *lapping diagram* (Fig. 1.26). Rows of dots represent needle positions in plane view. The numbering of needles assumes that the pattern mechanism is on the right side. As the guides position themselves in the spaces between needles, the positions

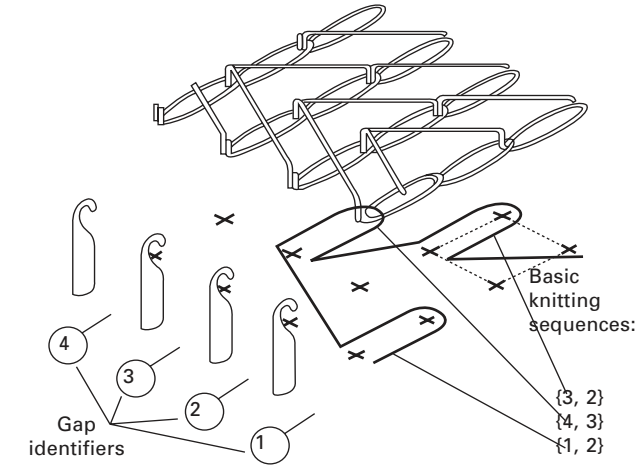

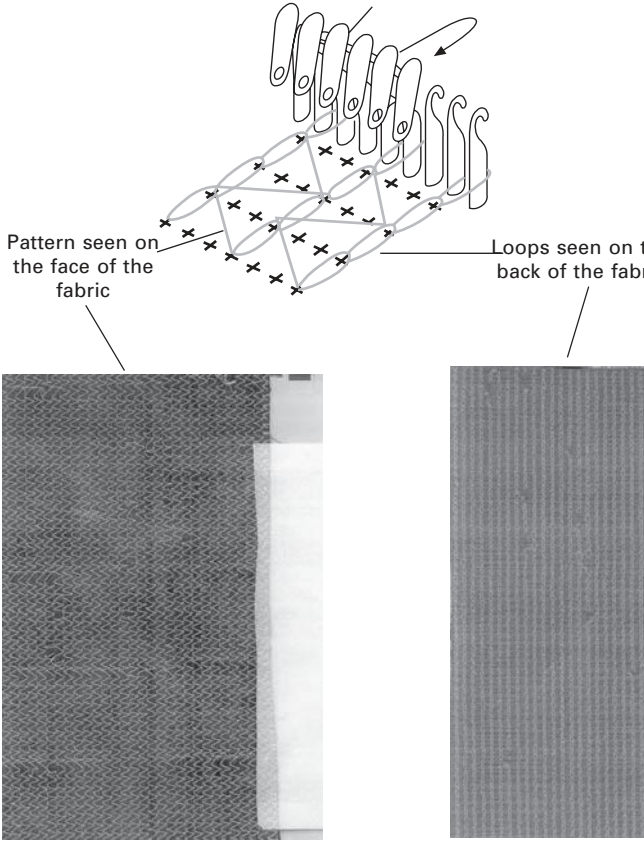

1.26 Warp-knit pattern formation and coding.

between vertical columns of dots represent lateral shifts of the guides. The pattern is a sequence of these numbers:

$$s_1–S_1/s_2–S_2/ \ \ldots \ / \ s_N–S_N \qquad 1.37$$

where s_i and S_i are the positions of the guide forming the ith loop and N is the number of knitting cycles in the pattern. Positions s_i and S_i refer to gaps between needles where the elementary movement of guides start. A pair $s_i–S_i$ represents an overlap motion (guides move behind needles) while S_i/s_{i+1} is an underlap motion (guides move in front of needles). The following consider patterns where overlaps extend by one needle only, i.e. $|s_i–S_i| = 1$.

When fibrous plies are stitched, the pattern is seen on the face of the fabric (Fig. 1.26). These yarns are laid on the face of the fabric by the guides. On the back of the fabric chains of loops are seen, extending in the machine direction. These loops are formed on separate needles and interconnect through the knitting action of the needles.

1.5.3 Internal geometry

Positions of the stitching sites

A stitching yarn pierces the fibrous plies at positions defined by the needle spacing in the needle bed (spacing in cross direction A) and by the speed of the material feeding in the knitting device (spacing in machine direction B). The value of A is also expressed by the *machine gauge*, a number of needles per inch. In a warp-knitted fabric devoid of fibrous plies, yarn tension leads to significant deviations of the actual loop spacing in the relaxed fabric. In the case of multiaxial multiply fabrics the stitching yarn is fixed by the fibrous plies, resulting in fairly regular spacing. Figure 1.27 gives an example of spacing variability for such a fabric. Deviations in the positions of stitching lead to deviations of the loops from the ideal machine direction; the deviation can be as high as 15°.

Geometry of the stitching loop

The loop geometry can be assumed using a geometric approach or described using a mechanical approach where the shape is calculated from equilibrium equations applied to the looped yarns. The latter approach is unsuitable here as loop positions are set by the plies, and large fluctuations of loop shapes are observed in practice. Hence the geometric approach is considered more appropriate.

Stitching yarns normally have a low linear density of around 10 tex with tyically 15 filaments, and low twist (<100 m^{-1}). They are easily compressible, which explains the large observed variations of their dimensions. Stitch yarn

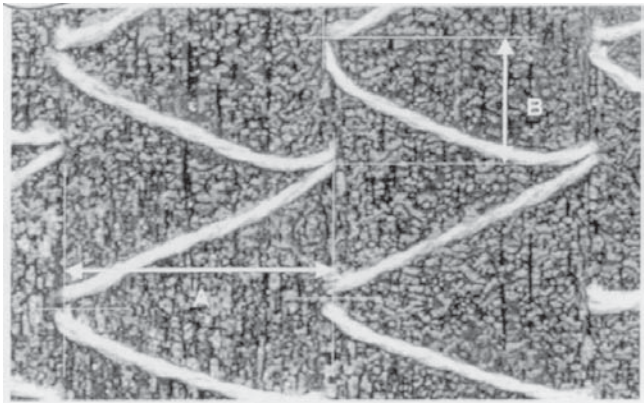

(a)

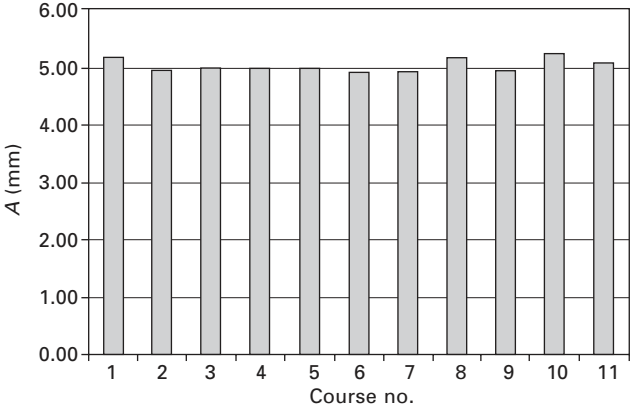

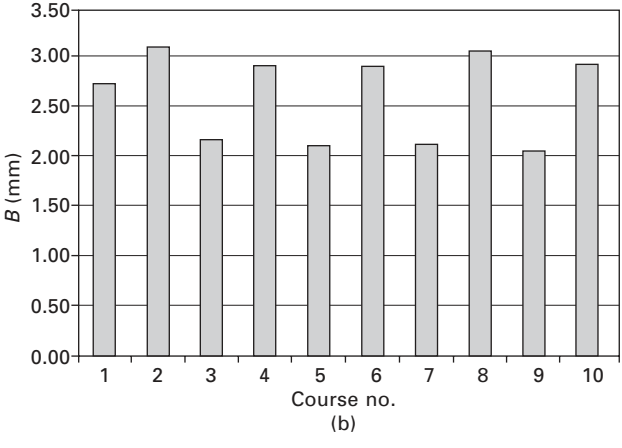

(b)

1.27 Spacing of the stitching loops for a carbon 0/–45/50 fabric: (a) definition of *A* and *B* and (b) measured values for adjacent wales.

shapes are observed to vary within the repeating pattern, with cross-sections ranging from circular to flattened (elliptical) and with varying dimensions[14].

The geometry of the yarn centreline is defined by identifying a set of anchor points A–M along the loop and approximating the centreline between the anchor points by straight lines or circular arcs. In Fig. 1.28 h is the total thickness of the plies; arcs AB, CD, FE, GH, IJ and KL have constant radii and diameter d_0. The loop width w depends on knitting tension. Considerable tension produces narrow loops with $w \approx 3d_0$; lesser tension increases w to 4 to 5 times d_0.

Interactions of the stitching with fibrous plies

Stitching causes deviations to fibre orientations. These deviations can result in linear channels (Fig. 1.29a), or be localised near stitching sites as *cracks* (Fig. 1.29b). Localised cracks have a rhomboidal shape of width b and length l. A channel is formed when localised cracks touch or overlap. The direction of cracks and channels corresponds to that of fibres in the ply. The cracks/channels are also evident inside the fabric, where they provide routes for resin flow. In a composite they create resin rich zones which can play an important role in the initiation of damage.

Crack and channel dimensions feature much scatter (Fig. 1.29c). Table 1.2 shows measured crack and channel dimensions for various fabrics. Crack widths are approximately proportional to the thickness of the stitch yarn, so that an empirical coefficient k can be used to calculate $b = kd_0$, where d_0 is the compacted stitch diameter. Fibres in a powdered fabric are more difficult to displace, explaining the low values of k and l/b for the latter fabric. In non-powdered fabrics channels are wider than cracks, with rough k averages of 4 (cracks) and 7 (channels) and l/w values for cracks of about 20. Dimensions are also influenced by knitting tension.

When large channels extend along the machine direction, stitch yarn sections on the fabric face or loops on the back can sink in the channels. This phenomenon plays a major role in nesting of non-crimp fabric layers in laminates. When this sinking occurs the layers can come closer, closing any gap between them that might be introduced by stitched yarns laying on the surface of the fabric. This is evidenced by compression curves of multiple layers of fabric such as a biaxial 'B' –45°/45° and quadriaxial 'Q' 0°/–45°/90°/45°; Fig. 1.30. In the former, stitch yarns extend across the fibre direction and cannot sink in cracks. The face of the latter textile has wide channels into which stitches sink deeply (Fig. 1.30a), allowing nesting. Hence the thickness per layer of the compressed fabric 'Q' decreases with an increase in number of layers while it stays constant for fabric 'B'.

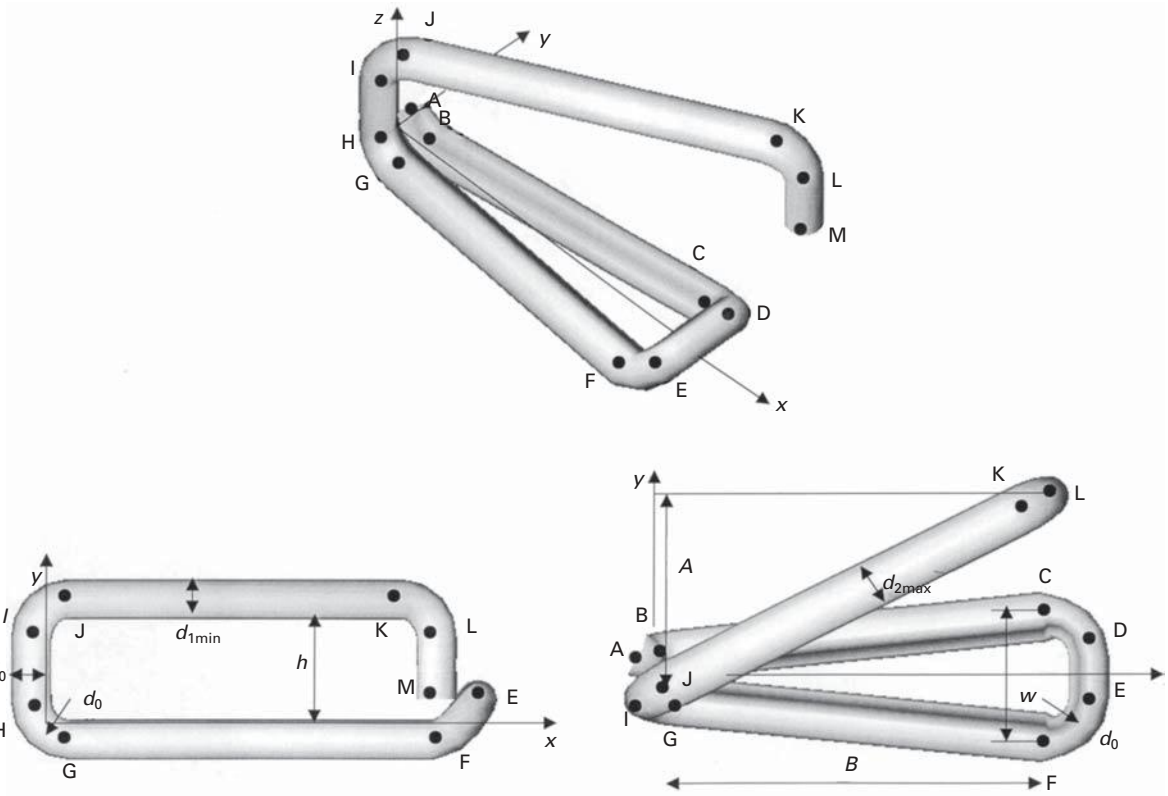

1.28 Geometry of the stitching loops, showing positions of anchor points.

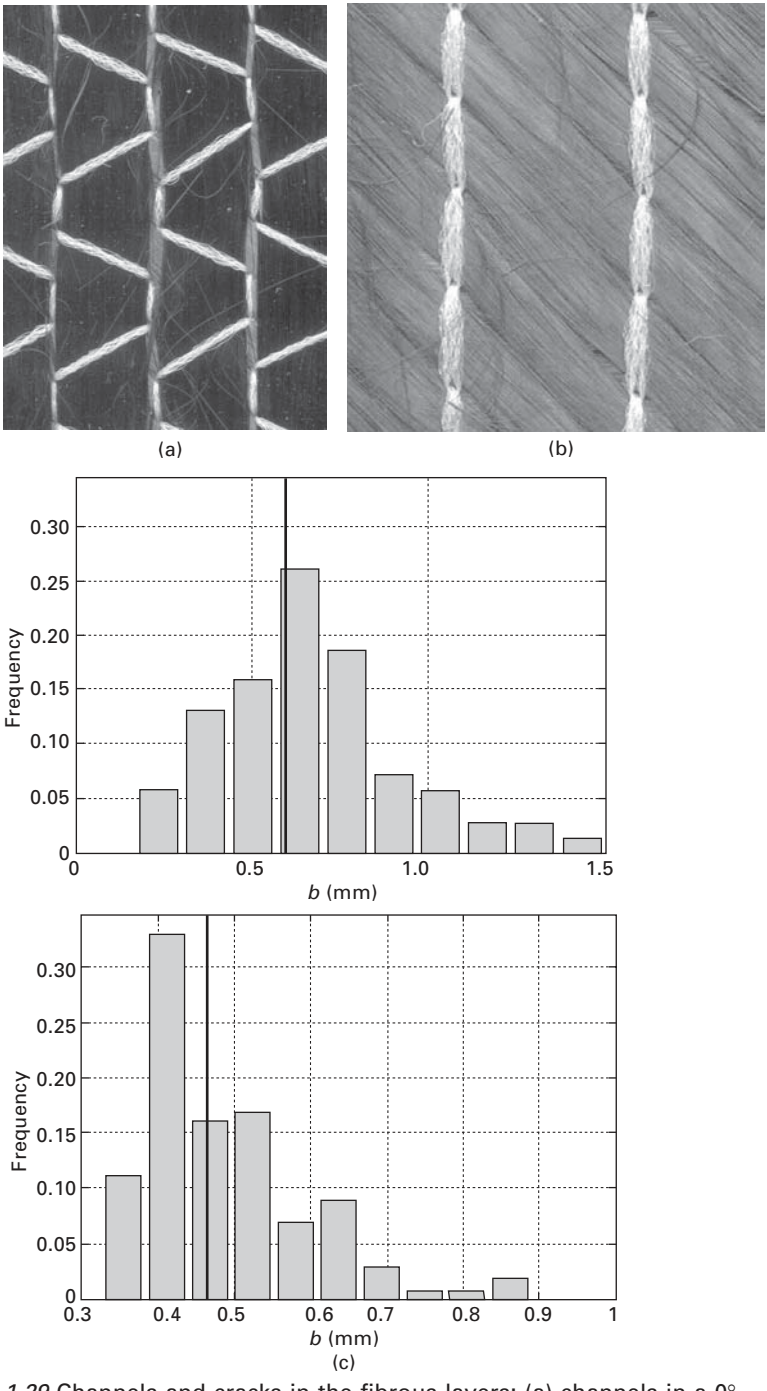

1.29 Channels and cracks in the fibrous layers: (a) channels in a 0° (face) ply; (b) crack in a 45° (back) ply; (c) distribution of channel/crack widths.

Table 1.2 Dimensions of channels and cracks in multiaxial multiply carbon fabrics

Fabric	Stitching		Crack/channel	w (mm)	l (mm)	k	l/w
	Material, linear density	d_0 (mm)					
–45/–45, 12K	PES, 7.6 tex	0.088	Face cracks	0.276	5.05	3.13	18.3
			Back cracks	0.434	7.15	5.39	16.5
0/90, 24K	PES, 7.6 tex	0.088	Face channels	0.62	n/a	7.04	n/a
			Back channels	0.36	n/a	4.09	n/a
0/–45/90/45	PES, 7.6 tex	0.088	Face channels	0.658	n/a	7.47	n/a
			Back cracks	0.483	7.28	5.48	15.0
45/–45, 12K	PES, 6 tex	0.071	Face cracks	0.28	7.43	3.94	26.5
			Back cracks	0.27	7.85	3.80	29.1
0/90, 12K, powdered	PA, 10 tex	0.107	Face channels	0.18	n/a	1.68	n/a
			Back cracks	0.53	3.46	4.95	6.53

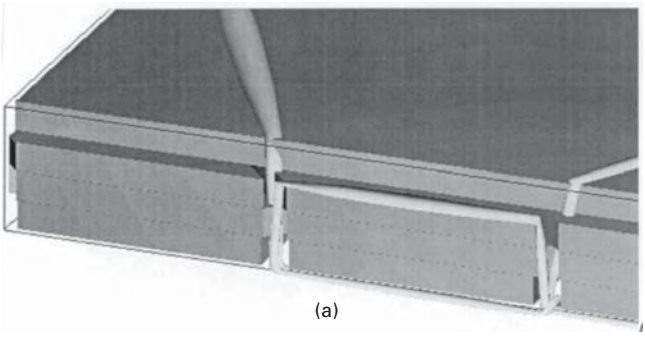

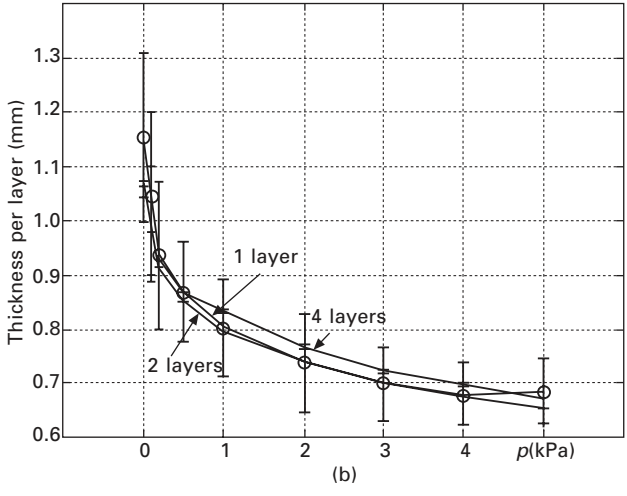

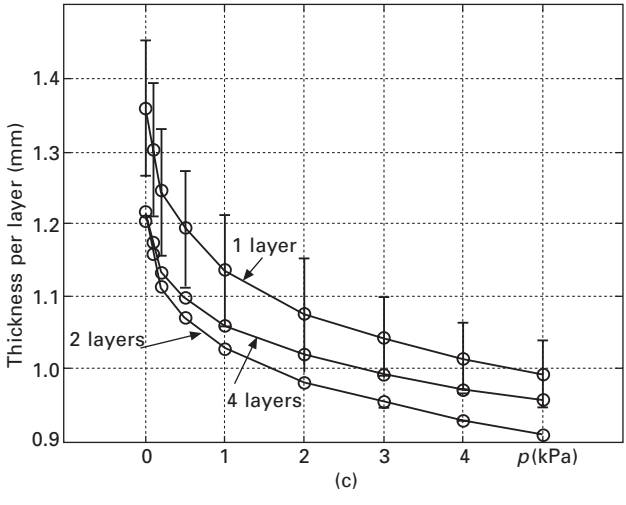

1.30 Sinking of the stitching in channels in the fibrous plies: (a) fabric 'Q' (see text), photo and schematic, and compression curves for (b) biaxial fabric 'B' and (c) quadriaxial fabric 'Q'.

1.6 Modelling of internal geometry of textile preforms

Textiles are hierarchically structured fibrous materials. As discussed in the classic paper by Hearle *et al*.[15] this description of the nature of textiles allows efficient construction of mathematical models for the geometry and the mechanical behaviour of textile structures. In spite of the generally recognised usefulness of this approach, it has not been used to its full strength for the creation of textile structure models. During the 1930s the first serious mechanical treatments of the structure of textile materials were published by Peirce[10], Pozdnyakov[16] and Novikov[17]. Since then, numerous publications have been proposed on the mechanical behaviour of textiles, culminating in a comprehensive treatment on *Mechanics of Flexible Fibre Assemblies* in 1980[18]. In the following years the ideas and approaches outlined in this book were pursued further. Textile mechanics at the outset of the 21st century includes models of the internal geometry of textile structures such as continuous-filament and staple yarns, random fibre mats, woven and knitted fabrics. The hierarchical description of textile structures is implemented using the minimum energy principle as introduced by Hearle and Shanahan[19] and de Jong and Postle[20]. This allows the decomposition of a structure into a set of structural elements, leading to models that are physically sound and computationally feasible. It should be noted that the principle of minimum energy is heuristic when applied to non-conservative mechanical systems such as textiles.

Following the hierarchical approach one can consider a description of the internal geometry of a fabric on two different levels: the y*arn paths mode* describing the spatial configuration of yarns and the *fibre distribution mode* describing spatial distribution properties of the fibrous assembly. In the former case the fabric is regarded as an agglomeration of yarns – slender curved bodies. Their spatial positions are defined by description of yarn midlines and cross-section at each point of the midlines. The internal fibrous structure of the yarns is not considered. In the latter case the fibrous structure of yarns should be defined. The definition of the spatial positions of yarns states whether any point in the unit cell lies inside a yarn or not; if so, parameters of the fibrous assembly at this point are determined. The yarn path mode is sufficient for the calculation of simpler data related to the internal geometry, such as surface density, fabric thickness and local inter-yarn porosity. The fibre distribution mode is needed when detailed information on the fibrous structure is required.

1.6.1 Yarn path mode

Figure 1.31 illustrates the description of yarn spatial configuration. The midline of the yarn shown in Fig. 1.31b is given by the spatial positions of the

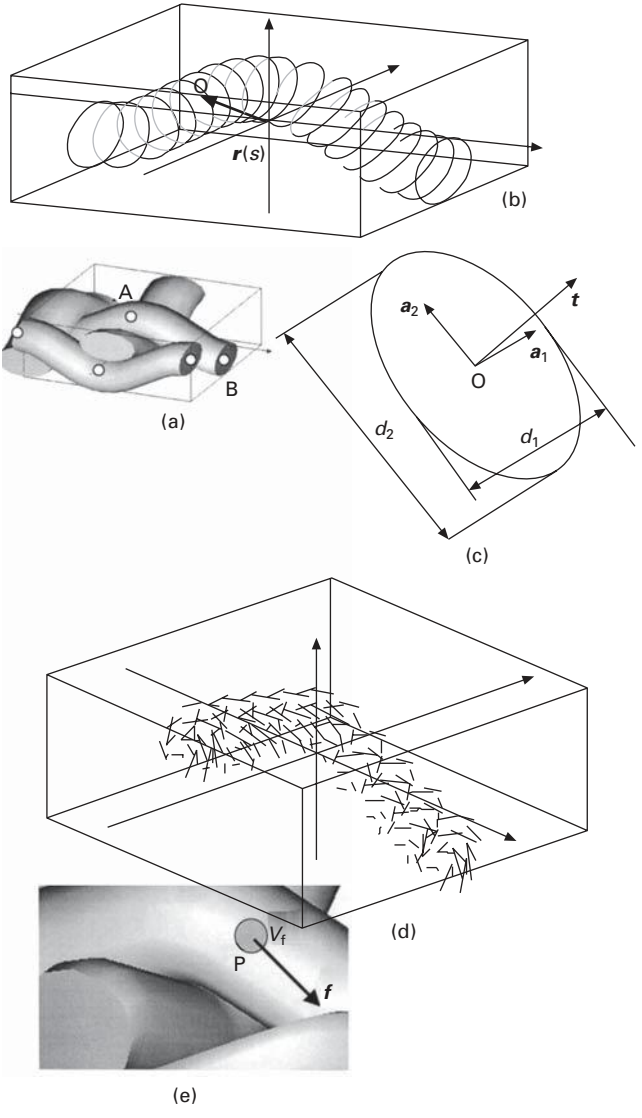

1.31 Models of textile structures: (a) yarn spatial positions; (b) yarn path mode; (c) parameters of a cross-section; (d) fibre distribution mode (fibre directions for a twisted yarn); (e) parameters of a fibrous assembly.

centres of the yarn cross-sections O: $\boldsymbol{r}(s)$ where s and $\boldsymbol{r}$ are coordinates along the midline and the radius-vector of point O. Let $\boldsymbol{t}(s)$ be the tangent to the midline at point O. The yarn cross-section is normal to $\boldsymbol{t}$ and defined by its dimensions $d_1(s)$ and $d_2(s)$ along axes $\boldsymbol{a}_1(s)$ and $\boldsymbol{a}_2(s)$, which are defined in the cross-section and rotate around $\boldsymbol{t}(s)$ if the yarn twists along its path.

Because of this rotation the system $[\boldsymbol{a}_1\boldsymbol{a}_2\boldsymbol{t}]$ may differ from coordinate system along the path.

A definition of the spatial position of a yarn with a given cross-section shape therefore consists of the five functions $\boldsymbol{r}(s)$, $\boldsymbol{a}_1(s)$, $\boldsymbol{a}_2(s)$, $\boldsymbol{d}_1(s)$, $\boldsymbol{d}_2(s)$. Models defining these functions for different textile structures were described in previous sections. Two approaches are possible for definition of the midline path $\boldsymbol{r}(s)$: a simpler geometric and a more complex mechanical one.

Geometric approach

In the geometric approach, midline anchor points are defined from topological information for the textile structure. These points can be located at yarn contacts or crossovers for some textiles, as the distance between contacting yarns is known from cross-section dimensions. For more complex textiles in may be necessary to introduce additional points to represent some curvatures. Yarn midlines are represented by smooth lines going through these points; typically Bézier curves are used[21–23].

The main advantage of the geometric approach is that it can represent any textile structure under one single format while producing simple and portable definitions. As a result, downstream models of the physical properties of textiles and their composites can be used with these geometric definitions, regardless of the textile manufacturing process. Furthermore, the format is equally well suited to simpler closed-form physical property models as it is to more computationally intensive ones. The philosophy behind the geometric approach consists in creating geometric models that are ensured to be appropriate, devoid of interference for example, with the view of refining the assumed initial geometry through mechanical methods, and this for any textile and manufacturing processes. Figure 1.32 shows diverse examples, with anchor points forming 3D linear segments represented as vectors on the left and the resulting geometric models on the right. Any interferences resulting from user input were corrected by a geometric algorithm where sections are modified arbitrarily and yarn V_f remains constant. Another major advantage is that it allows explicit consideration of important practical phenomena such as the statistical variation of dimensions inherent within actual textiles.

Although the geometric approach method offers the advantages of simplicity, speed and certainty over aspects such as interference, the models that it produces clearly depend on user input. The anchor points are predefined and assumptions are made about yarn interaction or crimp height, for example. Symmetry considerations can assist but only to a certain extent, and in its basic form predictive geometry determination is not possible. For an accurate description, dimensions must be measured from real fabrics.

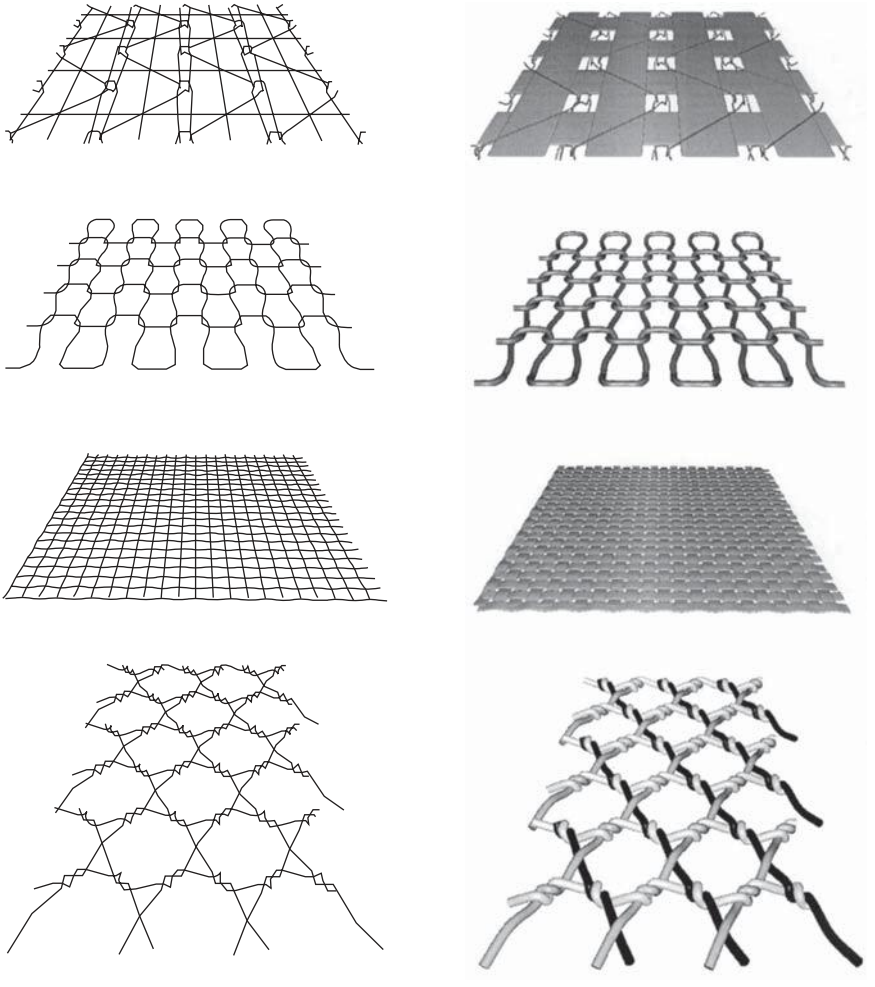

1.32 Geometric approach to textile modelling for a range of textiles, showing vectorial description of yarn paths (left) and resulting textile models (right).

Mechanical approach

A mechanical approach to the modelling of yarn paths requires a mathematical description of the interaction of contacting yarns. In relaxed fabrics this involves bending and compression of yarns; twisting may also be present. Therefore, it also requires appropriate experimental data for the yarns in these deformation modes. If this is available, the model must account for contacts between interacting yarns and describe the equilibrium of the final configuration. The minimum energy principle is normally used for this description. Examples of such models were shown above for weaves and braids.

Computational efficiency is critical in the mechanical approach and therefore the definition of fabric geometry should use the principle of hierarchy and structure decomposition. The repeat is a natural structural unit for fabrics and contains a number of yarns $\{Y\}$ that contact others. The contact regions occupy certain zones on the yarns. Characteristic points provide natural boundaries for *structural elements* of the repeat (Fig. 1.31a). In a woven fabric the structural elements consist of intervals of warp and weft yarns located between subsequent crossovers, where characteristic points are located.

A yarn Y consists of a set of structural elements $\{e\}_Y$, each characterised by the coordinates of its end points A_{Ye} and B_{Ye}, the dimensions of the contact regions near the end-points, and the forces acting on the contact regions. The exact shape and dimensions of the contact regions on a structural element and the forces acting on them are determined by yarn interactions in the structure.

The basic assumption of the decomposition routine is that the spatial positions of the end-points of structural elements play a central role in calculating the geometry of that element. Supposing that the end positions of the structural elements for all yarns in a repeat are known and fixed, contact regions develop near the end-points due to yarn interactions, and internal forces arise in the contact zones. Geometric constraints imposed on the structure by the end-point positions determine the local deformations of yarns at contact regions and the shape and dimensions of these regions, which in turn determine the contact forces.

In general cases a set of parameters q_1, q_2, q_3, … are designated that determine the complex mechanical behaviour of structural elements. Relating to the assumption formulated in previous paragraphs, these parameters consist of the positions of end-points of the structural elements, $\{q_i\} = \{A, B\}$.

Consider now the problem of computing the spatial position of yarns in the fabric repeat space. Let $\boldsymbol{r}_Y(s)$ be the parametric representation of the centreline of yarn Y. According to the minimum energy principle the set of $\boldsymbol{r}_Y(s)$ for all yarns in the fabric repeat should satisfy:

$$\sum_{(Y)} W[\boldsymbol{r}_Y(s)] \rightarrow \min \tag{1.38}$$

If $\boldsymbol{r}_Y(s)$ is split into separate functions for each structural element e on yarn Y this takes the form:

$$\sum_{(Y)} \sum_{(e)} W[\boldsymbol{r}_{Ye}(s)] \rightarrow \min \tag{1.39}$$

which can be recast as:

$$\sum_{(Y)} \sum_{(e)} W[\boldsymbol{r}_{Ye}(s; q_1, q_2, q_3 \ldots)] \rightarrow \min \tag{1.40}$$

This global minimisation problem can be reformulated as a series of minimisation problems for structural elements:

$$\min_{\boldsymbol{r}(s)} \sum_{(Y)} \sum_{(e)} W[\boldsymbol{r}_{Ye}(s; q_1, q_2, q_3 \ldots)]$$

$$= \min_{q_1, q_2, q_3 \ldots} \sum_{(Y)} \sum_{(e)} \min_{\boldsymbol{r}(s)} \{W[\boldsymbol{r}_{Ye}(s \mid q_1, q_2, q_3 \ldots)]\} \quad 1.41$$

Each minimisation problem should be solved with parameters $\{q_i\}$ fixed, yielding the solution:

$$\min_{\boldsymbol{r}(s)} \{W[\boldsymbol{r}(s \mid q_1, q_2, q_3 \ldots)]\} \Rightarrow \boldsymbol{r}(s \mid q_1, q_2, q_3 \ldots) \quad 1.42$$

which is used to calculate the energy of the structural element:

$$\boldsymbol{r}(s \mid q_1, q_2, q_3 \ldots) \Rightarrow W(q_1, q_2, q_3 \ldots) \quad 1.43$$

The function W, which depends only on parameters of the structural element, is termed the *characteristic function* of the structural element. The minimisation problem (1.40), which has the *functions* $\boldsymbol{r}_Y(s)$ as arguments, is reduced to the following minimisation problem:

$$\sum_{Y} \sum_{e} W_{Ye}(q_1, q_2, q_3 \ldots) \rightarrow \min \quad 1.44$$

where the arguments are a set of *scalar parameters* $\{q_i\}$. This leads to a system of non-linear algebraic equations instead of differential or integral equations, which would result from eqn 1.38. A practical application of this appears in section 1.3.3 for a simple weave. Note that the energy functions involved in eqn 1.44 may represent bending, compression and torsion and accounting for non-linearity.

Mechanical models aim to be predictive and to determine the structure of fabrics from independent measurements of yarn properties. In some cases this cannot be achieved as yarns undergo mechanical loading during fabric manufacture and the resulting deformations are not relaxed, leading to deviations between reality and analysis based on equilibrium in the relaxed state. This is especially true for cases when manufacturing tensions are extreme, say for example in 3D weaving. For such cases one must rely on a geometric model coupled with physical measurements taken from the fabric.

Using yarn path mode

The yarn path mode (mesoscopic geometric model) is a necessary step in building models at the microscopic scale (fibre distribution mode). Mesoscopic models also have inherent value: they define yarn volumes and therefore inter-yarn porosity, as well as local fibre directions of yarns. Information on

the *local direction of the yarns* is essential for most predictive models of the physical properties of textiles, say for example in micro-mechanical models of composites to calculate the homogenised stiffness matrix of the unit cell, or in permeability models for composites processing. One approach to the former consists in defining ellipsoidal inclusions with stiffness properties equivalent to those of elements of the impregnated yarn, and then using the solution of Eshelby for homogenising the stiffness of agglomerated inclusions[24]. Both approaches rely on a representation of the local, microscopic fibrous structure as a unidirectional array of fibres, the equivalent stiffness of which is obtained from empirical formulae[25] or finite element analysis results[26]. These issues are discussed further in Chapter 8.

The second use of the yarn path mode is related to numerical modelling. The geometry of *yarn volumes* can be easily transferred to mesh generators; (Fig. 1.33). Yarn segments can be assembled into solid models of fabrics and meshed. The geometry of the empty volumes extending between the yarns is far more intricate; this must also be meshed for problems of flow and heat transfer through textiles and for all problems related to textile composites. Although commercial solid modellers can sometimes process this, good results often require very high mesh densities. Other solution techniques that do not use conformal meshing, or that simplify the problem, constitute important topics towards the routine use of such tools as a support to industrial design of textile applications. Figure 1.34 shows a 2.5D mesh used for calculating in-plane permeability tensors of textile reinforcements based on a simplified, efficient technique[27].

1.6.2 Fibre distribution mode

Yarn path mode geometric modelling describes yarn volumes but says nothing about the fibrous structure of yarns, unit cells or fabrics. The fibre distribution mode provides such information. Consider a point P (Fig. 1.31e) and a fibrous assembly in the vicinity of this point. The assembly can be characterised by different parameters including physical and mechanical properties of the fibres near point P (which may vary throughout the fabric), fibre volume fraction V_f and direction $\boldsymbol{f}$. Length distribution of fibres near the point, average curvature and other parameters can be specified if the point is in a yarn. A fibre distribution mode model should provide such information for any point P.

Using fibre distribution mode

The ability to query the fibrous structure near arbitrary points can be used in many applications dealing with mesh representations of heterogeneous media. In *finite element* representations of fabrics the fibre distribution mode is used to determine mechanical properties for each element. Figure 1.33(c) illustrates

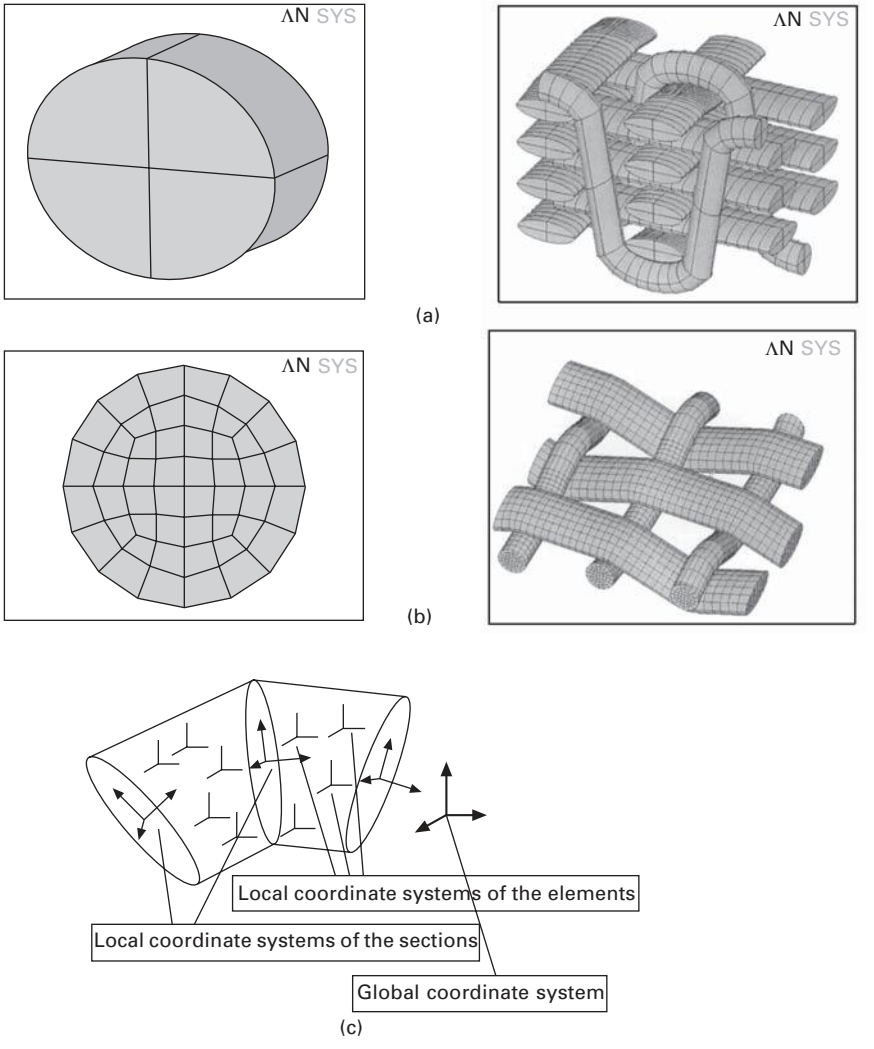

1.33 Transformation of yarn path mode model into finite element description: (a) yarn volumes; (b) mesh on the yarns; (c) local coordinate systems, representing fibre directions.

local coordinate systems for each element, aligned with the average fibre direction; this allows correct representation of anisotropy. Mechanical properties of a dry fabric include the tensile stiffness along the fibres and the compression stiffness through thickness (see Chapter 2). For composite materials, the homogenised stiffness of unidirectional fibre reinforced composite and local fibre volume fraction are required. The same is done in *cell models* of composite materials[28]. In such models a unit cell is subdivided into sub-cells (quasi-

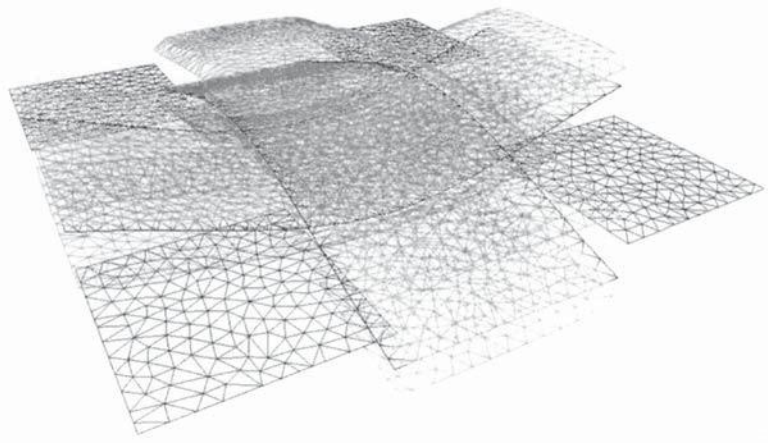

1.34 Mesh representing local yarn and resin/free volume mid-planes for a single crossover of a plain weave. Each element has an associated thickness (free volumes) or permeability (yarn). This model is used for the 'streamsurface' permeability prediction method[27].

finite elements), the effective stiffness of which is calculated from average properties of the local fibrous assembly or matrix.

In *models of flow* through the reinforcement, a regular mesh or lattice is defined in the unit cell. Nodes of the lattice can lie outside or inside the yarns. In the former case the Navier–Stokes equation governs the fluid flow near the node. In the latter case the flow is described by the Brinkmann equation. The local permeability of the media is calculated using a unidirectional description of the fibrous assembly near the node. These equations are solved simultaneously for all the nodes in the unit cell, using, for example, the lattice Boltzmann method[29] or commercial software[30].

1.6.3 Implementation of textile hierarchical model

Table 1.3 shows the hierarchy of structural elements in textile composites, and the modelling problems associated with each scale. Unnecessary mixture of hierarchical levels should be avoided: yarn data should be used to predict behaviour of fabrics as opposed to fibre data, and so forth. Each hierarchy level is occupied by models which use data from that level and the next lower to predict properties of the defined structure at the next upper level.

Object oriented programming provides a powerful tool for the construction virtual textiles. Associated data fields and methods are outlined in Table 1.4. The results of geometric modelling serve as crucial input to models of composites processing and mechanical behaviour. The main advantage is that local variations in textile geometry, and hence in physical properties,

Table 1.3 Hierarchy of structure and models of a textile composite

Structure	Elements	Models
Yarn (tow)	Fibres	Fibre distribution in the yarn and its change under load/strain Mechanical properties of the yarn
Fabric (woven, knitted…)	Yarns	Geometry of yarns in the fabric and its change under load/strain Mechanical behaviour of the fabric repeat under complex loading
Composite unit cell	Fabric	Mechanical properties (stiffness matrix/non-linear law; strength)
	Matrix	Permeability tensor
Composite part	(Deformed/ draped) unit cells	Behaviour under loading Flow of the resin Behaviour in the forming process

can be accounted for explicitly. A composite material, as the final product in the sequence 'fibre to yarn to textile to preform to composite', is included in the hierarchical description of the textile, taking full advantage of the versatility of the approach.

Fabrics are usually assembled into laminates to form reinforcements with appropriate thickness. The layers of the laminate are not precisely positioned one against another, causing a geometric and mechanical phenomenon of nesting. Nesting plays an important role in determining the physical properties of dry laminated reinforcements and composite parts. It causes statistical distribution of the laminate properties, both within one part and between different parts. A study of the nesting effect is therefore important for the correct representation of the internal geometry in predictive models of processing and performance and for the assessment of the statistical characteristics of properties, determining processing parameter windows and confidence intervals for the performance indicators. Such an approach is possible using a hierarchical model of the type described here[31].

Table 1.4 Implementation of virtual textile model via OOP approach

Object	Data		Methods
	Group	Fields	
Fibre	General	Linear density (tex) Diameter (mm) Density (g/cm^3)	
	Mechanics	Elastic constants Tenacity (MPa) Ultimate elongation	
Yarn	General	Yarn type: monofilament, continuous filament or spun Linear density (tex)	Compute mass for a given length
	Geometry of the cross-section	Assumed shape: elliptical/ lenticular/rectangular Dimensions of cross-section in free state d_{01}, d_{02} (mm)	Compute volume of the given yarn length Determine, whether the given point (x, y) lies inside the yarn
	Compression	Type of compression behaviour: no compression, specified compression law Compression coefficient $\eta_1 = d_1/d_{10}$/ function of compressive force Q per unit length Flattening coefficient $\eta_2 = d_2/d_{20}$/ function of compressive force Q per unit length	Compute compressed yarn dimensions under a given force per unit length Compute compression of two intersecting yarns for given normal force and intersection angle
	Bending	Bending curve 'torque–curvature' (linear for constant bending rigidity) $M(\kappa)$	Compute bending rigidity value B for a given curvature

(Contd)

Table 1.4 (Continued)

Object	Data		Methods
	Group	Fields	
	Friction	Friction law yarn-yarn in the form $F = fN^n$, where N is a normal force	Compute friction force for a given normal force
Yarn with fibre data	Inherits data and methods of yarn. Adds the following and replaces (**bold**) some of yarn methods		
	General	Twist (1/m)	Compute the twist angle
		Twist direction (*S* or *Z*)	Compute linear density from fibre data
	Fibre	Fibre data (*fibre* object)	Compute fibrous content and fibre direction in the vicinity of the given point (*x*, *y*).
		Number of fibres in cross-section	
		Fibre distribution in the yarn	
	Compression		Compute compressed yarn dimensions **and fibre distribution in it**
	Bending		Compute bending resistance from fibre data
Yarn path		Implements yarn path mode	
	Fibrous assembly	Holds a reference to yarn with fibre data object	
	Yarn path	Array of descriptions of dimensions and orientation of yarn cross-sections	Compute yarn volume, length and mass
			Compute average fibre volume fraction
Fabric		Generic description of a fabric	
	Fibrous assembly	Array of *yarn path* objects	Build the yarn descriptions (abstract).
			Compute overall fabric parameters: dimensions of unit cell, areal density, fibre volume fraction
			Compute local fibre data at given point

Table 1.4 (Continued)

Object	Data		Methods
	Group	Fields	
			Visualise the fabric Export data for micro-mechanical and permeability analysis
Woven fabric	Inherits from *fabric* object. Adds and replaces (**bold**) the following		
	Topology	Weave coding	
	Yarns	References to *yarn with fibre data* objects for all yarns in fabric repeat	
	Spacing	Ends/picks count	
	Fibrous assembly		Build the yarn descriptions

References

1. Kurashiki T., Zako M. and Verpoest I., 'Damage development of woven fabric composites considering an effect of mismatch of lay-up', *Proc. 10th European Conf. on Composite Materials*, Brugge, June 2002 (CD edition).
2. Kawabata, S., *The Standardisation and Analysis of Hand Evaluation*, Osaka, Textile Machinery Society of Japan, 1975.
3. Hearle J.W.S., Grosberg P. and Baker S., *Structural Mechanics of Fibres, Yarns and Fabrics*, New York, Wiley Interscience, 1969.
4. Abbot G.M., 'Yarn-bending and the weighted-ring stiffness test', *J. Textile Institute*, 1983 **74**(5) 281–286.
5. Lomov S.V., Truevtzev A.V. and Cassidy C., 'A predictive model for the fabric-to-yarn bending stiffness ratio of a plain-woven set fabric', *Textile Research J.*, 2000 **70**(12) 1088–1096.
6. Grishanov S.A., Lomov S.V., Harwood R.J., Cassidy T. and Farrer C., 'The simulation of the geometry of two-component yarns. Part I. The mechanics of strand compression: simulating yarn cross-section shape', *J. Textile Institute*, 1997 **88 part 1**(2) 118–131.
7. Harwood R.H., Grishanov S.A., Lomov S.V. and Cassidy T., 'Modelling of two-component yarns. Part I: The compressibility of yarns', *J. Textile Institute*, 1997 **88 Part 1** 373–384.
8. Potluri P., Wilding M.A. and Memon A., 'A novel stress-freezing technique for studying the compressional behaviour of woven fabrics', *Textile Research J.*, 2002 **72**(12) 1073–1078.
9. Love A.E.H., *A Treatise on the Mathematical Theory of Elasticity*, New York, Dover Publications, 1944.
10. Peirce F.T., 'The geometry of cloth structure', *J. Textile Institute*, 1937 **28**(3) T45–T96.
11. Long A.C., 'Process modelling for liquid moulding of braided preforms', *Composites Part A*, 2001 **32**(7) 941–953.
12. Kessels J.F.A. and Akkerman R., 'Prediction of the yarn trajectories on complex braided preforms', *Composites Part A*, 2002 **33**(8) 1073–1081.
13. Byun J.H. and Chou T.W., 'Process–microstructure relationships of 2-step and 4-step braided composites', *Composites Sci. Technol.*, 1996 **56** 235–251.
14. Lomov S.V., Belov E.B., Bischoff T., Ghosh S.B., Truong Chi T. and Verpoest I, 'Carbon composites based on multiaxial multiply stitched preforms. Part 1. Geometry of the preform', *Composites Part A*, 2002 **33**(9) 1171–1183.
15. Hearle J.W.S., Konopasek M. and Newton A., 'On some general features of a computer-based system for calculation of the mechanics of textile structure', *Textile Research J*, 1972 **42**(10) 613–626.
16. Pozdnyakov B.P., *Fabric Resistance to Tension in Different Directions*, Moscow-Leningrad, GIZLegProm., 1932, 70 (in Russian).
17. Novikov N.G., 'A fabric structure and its design with the geometrical technique', *Textilnaya Promishlennost*, 1946 **6**(2) 9–17 (in Russian).
18. Hearle J.W.S., Amirbayat J. and Twaites J.J. (editors), *Mechanics of Flexible Fibre Assemblies*, Alphen aan den Rijn, Sijthoff and Nordhof, 1980.
19. Hearle J.W.S. and Shanahan W.J., 'An energy method for calculations in fabric mechanics', *J Textile Institute*, 1978 **69**(4) 81–110.
20. de Jong S. and Postle R., 'A general energy analysis in fabric mechanics using optimal control theory', *Textile Research J.*, 1978 **48**(3) 127–135.

21. Robitaille F., Clayton B.R., Long A.C., Souter B.J. and Rudd C.D., 'Geometric modelling of industrial preforms: woven and braided textiles', *Proc. Institution of Mechanical Engineers Part L*, 1999 **213** 69–84.
22. Robitaille F., Clayton B.R., Long A.C., Souter B.J. and Rudd C.D., 'Geometric modelling of industrial preforms: warp-knitted textiles', *Proc. Institution of Mechanical Engineers Part L*, 2000 **214** 71–90.
23. Goktepe O. and Harlock S.C., 'Three-dimensional computer modelling of warp knitted structures', *Textile Research J*, 2002 **72**(3) 266–272.
24. Huysmans G., Verpoest I. and Van Houtte P., 'A poly-inclusion approach for the elastic modelling of knitted fabric composites', *Acta Materials*, 1998 **46**(9) 3003–3013.
25. Chamis C.C., 'Mechanics of composite materials: past, present and future', *J. Composites Technol. Res.*, 1989 **11**(1) 3–14.
26. Carvelli V. and Poggi C., 'A homogenization procedure for the numerical analysis of woven fabric composites', *Composites Part A*, 2001 **32**(10) 1425–1432.
27. Robitaille F., Long A.C. and Rudd C.D., 'Geometric modelling of textiles for prediction of composite processing and performance characteristics', *Plastics Rubber and Composites*, 2002 **31**(2) 66–75.
28. Vandeurzen P., Ivens J. and Verpoest I., 'Micro-stress analysis of woven fabric composites by multilevel decomposition', *J. Composite Materials*, 1998 **32**(7) 623–651.
29. Belov E.B., Lomov S.V., Verpoest I., Peters T., Roose D., Parnas R.S., Hoes K. and Sol V., 'Modelling of permeability of textile reinforcements: lattice Boltzmann method', *Composites Sci. Technol.*, 2004 **64**(7–8) 1069–1080.
30. Long A.C., Wong C.C., Sherburn M. and Robitaille F., 'Modelling the effect of fibre architecture on permeability for multi-layer preforms', *Proc 25th SAMPE Europe Int. Conf., Paris*, March/April 2004, pp. 325–330.
31. Lomov S.V., Verpoest I., Peeters T., Roose D. and Zako M., 'Nesting in textile laminates: geometrical modelling of the laminate', *Composites Sci. Technol.*, 2003 **63**(7) 993–1007.

2

Mechanical analysis of textiles

A C LONG, University of Nottingham, UK,
P BOISSE, INSA Lyon, France and
F ROBITAILLE, University of Ottawa, Canada

2.1 Introduction

This chapter describes the mechanical behaviour of textile reinforcements, with the primary aim of understanding their behaviour during forming and consolidation processes. A number of deformation mechanisms are available. However, during typical composites manufacturing processes, it is generally agreed that the most important of these are in-plane shear and tensile behaviour and through-thickness compaction. Of these mechanisms, the ability of fabrics to shear in-plane is their most important feature during forming, although given their low shear stiffness, in-plane tensile behaviour represents the largest source of energy dissipation. Compaction behaviour defines the fibre volume fraction that can be obtained after manufacturing. Other properties such as fabric bending and ply/tool friction are not considered here, primarily because these have received relatively little attention elsewhere and little data are available.

This chapter introduces a number of experimental methods for characterising the deformation of textiles. These methods have been developed within research studies, usually to obtain material data for manufacturing simulation (see Chapter 4). One important consideration here is that none of these tests is standardised – and in fact nearly all published studies use slightly different test methods and specimen dimensions. This issue is being addressed at present as part of a round-robin exercise[1]. Several standard tests are used in the wider textiles community (e.g. BS ISO 4606:1995, BS 3356:1990, BS 3524-10:1987). Of particular relevance here is the 'Kawabata Evaluation System for Fabrics (KES-F)', a series of test methods and associated testing equipment for textile mechanical behaviour including tensile, shear, bending, compression and friction[2]. However, while this system has been used widely for clothing textiles, its application to reinforcement fabrics has been limited[3]. This is probably because KES-F provides single point data at relatively low levels of deformation, coupled with the limited availability of the (expensive) testing equipment.

As discussed in Chapter 1, the geometry of textile reinforcements can be described at a number of length scales. Individual fibres represent the microscopic scale, with large numbers of fibres (typically several thousand) making up the tow or yarn. The scale of the yarns and of the fabric repeating unit cell is the mesoscopic scale. Finally, the fabric structure constitutes the macroscopic scale. The macroscopic mechanical behaviour of fabrics depends on phenomena at smaller scales, and in particular it is dependent on geometric and contact non-linearities. Such considerations will be used throughout this chapter to develop predictive models for textile mechanical behaviour.

2.2 In-plane shear

2.2.1 Characterisation techniques

As mentioned above, in-plane (or intra-ply) shear is generally considered to be the primary deformation mechanism during forming of textile reinforcements to three-dimensional geometries. Characterisation of this mechanism has therefore received a great deal of attention. The objectives are usually twofold: to measure the non-linear mechanical response of the material during shear, and to characterise the limit of deformation. At the simplest level, mechanical behaviour is of interest for ranking of materials in terms of ease of forming. More recently such data have been required for mechanical forming simulation software based on finite element analysis (see Chapter 4). Here shear force should be normalised by a representative length to eliminate sample size effects. The limit of forming is often characterised by measurement of the 'locking angle', which represents the maximum level of shear deformation that can be achieved before fabric wrinkling occurs. In practice this limit varies widely and is highly dependent on the test method employed. The primary use of locking angle data is to identify areas of wrinkling within kinematic draping codes for fabric forming.

The majority of published studies have characterised resistance to intra-ply shear using two approaches (Fig. 2.1). Bias extension tests, involving uniaxial extension of relatively wide samples in the bias direction, are favoured by a number of researchers[4–6], as the testing procedure is relatively simple. However the deformation field within the sample is non-uniform, with maximum shear observed in the central region and a combination of shear and inter-yarn slip observed adjacent to the clamped edges. In addition the shear angle cannot be obtained directly from the crosshead displacement, so that the test must be monitored visually to measure deformation. Nevertheless this test can provide a useful measure of the locking angle, which in this case represents the maximum shear angle achieved during the test. Above this angle deformation occurs entirely by inter-yarn slip, indicating that the energy required to achieve shear deformation has reached a practical limit. Although

this may not indicate the exact angle at which wrinkling would occur, its measurement is repeatable as the bias extension test is not affected significantly by variability in boundary conditions. Bias extension testing is discussed in more detail in Chapter 3, in the context of forming of pre-impregnated composites.

The other popular test method for shear resistance of textile reinforcements is the picture frame test[7–10]. Here the fabric is clamped within a frame hinged at each corner, with the two diagonally opposite corners displaced using a mechanical testing machine. Cruciform specimens are used typically, with the corners of specimens removed adjacent to the bearings in the corners. Samples must be mounted such that the fibres are parallel to the sides of the picture frame prior to testing. Any small misalignment will lead to tensile or compressive forces in the fibre directions, resulting in large scatter in measured force readings. Nevertheless the picture frame test has proved popular as it produces uniform shear deformation (if performed with care).

A number of picture frame test results obtained at Nottingham are reported here as examples of typical behaviour. The picture frame shearing equipment used is illustrated in Fig. 2.1, where the distance between the clamps (l) is 145 mm. Crimped clamps are used typically to ensure that the fabric does not slip from the grips during testing. The apparatus is operated using a Hounsfield mechanical testing machine, which monitors axial load versus crosshead displacement. Here the results are converted into shear force versus shear angle using the following relationships. The shear force (F_s) can be obtained from the measured force in the direction of extension (F_x) using:

$$F_s = \frac{F_x}{2 \cos \Phi} \qquad 2.1$$

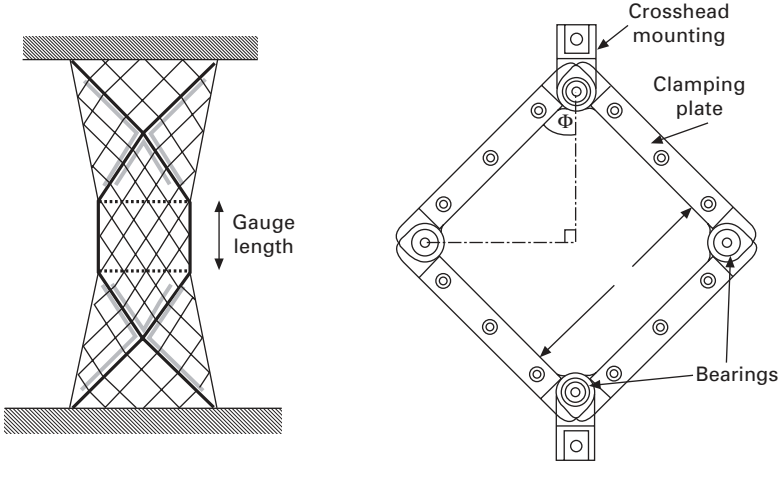

2.1 Characterisation tests for in-plane shear of biaxial fabrics – bias extension (left) and picture frame shear (right).

where the frame angle Φ is determined from the crosshead displacement D_x and the side length of the shear frame (l) using:

$$\Phi = \cos^{-1}\left[\frac{1}{\sqrt{2}} + \frac{D_x}{2l}\right] \quad 2.2$$

The shear angle (reduction in inter-yarn angle) is given by:

$$\theta = \frac{\pi}{2} - 2\Phi \quad 2.3$$

For tests reported here, a pre-tensioning rig was used to position dry fabrics within the picture frame. This consists of a frame within which fabric samples are clamped prior to mounting in the picture frame. Two adjacent sides of the pre-tensioning frame are hinged, to which a measured force is applied to impart tension to the fabric. This device serves two purposes, to align the material within the rig and to enhance repeatability. For the results reported here, a tension of 200 N was applied to fibres in each direction. All tests were conducted at a crosshead displacement rate of 100 mm/min, although experiments at other rates for dry fabric have produced almost identical results[11]. A minimum of six tests were conducted for each fabric, with error bars produced using the t-distribution at 90% confidence limit.

Initial yarn width and pitch (centreline spacing) values were measured using image analysis from digital images oriented normal to the fabric. Video images were also used to estimate the locking angle, although here the procedure was more effective with the camera placed at an oblique angle to the plane of the fabric. Samples were marked with horizontal lines, which buckled when wrinkling occurred. A range of glass fibre reinforcements were tested, including woven fabrics and non-crimp fabrics (NCFs). Descriptions of the fabrics tested are given in Table 2.1, which also includes locking angles averaged for at least four samples.

As shown in the table, for woven fabrics shear angles of at least 55° were achieved before wrinkling was observed. Skelton[5] proposed a lower limit when adjacent yarns come into contact (i.e. yarn width is equal to yarn pitch). Application of this model to the fabrics described in Table 2.1 is of limited use, as the predicted locking angles are typically 20° lower than those measured. Here, fabric locking occurred some time after adjacent yarns came into contact. For the light plain weave (P150), the relatively large spacing between the yarns permitted large shear angles, and in fact only three of the six samples wrinkled before the end of the shear test. The locking angle was lower for the heavier plain weave (P800). Woven fabrics can be ranked for locking angle using the ratio between initial yarn (tow) pitch and width, which is sometimes referred to as the *fabric tightness*. For woven fabrics a high ratio appears to indicate a high locking angle. The same procedure appears to apply to non-crimp fabrics, although ratios here are

Table 2.1 Fibre architecture descriptions and measured locking angles for woven and non-crimp glass fabrics characterised in shear. In each case, tow properties and spacings were identical in warp and weft

Fabric ID	Style	Fibre angles (°)	Surface density (g/m^2)	Tow linear density (tex)	Tow pitch (mm)	Tow width (mm)	Tow pitch/ width	Locking angle (standard deviation)
P150	Plain weave	0/90	147	150	2.04	1.22	1.67	≈68° (–)
P800	Plain weave	0/90	800	1600	4.01	3.09	1.30	60° (1.4)
S800-01	4-Harness satin	0/90	800	270	0.68	0.62	1.10	55° (1.7)
S800-02	4-Harness satin	0/90	788	1450	3.70	2.80	1.32	61° (1.6)
T800	2:2 Twill weave	0/90	790	2500	6.30	4.40	1.43	62° (1.7)
Ebx936	Tricot 1&1 NCF	±45	936	388	0.82	0.70	1.17	62° (–)
Ebx318*	Pillar NCF	±45	318	99	0.62	0.47	1.32	37°/64° (–)

*Locking angle for this material depends on direction of testing. Value for fabric sheared parallel to stitching is significantly lower than value when sheared perpendicular to stitch.

generally lower than those for woven fabrics with similar locking angles. In addition, for these materials the locking angle can depend on the direction of testing, with different behaviour observed when the fabric is sheared parallel or perpendicular to the stitching thread (as discussed below).

Typical shear compliance curves for woven fabrics are shown in Fig. 2.2. Figure 2.2(a) compares the behaviour of fabrics with similar surface densities

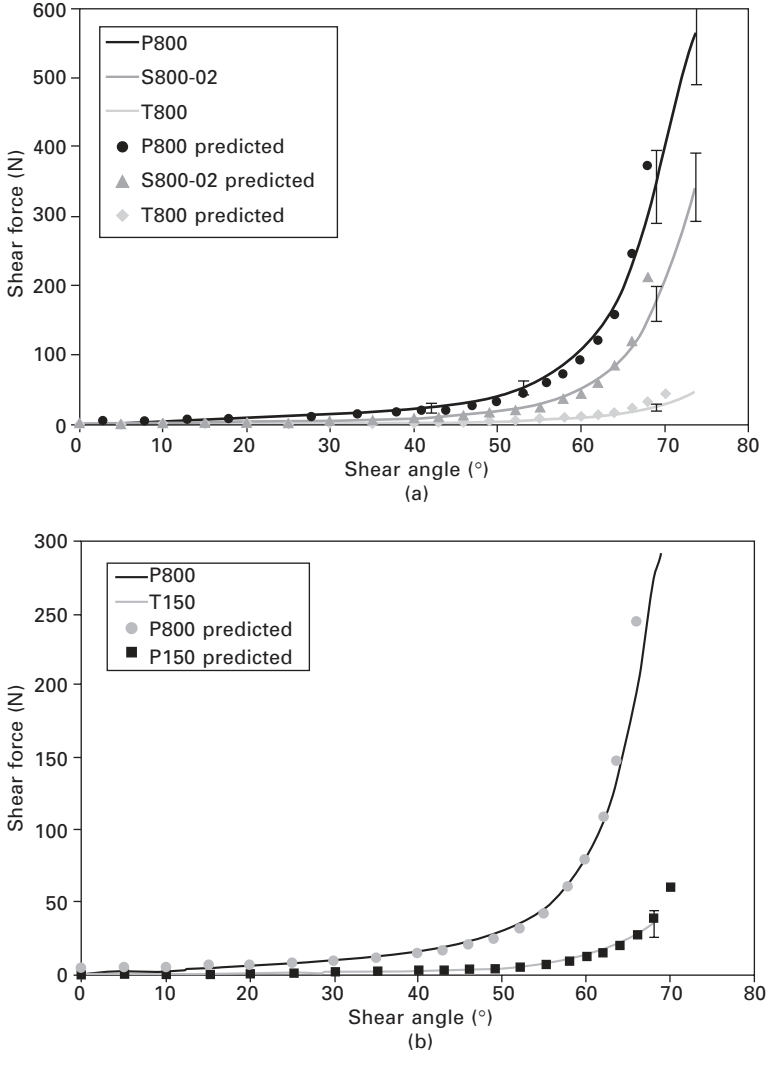

2.2 Experimental and predicted shear compliance curves for woven fabrics. (a) Effect of weave pattern: plain weave (P800), 4-harness satin weave (S800-02) and 2:2 twill weave (T800). (b) Effect of surface density for plain weave: P150 (150 g/m^2) and P800 (800 g/m^2).

but different fibre architectures. The plain weave (P800) requires the highest force to achieve a particular shear angle, while the twill weave (T800) is the most compliant. Clearly this is related to the ratio between yarn width and pitch as described above, although difference in weave style is also significant (as discussed in the next section). Similar observations can be made from Fig. 2.2(b), which compares the behaviour of a two plain weaves with different surface densities. For all fabrics tested, two distinct regions may be identified within the shear compliance curve. The initial resistance to shear is relatively low, and is likely to be caused by friction at the yarn crossovers as suggested by Skelton[5]. Once adjacent yarns come into contact, the resistance increases significantly as the yarns are compressed together. This is the region where wrinkling is usually observed. If the test were continued, the curve would tend towards an asymptote corresponding to maximum yarn compaction (i.e. close packing of the filaments within each yarn).

Figure 2.3 shows typical shear compliance curves obtained for NCFs with both tricot and pillar warp-knit stitching threads. The tricot warp-knit resembles a 'zigzag' pattern, whereas the pillar warp-knit is similar to a chain stitch. In both cases it is apparent that the compliance is lower when the fabric is sheared parallel to the stitching direction. Testing in this direction results in a tensile strain within the stitch, which causes an increase in shear force. The effect is more pronounced for the pillar warp-knit, as the majority of the stitching thread is aligned with the applied force. Here testing parallel to the stitch results in a linear increase in force until the stitching thread snaps. After this point the force is reduced until inter-yarn compaction occurs. The directionality exhibited by NCFs during shear can result in non-symmetric fibre patterns during forming, as described in Chapter 4.

2.2.2 In-plane shear modelling

Given the large number of reinforcements available, it is desirable to develop a model for fabric shear behaviour, both to predict resistance to shear and the change in fabric geometry. Broadly, this must capture the evolution of the fabric geometry during shear, and include contributions from each deformation mechanism to the overall shear behaviour. From the experimental analyses above, it may be concluded that the primary mechanisms are shear at yarn crossovers and friction between yarns, both at crossovers and between parallel yarns. NCFs also dissipate energy via relative displacement and stretching of the stitching threads. The geometry of the fabric can be relatively complex, so that precise determination of forces or energy dissipated via any individual mechanism may be difficult to determine. For example in woven fabrics parallel yarns are only in contact with each other over a fraction of their lengths, and crossover contact may act over relatively complex curved surfaces. Hence to produce an analytical model, a number of simplifications are required.

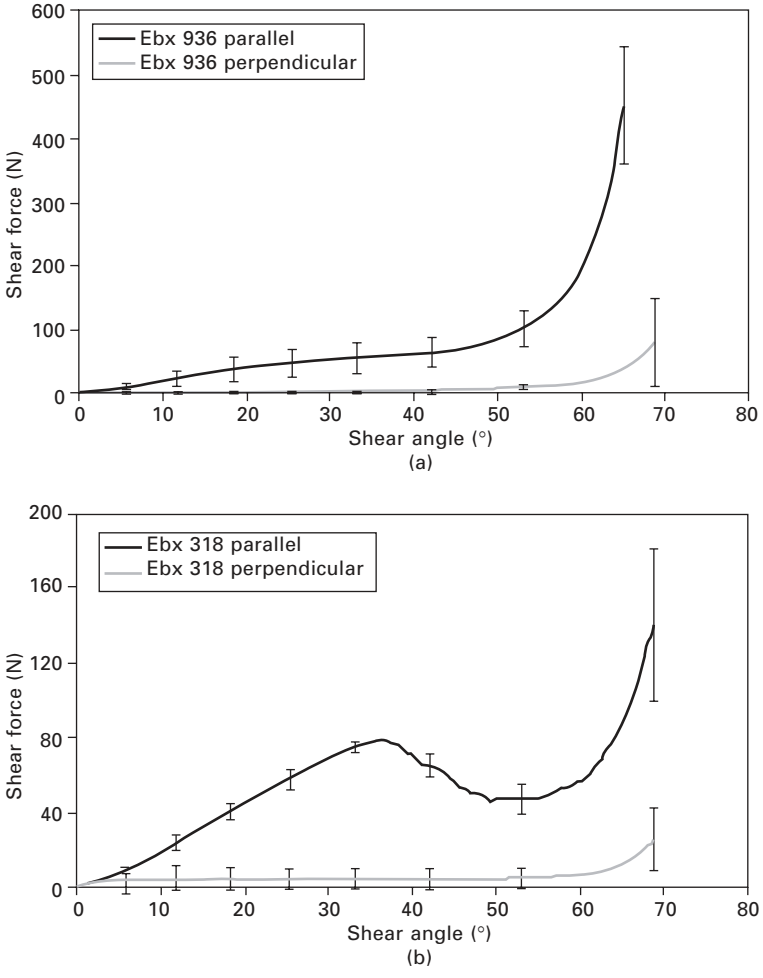

2.3 Shear compliance curves for ±45° NCFs tested parallel and perpendicular to the stitch. (a) tricot 1&1 warp-knit (Ebx936); (b) pillar warp-knit (Ebx318).

Skelton[5] suggested that resistance to in-plane shear for woven fabrics was a result of friction at yarn crossovers, and developed an expression for shear stiffness as a function of the number of crossovers. However, this implied a linear relationship between shear force and shear angle, which is not the case for large deformations (as illustrated above). Kawabata *et al.*[12] performed a more detailed study for a plain woven fabric. In this work the torque required to rotate a single yarn crossover was expressed as an empirical function of contact force and shear angle. Yarn paths were modelled using a saw tooth pattern (straight lines between crossovers), which allowed the contact force

to be derived from the tensile forces in the yarns. This model is described in detail in section 2.3.4 in the context of in-plane tensile behaviour. However, it is of limited use for modelling of fabric shear, as it relies on specialised equipment to determine the parameters for the yarn interaction model.

McBride and Chen[13] modelled the yarn paths using sinusoidal curves, which were allowed to evolve during shear deformation. Bias extension tests were performed for a number of plain weave reinforcements, with image analysis used to study the evolution in yarn spacing and yarn width during shearing. Yarn width was found to remain constant until adjacent yarns came into contact, after which the yarns were compacted. For all materials, fabric thickness (measured using a fabric micrometer) remained constant prior to wrinkling. These results may be explained by the fact that an increase in thickness would require elongation of the yarns, resulting in forces significantly higher than those measured above.

Souter[11] developed a general model for shear resistance of woven fabrics. A combination of inter-yarn friction at rotating crossovers and compaction between adjacent yarns was used to predict shear resistance. Yarn cross-sections were assumed to be lenticular based on microscopy, with yarns in intimate contact at crossovers and following straight paths between crossovers. The distance between yarn crossovers along each yarn remained constant (i.e. inter-yarn slip was neglected), whereas the yarn width reduced once yarns came into contact. Fabric thickness was assumed constant during shearing, based on experimental observations by the authors and supported by those from McBride and Chen[13].

The resistance to shearing at each yarn crossover was modelled by considering the torque (T_c) required to rotate a yarn crossover, defined by Kawabata *et al.*[12] as:

$$T_c = \mu_c \times F_c \times R_{eff} \qquad 2.4$$

where μ_c is the coefficient of friction (taken as 0.3), F_c is the contact force between the yarns and R_{eff} is the effective radius of rotation of the contact area (i.e. the radius of a circle with the same area as the yarn crossover). Yarn width was assumed to remain constant until adjacent yarns came into contact (i.e. the yarn width is equal to the yarn pitch). After this point the yarn width was reduced to prevent adjacent yarns passing through each other.

Inter-yarn contact force was calculated by resolving the contributions from yarn tension and compaction into the direction normal to the crossover. The resulting contact force depends on the weave style, as woven fabrics can consist of a number of contact geometries as illustrated in Fig. 2.4. Compaction was modelled here using the model from Cai and Gutowski[14], who developed the following equation for the fibre bundle pressure:

$$\sigma_b = \frac{e_b F_{11}}{(F_{bb} F_{11} - F_{b1}^2)} \qquad 2.5$$

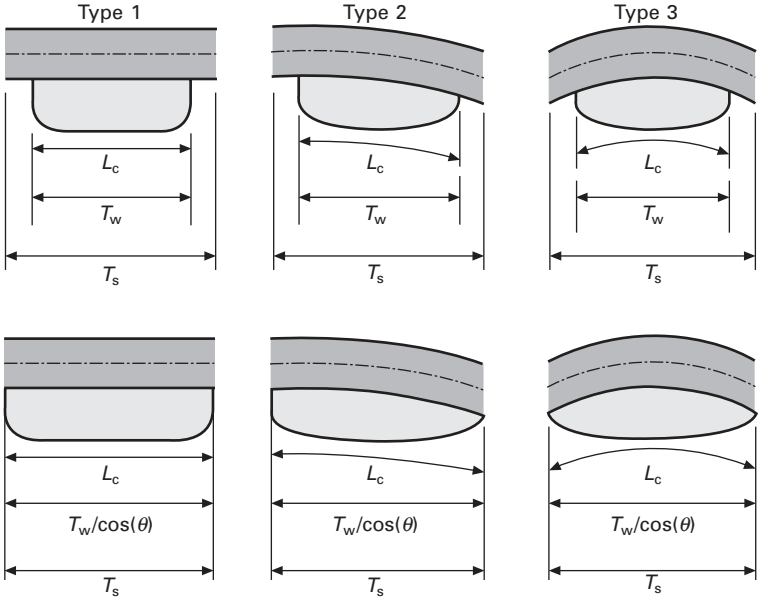

2.4 Three different types of tow crossover: before shearing (top) and during shearing (bottom). L_c = *contact length;* T_w = *tow width;* T_s = *tow spacing.*

where the bulk strain in the yarn is defined as:

$$e_b = 1 - \sqrt{\frac{v_f}{v_{f0}}} \qquad 2.6$$

In the above, v_f and v_{f0} are the current and initial fibre volume fractions, and F_{11}, F_{b1} and F_{bb} are terms of the yarn compliance tensor, which are functions of fibre modulus, fibre waviness (wavelength divided by amplitude for a notional sinusoidal fibre path) and maximal fibre volume fraction. Parameters determined by McBride[15] for compaction of unidirectional yarns were used in the present study.

The torque required to shear the fabric is obtained by summing the torque for each crossover (T_c). The shear force for each specimen can then be calculated from the number of unit cells it contains (N):

$$F_s = \frac{1}{l \cos \theta} \sum_{i=1}^{N} T_{c_i} \qquad 2.7$$

This method of analysis was applied to the four different woven fabrics described in Table 2.1. Results from the model are included in Fig. 2.2, showing good agreement with experimental data. In particular, the model represents the two observed regions within the shear compliance curve very

clearly. Before yarns come into contact, the resistance to shear is small as the yarn contact force is low. Once yarns contact the shear force increases significantly as the contact force includes an additional (and substantial) contribution from yarn compaction.

The above modelling approach has recently been extended to NCFs[16]. The primary differences here are that the yarns are assumed to be perfectly straight, so that significant energy is dissipated via shearing and compaction between parallel yarns. In addition the stitch contributes a significant resistance to shearing via stitch tension and inter-stitch friction. These were modelled using a simple geometric representation for a tricot stitch (Fig. 2.5). Results from this model are shown in Fig. 2.6, which illustrates the difference in shear behaviour predicted for two ±45° tricot-stitched fabrics with different stitch lengths. The model is able to represent the asymmetric shear behaviour typical of NCFs, and also predicts the effect of the stitch geometry on this behaviour.

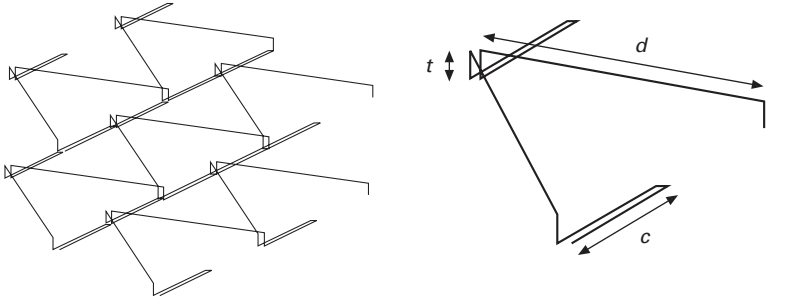

2.5 Tricot stitch pattern for NCF model (left), and stitch unit-cell (right). It is assumed that fabric thickness (*t*) remains constant, and dimensions *c* and *d* evolve as the fabric is sheared.

This section has presented approaches based on analytical modelling to predict the shear response of textile reinforcements. An alternative here is to use 3D finite element analysis to predict fabric shear behaviour. This approach has many attractions, eliminating many of the simplifying assumptions required by analytical models. The approach described in section 2.3.5 has recently been applied to this problem. Such techniques are very useful in the design of reinforcement materials, allowing behaviour to be predicted prior to fabric manufacture and providing useful information to the fabric designer. To assess the effects of fabric mechanics on forming, predictions from these approaches can be used directly as input data for simulations of fabric forming[17], which may allow fabric formability to be optimised for a particular component.

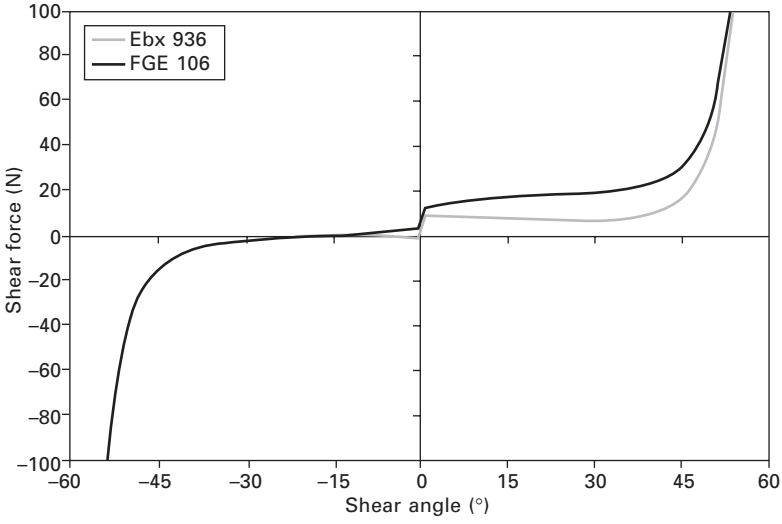

2.6 Predicted shear compliance curves for two ±45° tricot stitched NCFs with different stitch lengths (Ebx 936 c = 2 mm; FGE 106 c = 2.5 mm). Positive shear angles represent shearing parallel to the stitch, whereas negative values represent shearing perpendicular to the stitch.

2.3 Biaxial in-plane tension

2.3.1 Introduction to tensile behaviour of textiles

This section concentrates on tensile behaviour of textile reinforcements when loaded in the fibre directions. Whereas NCFs exhibit relatively linear behaviour, as the fibres remain largely parallel to the plane of the fabric, woven fabrics are well known to have non-linear mechanical properties. Hence woven fabrics form the focus of this section. The diameter of individual fibres within the yarns is very small (5–7 μm for carbon and 5–25 μm for glass) compared with their length. Consequently they can only be submitted to a tensile stress in the fibre direction $\boldsymbol{h}_1$:

$$\sigma = \sigma^{11}\, \boldsymbol{h}_1 \otimes \boldsymbol{h}_1 \quad \sigma^{11} \geq 0 \qquad 2.8$$

Fibres are assembled into yarns. Different yarn structures can be obtained according to the fibre arrangement within the yarn. This section considers yarns that are simply juxtaposed (untwisted). This permits relative sliding of the fibres if yarns are subjected to bending, so that the stress state in the yarn defined by eqn 2.8 remains valid.

From the stress state, it is convenient to define the tension in the yarn:

$$T^{11} = \int_{A_y} \sigma^{11} \mathrm{d}S, \quad \boldsymbol{T} = T^{11} \boldsymbol{h}_1 \otimes \boldsymbol{h}_1 \qquad 2.9$$

where A_y is the sum of the surfaces of the fibres constituting the yarn.

If two yarn networks in directions $\boldsymbol{h}_1$ and $\boldsymbol{h}_2$ are considered (Fig. 2.7a), the stress state for the domain defined by these two yarn networks is of the form:

$$\sigma = \sigma^{11}\boldsymbol{h}_1 \otimes \boldsymbol{h}_1 + \sigma^{22}\,\boldsymbol{h}_2 \otimes \boldsymbol{h}_2 \qquad 2.10$$

and the tensor of the tensions that can be transmitted:

$$\boldsymbol{T} = T^{11}\boldsymbol{h}_1 \otimes \boldsymbol{h}_1 + T^{22}\boldsymbol{h}_2 \otimes \boldsymbol{h}_2 \qquad 2.11$$

$$T^{11} = \int_{A_{y1}} \sigma^{11}\mathrm{d}S,\; T^{22} = \int_{A_{y2}} \sigma^{22}\mathrm{d}S,\; T^{11} \geq 0,\; T^{22} \geq 0 \qquad 2.12$$

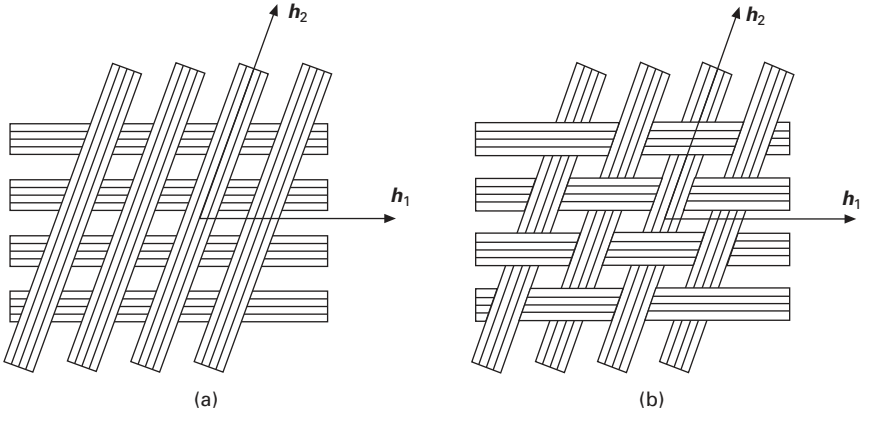

2.7 Bidirectional textile domains: (a) non-woven; (b) woven.

In the above, superscripts 11 and 22 indicate loading parallel to the two yarn directions. When the warp and weft yarns are woven, T^{11} and T^{22} interact because of the interlaced structure. Yarns within woven fabrics are 'wavy' or crimped (Fig. 2.8). Under tensile loads, yarns tend to straighten and to become flattened. In the extreme case, where transverse yarns are free to displace, loaded yarns become totally straight, with transverse yarns becoming highly crimped (Fig. 2.8, $T^{22} = 0$). In intermediate cases, an equilibrium state is reached where the two directions show undulation variations. It is clear that this phenomenon is biaxial and that the two directions interact. The tensile behaviour of woven fabrics is non-linear at low tensions, even if the yarn is linear in tension (Fig. 2.9). As will be shown in the following sections this response depends on the ratio between warp and weft strains. This non-linear phenomenon is observed in the macroscopic tensile behaviour of fabrics, but it is due to geometrical non-linearities at the mesoscopic (repeating unit-cell) scale and is amplified by yarn compaction at the microscopic scale.

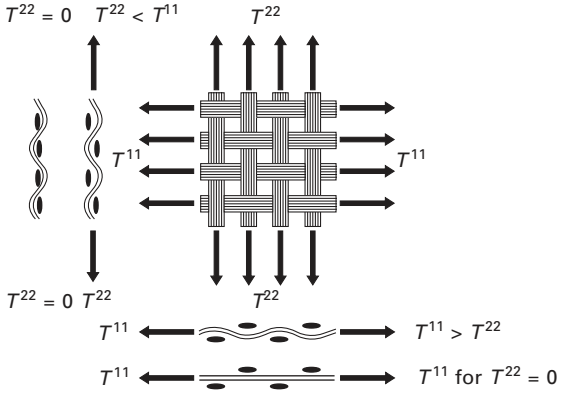

2.8 Tension interactions due to interlacing in woven fabrics.

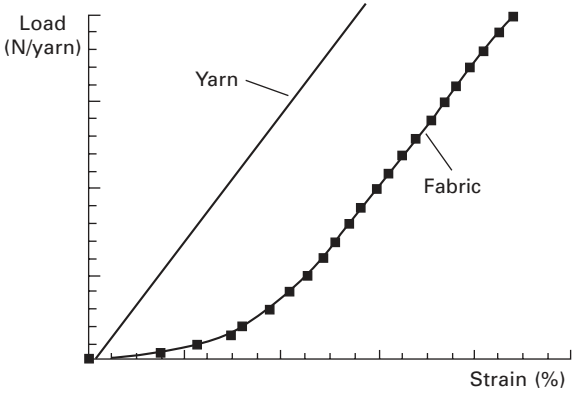

2.9 Non-linear tensile behaviour for woven fabrics based on linear elastic yarns.

2.3.2 Tensile behaviour surfaces

For a woven domain subjected to in-plane tension (Fig. 2.7), the stress state can be described by the tension tensor, which is of the form:

$$\boldsymbol{T} = T^{11}(\varepsilon_{11}, \varepsilon_{22})\, \boldsymbol{h}_1 \otimes \boldsymbol{h}_1 + T^{22}(\varepsilon_{11}, \varepsilon_{22})\, \boldsymbol{h}_2 \otimes \boldsymbol{h}_2 \qquad 2.13$$

The tensions in warp and weft directions, T^{11} and T^{22}, depend on both axial strains, ε_{11} and ε_{22}, because of warp and weft interactions as described above. For a woven domain made of n_{cell} elementary woven cells submitted to in-plane biaxial tension, the dynamic equation can be written in the following form:

$$\sum_{p=1}^{n_{\text{cell}}} {}^{p}\varepsilon_{11}(\eta)\, {}^{p}T^{11}\, {}^{p}L_1 + {}^{p}\varepsilon_{22}(\eta)\, {}^{p}T^{22}\, {}^{p}L_2 - T_{\text{ext}}(\eta) = \int_{\Omega} \rho \ddot{u}\, \eta \, \mathrm{d}V \qquad 2.14$$

$$\forall\ \eta / \eta = 0 \text{ on } \Gamma_{\text{u}}$$

$T_{ext}(\eta)$ is the virtual work due to exterior loads:

$$T_{ext}(\eta) = \int_{\Omega} \boldsymbol{f}\,\eta\,dV - \int_{\Gamma_t} \boldsymbol{t}\,\eta\,dS \qquad 2.15$$

In the above, $\boldsymbol{f}$ and $\boldsymbol{t}$ are the prescribed volume and surface loads, respectively. Γ_u and Γ_t are boundaries of the fabric domain (Ω) with prescribed displacements and surface loads, respectively. L_1 and L_2 are yarn segment lengths in the two yarn directions for an individual cell, and ρ is the material density.

In eqn 2.13 the tensile mechanical behaviour of the fabric reinforcement is defined by relations between the yarn tensions, which in turn are functions of both yarn strains. Woven fabric tensile behaviour is defined by two biaxial mechanical surfaces, which define the warp or weft loads as a function of the biaxial strains. These are identical if the fabric is balanced, i.e. if the yarns and their paths are the same in the warp and weft directions. Three different analysis techniques are presented for this behaviour in the following sections: experimental measurement, simplified analytical models and 3D finite element analysis.

2.3.3 Experimental analysis of the biaxial tensile behaviour

In this section biaxial tensile experiments are described, the primary aim of which is to determine the two tension surfaces linking warp and weft tensions to the corresponding strains. A number of specialist biaxial tensile devices have been designed for fabric testing[18, 19]. The device used in this study is operated using a conventional tensile/compressive testing machine, and needs no servo-control between the two tensile axes. It is an extension of devices developed for sheet metal, and works via two deformable lozenges[20, 21] as illustrated in Fig. 2.10. When the machine crosshead is raised, it compresses the whole system. This generates a displacement in both the warp and weft directions within a specimen set in the middle of the device. A cruciform specimen is used, where only the square central region (50 mm wide) is of interest. The arms of the cruciform have the transverse yarns removed, so that these regions are uncrimped. This is essential to avoid the use of systems that allow transverse deformation (as required in the Kawabata device, for example[18, 19]).

Various ratios (denoted k) between strains in the warp and weft directions can be imposed by adjusting the dimensions of the testing fixture in one direction. In addition a regulation system allows the inter-yarn angle to be modified from 90° (i.e. effects of fabric shear on tensile behaviour can be measured). Load cells, positioned directly behind the specimen, give the total load in each direction. Strain measurements are performed using either

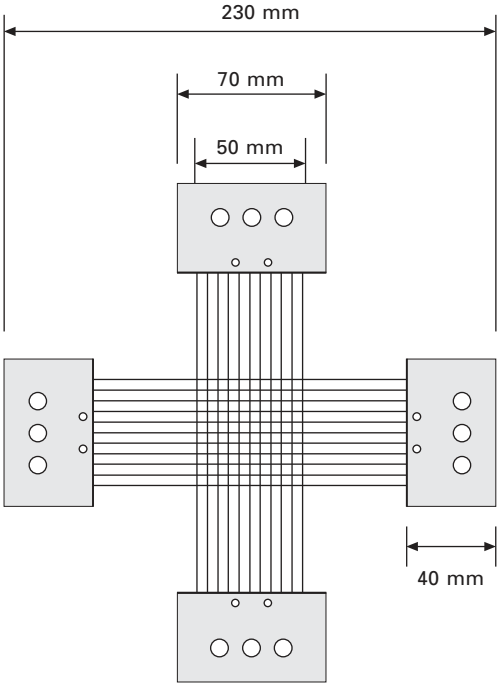

2.10 Biaxial tensile testing device and cruciform specimen.

optical method[22, 23] or extensometers. The two methods lead to results in good accordance; optical strain measurements are particularly useful as they allow the full strain field across the central woven region to be assessed. Such analyses have confirmed that the strain field is uniform and homogeneous, even in the inner corners that pose problems for materials with higher in-plane shear stiffness (as is the case for metals[20]).

Results from tests on three fabrics are presented here to illustrate typical biaxial behaviour. These materials are used to produce preforms for the RTM (resin transfer moulding) process. Data are presented for several strain ratios $k = \varepsilon_1/\varepsilon_2$ (1 is the direction under consideration, which may be warp or weft). The fabric density in one direction is the number of yarns per unit fabric length; the crimp characterises undulation and is defined as:

$$\text{Crimp } (\%) = \frac{\text{yarn length} - \text{fabric length}}{\text{fabric length}} \times 100 \qquad 2.16$$

Balanced glass plain weave

This fabric is approximately balanced (the properties in the warp and weft directions are almost identical). The yarn density is 0.22 yarns/mm and the

crimp is 0.4%. The individual yarns have slightly non-linear tensile behaviour because fibre cohesion in the yarn is not particularly efficient and the filaments are not rigorously parallel. The tenacity of the glass yarns is 350 N and their stiffness is 38 KN. Tension versus strain curves for the fabric are highly non-linear at low forces and then linear for higher loads (Fig. 2.11a). This non-linearity is a consequence of non-linear geometric phenomena occurring at lower scales, more precisely straightening at the mesoscale and compaction at the microscale. This non-linear zone depends on the prescribed strain ratio, which illustrates the biaxial nature of the fabric behaviour. The non-linear zone is largest for tests in which displacement in the other direction is free (i.e. uniaxial tests, $k = 0$). Here the yarns tend to become completely straight under very low loads. Once the yarns in one direction become straight, the behaviour of the fabric is very similar to that of the yarn alone. The value of the strain corresponding to this transition is representative of the fabric crimp in the loading direction. The experimental results are highly reproducible[24, 25]. From the tension–strain curves for different strain ratios it is possible to generate the experimental biaxial behaviour surface (Fig. 2.11b).

Balanced carbon 2 × 2 twill weave

This balanced fabric is made of yarns composed of 6000 high-strength carbon fibres. In both warp and weft directions the yarn density 0.35 yarns/mm. Their tenacity is 420 N, and their uniaxial tensile behaviour is approximately linear (Fig. 2.12a). The fabric crimp is 0.35%. Biaxial tensile curves for different strain ratios are presented in Fig. 2.12(a), and the tension surface is shown in Fig. 2.12(b). Although the yarns exhibit linear behaviour, the tensile force versus strain behaviour of the fabric is highly non-linear at low loads and then linear at higher loads. The non-linearity decreases as k is increased, in a similar manner to the glass plain weave fabric. Failure has been reached for $\varepsilon = 0.8\%$ ($k = 1$)[25] while the non-linear zone extends to approximately 0.3%. Consequently, when a woven material is loaded, for instance during forming, a major part of the fabric is in a state where its behaviour is highly non-linear; it is, then, important to describe this non-linearity in the mechanical behaviour.

Highly unbalanced glass plain weave

The stiffness of the weft yarn of this fabric is 75 kN per yarn and that of the warp is 8.9 kN per yarn. Consequently the fabric is very unbalanced. The behaviour of the fabric is thus significantly more non-linear than that of the individual yarns. The two warp and weft behaviour curves (and surfaces) are different (Figs 2.13a&b). The weft, which is much more rigid, has a behaviour that is influenced very little by the warp strain. The tension surface is obtained

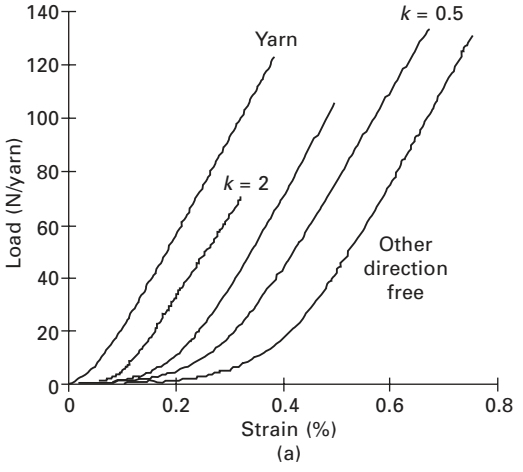

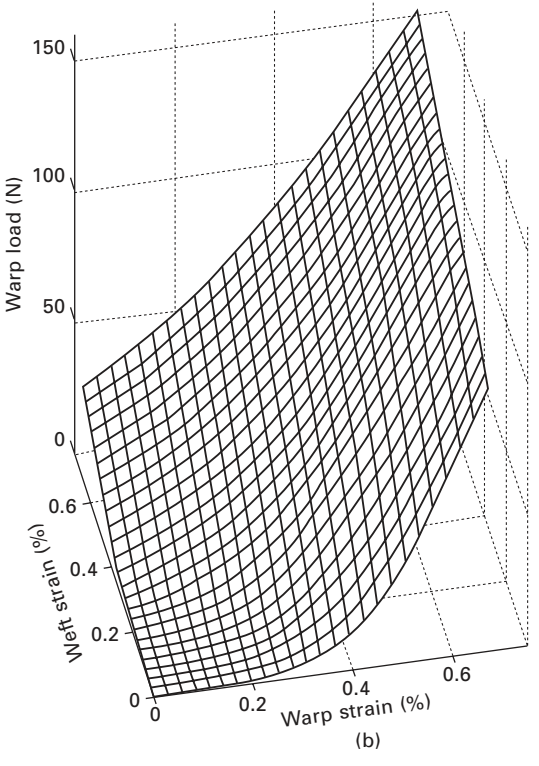

2.11 Results of biaxial tests for a glass plain weave: (a) load–strain curves; (b) tension surface.

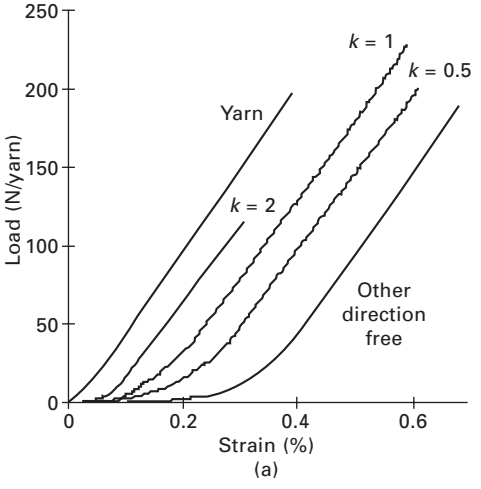

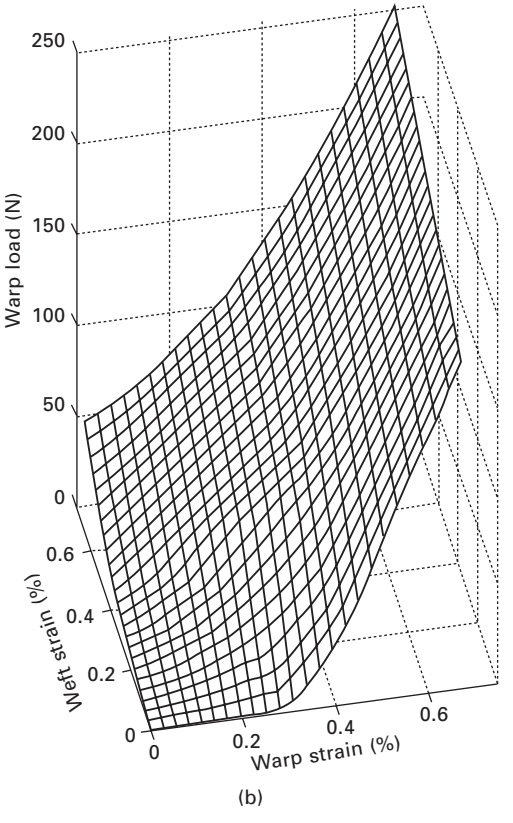

2.12 Results of biaxial tests for a carbon 2 × 2 twill weave: (a) load–strain curves; (b) tension surface.

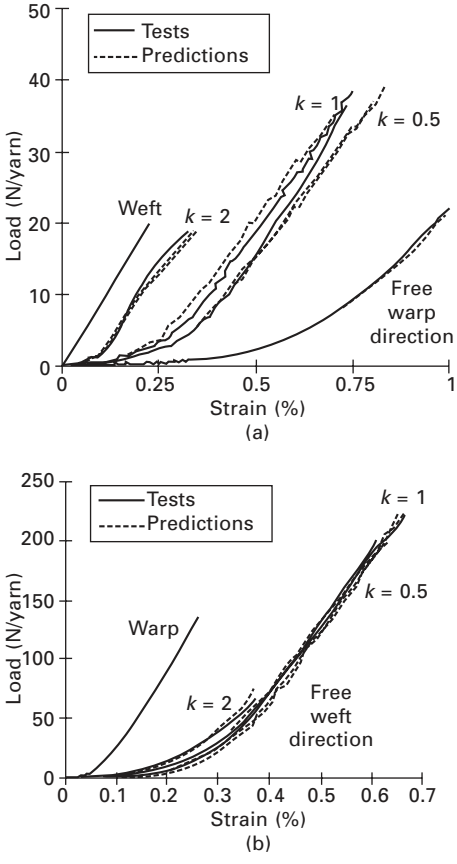

2.13 Results of biaxial tests for an unbalanced glass plain weave: (a) weft load–strain curve; (b) warp load–strain curve.

by a straight translation in the warp strain direction. In contrast, the warp strain depends strongly on the weft strain.

2.3.4 Analytical models

The biaxial experiments described above are rather difficult to perform and it is convenient to use simplified analytical models to predict the mechanical behaviour of the fabric from parameters related to the weave structure and the mechanical characteristics of the yarns. Such models can be very fast and can allow the influence of material parameters to be examined. Many models have been proposed in the textile science literature[18, 26–29]. Here the well-known Kawabata model[18] is described, and a second model that is consistent with the geometry of the woven fabric is presented.

Kawabata model

In this model, yarns within a plain weave are described by straight lines as shown in Fig. 2.14. From the geometry of the mesh the following equation can be derived for the strain in each yarn direction:

$$\varepsilon_{f\alpha} = \{4[e_{0\alpha} + (-1)^{\alpha} w_{\alpha}]^2 + L_{0\alpha}^2 (1 + \varepsilon_{\alpha})^2\}^{1/2} (L_{0\alpha}^2 + 4e_{0\alpha}^2)^{-1/2} - 1 \quad 2.17$$

The angle between each yarn and $\boldsymbol{x}_3$ is:

$$\cos \theta_{\alpha} = 2[e_{0\alpha} + (-1)^{\alpha} w_{\alpha}]\{L_{0\alpha}^2 (1 + \varepsilon_{\alpha})^2 + 4[e_{0\alpha} + (-1)^{\alpha} w_{\alpha}]^2\}^{-1/2} \quad 2.18$$

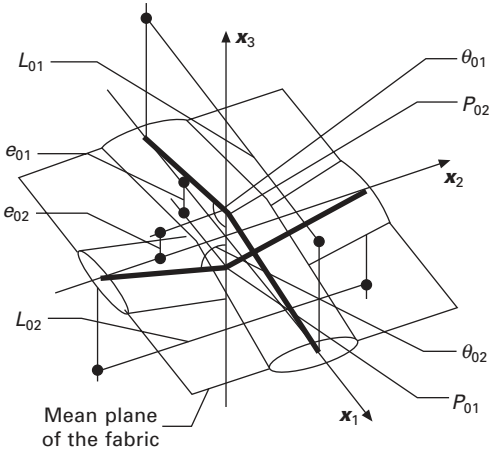

2.14 Geometric representation of a plain weave in Kawabata's model.

In the above, α (= 1 or 2) refers to the yarn direction, and w_{α} is the yarn displacement in the $\boldsymbol{x}_3$ direction. Other symbols are defined in Fig. 2.14. Equilibrium conditions and the projection of the loads onto the fabric mean plane leads to:

$$T_f^1 \cos \theta_1 = T_f^1 \cos \theta_2 \quad T^{\alpha\alpha} = T_f^{\alpha} \sin \theta_{\alpha} \quad F_c = 2T_f^{\alpha} \cos \theta_{\alpha} \quad 2.19$$

where F_c is the compressive force between yarns along $\boldsymbol{x}_3$. The tensile behaviour of each yarn is given by:

$$T_f^{\alpha} = g(\varepsilon_f^{\alpha}) \quad 2.20$$

A large number of studies have been published concerning the mechanics of yarn compression[14, 18, 29–32], and this is discussed in the context of fabric compaction in section 2.4. Here an empirical compaction law is used, which is different from that proposed by Kawabata[18]:

$$\phi(F_c) = A[2 - \exp(-BF_c) - \exp(-CF_c)] = w_1 - w_2 \qquad 2.21$$

The compaction coefficients A, B and C are identified using an inverse method[33, 34] from the biaxial test at $k = 1$.

The system of equations given above can be reduced to one non-linear equation depending on transverse displacement, and can be solved by dichotomy if strains are imposed. If loads are known, it is necessary to solve the whole system; an iterative method (e.g. Broyden) can be used efficiently. Good agreement between the model and experimental results for different values of k is demonstrated in Fig. 2.15. Additional results for the fabrics presented in section 2.3.3 are given by Buet-Gautier & Boisse[25].

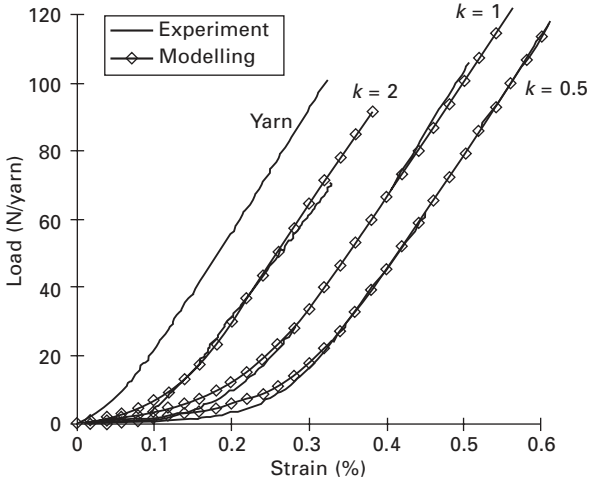

2.15 Comparison between Kawabata's model and experimental data for a glass plain weave.

This model is simple and efficient. However, the 3D geometry of the yarns built on the straight segments penetrate through each other, and in order to obtain good results as shown in Fig. 2.15 the values of parameters A, B and C are not consistent with physical values for the fabric. The goal of the next model is to avoid penetration of the yarns (to be geometrically consistent) and to work with physical values.

A geometrically consistent yarn model for fabric tensile biaxial behaviour

Here yarn longitudinal sections are curved lines with surfaces that are in consistent contact with each other at yarn crossovers. Yarn cross-sections are defined by the intersection of two circular arcs with different diameters. Between yarn crossovers, the yarns are assumed to follow straight paths.

Consequently, the yarn paths are represented by circular arcs and straight segments (Fig. 2.16). The geometry is defined in the general case (unbalanced fabric) by a set of seven material parameters. It is convenient to measure for the warp ($\alpha = 1$) and weft ($\alpha = 2$) direction, the crimp e_α, the interval between two yarns a_α and the yarn width c_α. The last parameter required is the thickness of the fabric w. It can be shown that the solution of this system can be reduced to two non-linear equations giving $\varphi_{\alpha 1}$:

$$\tan \varphi_{\alpha 1} \left\{ 4 \left[L_\alpha - \frac{1}{2} \frac{(a_{\alpha'} - c_{\alpha'})}{\cos \varphi_{\alpha 1}} \right]^2 a_{\alpha'}^{-1} - c_{\alpha'}^2 \right\}^{1/2} = c_{\alpha'} \qquad 2.22$$

where $\alpha' = 3 - \alpha$. If the fabric is balanced, only three parameters (crimp, yarn width and interval between two yarns) are necessary to define the whole geometry. For the balanced glass plain weave presented in Fig. 2.11, the geometric measurements are $c_\alpha = 3.80$ mm, $a_\alpha = 4.55$ mm and $e_\alpha = 0.40\%$. The geometric model leads to $\varphi_{\alpha 1} = 0.134$, $c_\alpha = 2.30$ mm, $b_\alpha = 0.130$ mm and $w = 0.710$ mm. These calculated quantities agree well with their physical measurements, for example the fabric thickness w. The 3D geometry obtained

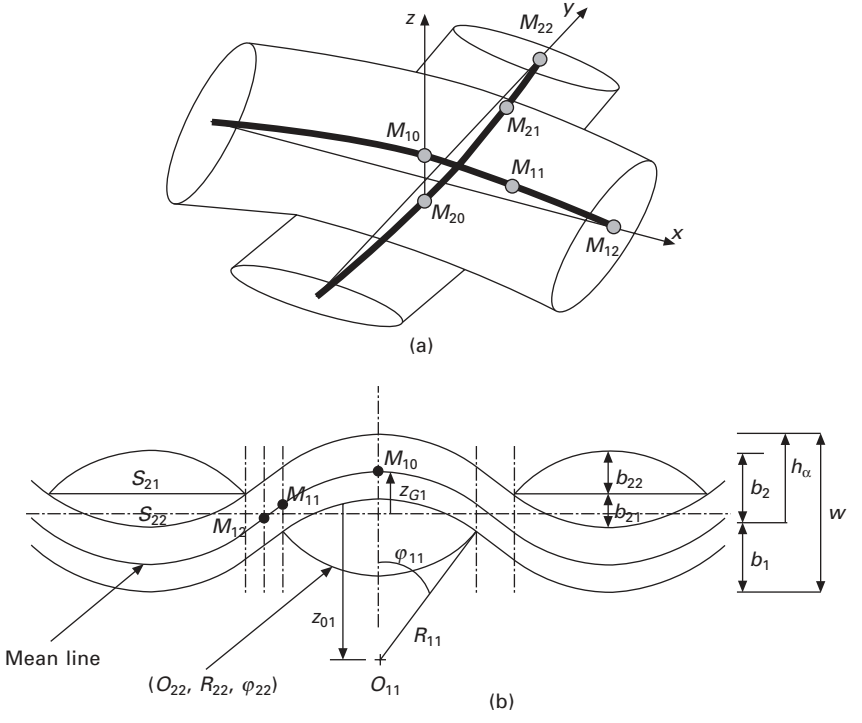

2.16 Geometry of the consistent model (a) and section through the model along one yarn direction (b).

can be used directly for generation of finite element meshes, as will be described in the following section.

The relations between the two strains and tensions in the warp and weft directions are obtained from equilibrium in the deformed configuration:

$$T_{\mathrm{f}}^{\alpha} = PR_{\alpha 1}\, R_{\alpha' 1}\, \varphi_{\alpha 1} \quad T^{\alpha\alpha} = T_{\mathrm{f}}^{\alpha} \cos \varphi_{1\alpha} \tag{2.23}$$

where P is the contact pressure between crossing yarns. Axial strains in the yarn direction (which are assumed to be small) and the strains in the plane of the fabric are respectively:

$$\varepsilon_{\mathrm{f}}^{\alpha} = \frac{L_{\alpha} - L_{\alpha 0}}{L_{\alpha 0}} \quad \varepsilon_{\alpha\alpha} = \frac{1}{2}\left(\frac{a_{\alpha^2} - a_{\alpha_0^2}}{a_{\alpha_0^2}} \right) \tag{2.24}$$

where the subscript 0 indicates the initial value (prior to loading). The tensile behaviour of the yarns is given by eqn 2.20. Transverse compaction stiffness is defined by relating the parameter $r = |z_2 - z_1|$, which describes the relative displacement between yarn paths, with the loads on the mesh. As suggested above, this stiffness depends both on the compaction state and the yarn tensions:

$$r = A\left[2 - e^{-\mathrm{BSP}} - e^{-\frac{C}{2}(T_{\mathrm{f}}^{1} + T_{\mathrm{f}}^{2})} \right] \tag{2.25}$$

where S is the yarn contact surface area. Considering the difficulty in performing a simple test to measure compaction of the yarn, the coefficients A, B and C are again determined by an inverse method using the result of the biaxial test for $k = 1$.

If a strain state of the fabric (ε_{11}, ε_{22}) is prescribed, the equations in the deformed state give the two warp and weft yarn tensions (T^{11}, T^{22}). It can be shown[21, 35] that this set of equations can be reduced to a non-linear system of two equations that can be solved using an iterative (Newton) method. The tension surface obtained in the case of the balanced plain weave glass fabric is compared with the experimental surface in Fig. 2.17. Both surfaces are in good agreement, particularly at low strains where non-linearity is most pronounced.

2.3.5 3D finite element analysis of the unit cell under tension

3D finite element (FE) analysis is an alternative to the two previous approaches to determine the biaxial tensile surfaces for fabric reinforcements. This gives information on local phenomena that influence the global fabric mechanical behaviour. It can be used before fabrication to define the geometrical characteristics and the types of yarn for a fabric in order to obtain the desired

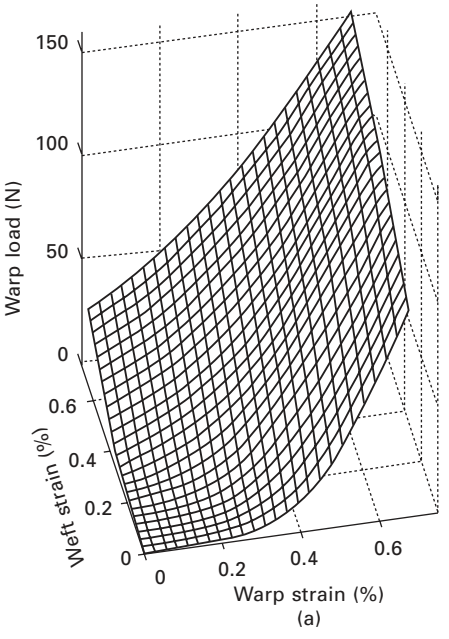

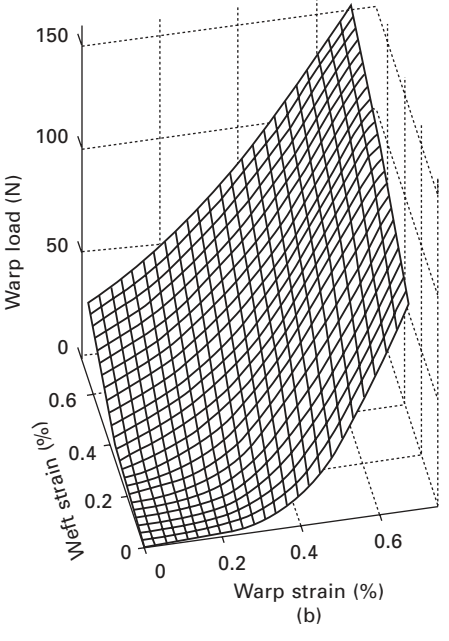

2.17 Tensile behaviour surface for balanced glass plain weave: (a) experimental and (b) geometrically consistent model prediction.

mechanical properties. This is particularly interesting for complex fabrics manufactured in small quantities and used in highly demanding structural applications such as aerospace components. In addition the FE approach allows the influence of material parameters (e.g. crimp, yarn density, weave pattern) on the biaxial mechanical properties of the fabric to be analysed in detail[36].

The yarn is composed of a large number of fibres with small cross-sections that are very flexible and can slide in relation to each other. Consequently yarn mechanical behaviour is highly non-linear, and exhibits very low rigidity in all directions other than parallel to the fibres. Furthermore, the transverse stiffness depends on yarn compaction and tension. The equivalent material used in 3D FE analysis must account for this behaviour. This can be achieved using an elastic orthotropic model where the principal frame is defined with direction 1 parallel to the yarn, with very small shear moduli (G_{12}, G_{13}, G_{23}) and Poisson ratios (ν_{12}, ν_{13}, ν_{23}), and with low transverse moduli (E_2, E_3) in comparison with the longitudinal modulus (E_1). Because local geometric non-linearities are of primary importance, the simulation must be performed using large strain theory. Since the axial (1 direction) and transverse moduli are very different, it is important to specify the mechanical characteristics in the appropriate directions during the analysis. Therefore, the yarn stiffnesses are prescribed in material directions, i.e. linked to the finite elements in their current position. In each of these material directions, hypoelastic behaviour is considered.

The longitudinal modulus may be constant or strain dependent, and can be determined by tension tests on single yarns. As already noted, yarn compaction plays a major role in the deformation of woven fabrics. In the current FE-based approach, local values of the mechanical properties are needed, so that to model compaction the transverse modulus E_3 is required. When the yarns are under tension, it can be observed that it is more difficult to compress them. It is therefore necessary to take this tension into account. Here, yarn compaction is represented by the evolution of the transverse modulus, which increases if transverse and longitudinal strains increase:

$$E_3 = E_\varepsilon + E_0 |\varepsilon_{33}^n| \varepsilon_{11}^m \qquad 2.26$$

where E_0, m and n are three material parameters. E_ε is the transverse Young's modulus in the unloaded state, which is almost zero for the fabric yarns described in section 2.3.3. Equation 2.26 is consistent with results given by global yarn compression models for the evolution of the yarn thickness[30, 31]. When loading starts, the transverse stiffness increases because the voids between fibres are reduced. Finally, the stiffness tends to an asymptotic value, which is very large in comparison with the value at low strain. As for the analytical models presented above, an inverse method[33, 34, 36] was used to determine the parameters E_0, m and n, using the results for a biaxial test with

$k = 1$. In this 3D simulation of the woven unit cell, a numerical difficulty comes from the very large difference between weak (or zero) values of some moduli (particularly shear modulus) and the modulus in the direction of the yarn. This can result in spurious zero energy modes. The hourglass control method, developed for finite elements with reduced integration, is used here to avoid this problem[37, 38]. A master–slave approach is used to model contact between the yarns. It has been observed that contact non-linearities are important for the twill weave, but less so for the plain weave.

Figure 2.18 presents the unit cell mesh for the carbon 2 × 2 twill weave (30 000 degrees of freedom), as described in section 2.3.3 The tensile behaviour surface obtained from computations under biaxial tensile loads with different strain ratios is also shown. This is in good agreement with the surface determined by experiments (Fig. 2.12); similarly good agreement between FE predictions and experimental data was obtained for the other fabrics described earlier[21]. Curves obtained from FE analysis are included in the graphs in Fig. 2.13 (dotted lines) for the unbalanced fabric, again demonstrating good agreement.

The 3D FE analyses show that yarn compaction is extremely important in most cases. This is particularly evident under equal biaxial strains (i.e. $k = 1$), where the yarn compaction (logarithmic) strain reaches a maximum value of 40% for the glass plain weave (Fig. 2.19). In contrast, under uniaxial loading ($k = 0$), compaction is negligible: the stretched yarn becomes straight while the undulation of the free yarn increases (Fig. 2.19a).

The 2.5D carbon fabric presented in Fig. 2.20 is used in aerospace structural components. The weave pattern is such that the weft yarns cross two warp layers, so avoiding delamination between the different plies. The FE model presented in Fig. 2.20 has 53 000 degrees of freedom. The warp yarns are initially straight. This explains why biaxial tests give the same response in the warp direction for different strain ratios, so that the tensile behaviour surface is flat (Fig. 2.20b). On the other hand, the response in the weft direction is non-linear and depends on the strain ratio (Fig. 2.20c). Given the complexity of such fabric reinforcements, 3D FE simulations can facilitate fabric design so that the appropriate type of yarn and weave pattern for a given application can be determined before fabric manufacture. Results of computations for other fabrics are given by Boisse and coworkers[21, 36].

2.4 Compaction

2.4.1 Importance of compaction in the processing textile preforms and composites

The widespread use of textile preforms and reinforcements for composites manufacturing results from the easy handling of large quantities of fibres

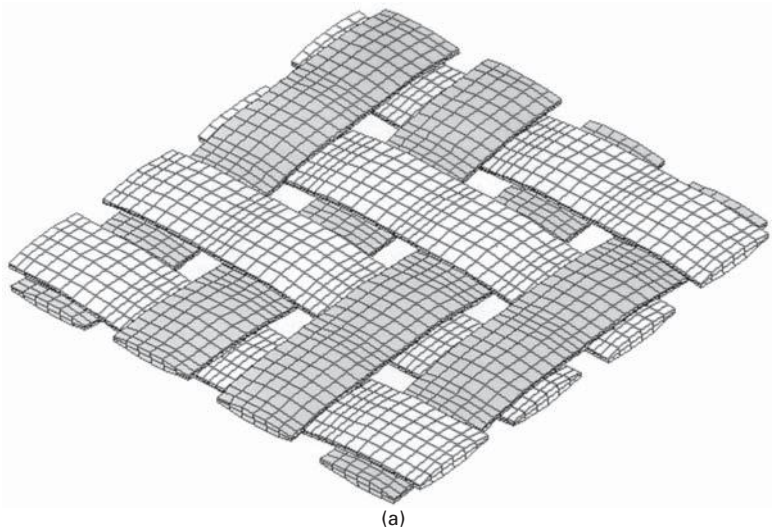

(a)

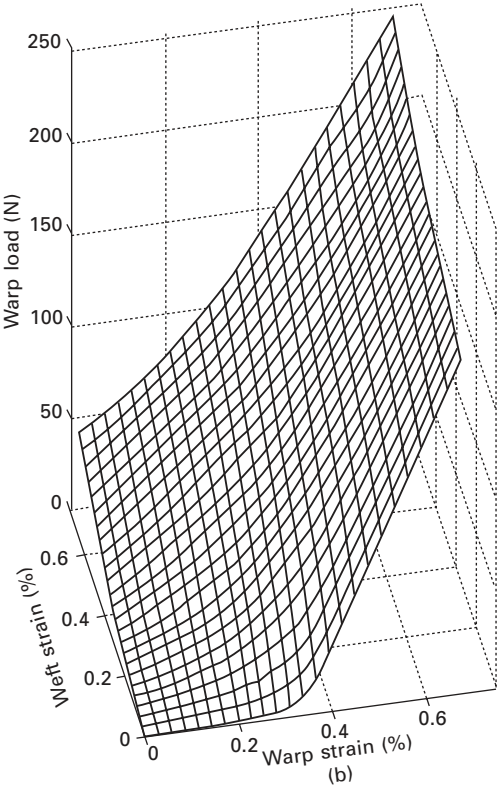

(b)

2.18 3D finite element analyses for biaxial tensile behaviour of carbon 2 × 2 twill weave. (a) FE mesh and (b) predicted tensile behaviour surface.

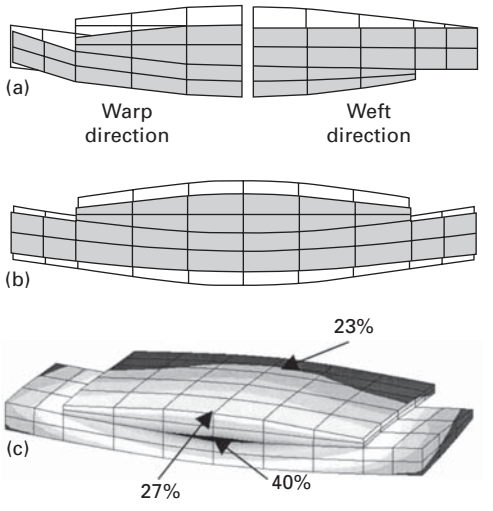

2.19 Yarn compaction during tensile loading of a plain weave, for strain ratios of (a) $k = 0$ and (b, c) $k = 1$.

offered by these material forms, which make fast and economical production possible. Despite lower costs, stringent imperatives on processing and performance are nonetheless present when manufacturing composites from textiles. Preforms must be processed in a configuration that eases manufacturing and maximises the properties of the final part.

In RTM (section 5.3.1), the injection of the resin through the preform is eased by low fibre volume fractions. These must be kept within a certain range, above a minimum value in order to prevent movement of the preform in the mould upon injection and below a maximum value to ensure that resin flows at sufficiently high rate under practicable injection pressures. Final parts must feature high fibre volume fractions as this ensures minimal resin usage and high specific properties, as well as limiting the possible occurrence of resin-rich areas.

Similar considerations apply to VI (vacuum infusion, section 5.3.2). In this process the vacuum level and the design of the mould and gates affect the thickness at each point of the part, in its final state and at all times during processing. In turn the thickness affects preform permeability, flow, filling dynamics and pressure distribution. Thickness and compaction behaviour of the textile reinforcement have a major influence on process kinetics for VI.

Compaction behaviour also plays an important role in the stamping of textile-reinforced thermoplastic composites. Here the reduction in thickness is an integral part of the manufacturing cycle, and must be timed accordingly. Initially, any air must be evacuated by flowing along and/or between solid fibres. Then the viscosity of the polymer (present as fibres or in partly

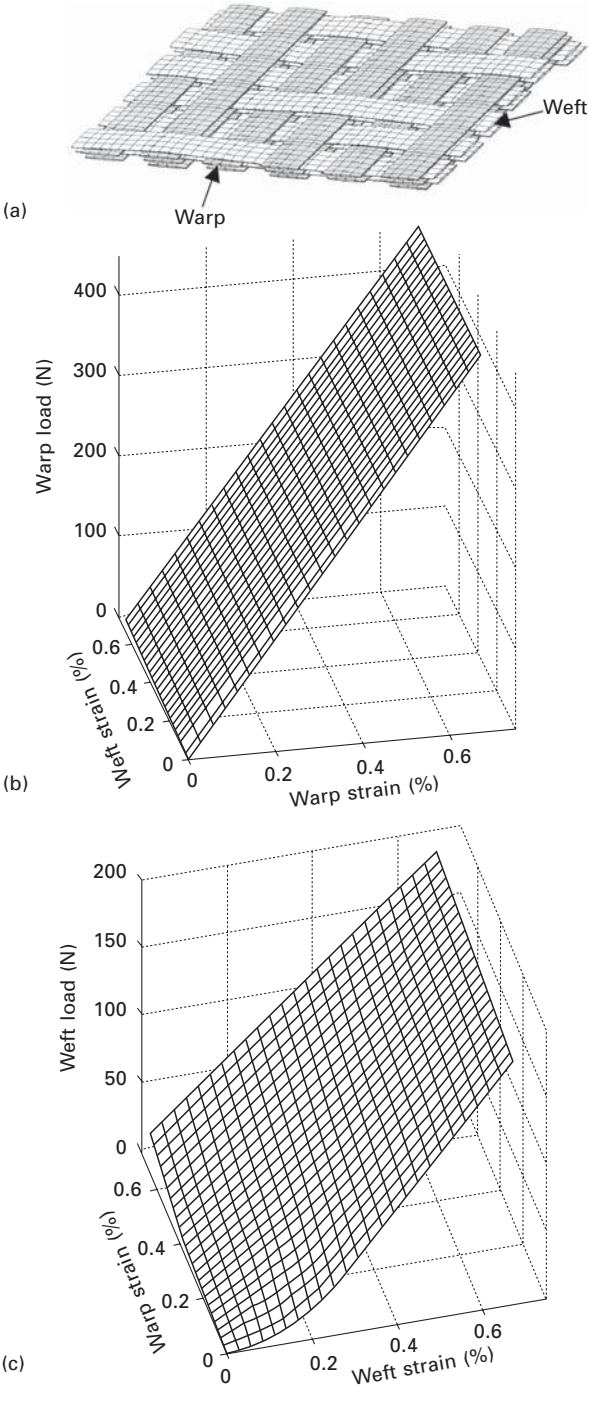

2.20 3D finite element analysis for biaxial tensile behaviour of a 2.5D fabric: (a) FE mesh and (b, c) predicted tensile behaviour surfaces.

consolidated form) is lowered throughout the preform, so that thorough consolidation can take place under increased compaction forces. Critically, these operations must be completed within a minimal cycle time. The thermal behaviour of the material throughout the cycle depends on the imposed compaction level. Knowledge of the fibre volume fraction in a part being processed is also critical to minimising voids.

Textiles in their unloaded state have a low fibre volume fraction (typically between 10 and 25%[39]) which must be increased during processing. The final fibre volume fraction and the rates at which it is increased are generally crucial to the economic production of quality parts. Hence control of the compaction is essential.

Predictive simulation tools for composites manufacturing processes are becoming increasingly available (see Chapters 4 and 7). Accurate predictions require accurate data, including compaction data. However, the usefulness of such compaction data extends beyond process modelling and control. Knowledge of the compaction behaviour is equally important to the specification of manufacturing equipment and textile reinforcements for RTM. Process engineers need to know what forces are involved in bringing a preform to a target fibre volume fraction, and which textiles may be most amenable to this. Similarly, when selecting a vacuum pump for VI moulding one needs to know what preform thicknesses can be achieved for a given port set-up and part dimensions, so that the manufacturing operation can be designed appropriately and operated with confidence.

The precise scope of this section is detailed below, followed by a description of the phenomena covered here. Further information on the effect of diverse parameters that relate to industrial situations is presented, and practical recommendations are made. While the information applies to any manufacturing process where textile reinforcements are used, throughout this section the concepts and their practical consequences are discussed for three processes, namely RTM, VI and thermoplastic stamping.

2.4.2 Scope of the section

This section describes the behaviour of textile reinforcements subjected to compaction forces normal to their plane. The focus is on the relation between the force F applied to the textile and its thickness h, which can be converted respectively to a pressure P by dividing by the projected area A, and to a fibre volume fraction v_f.

In manufacturing, pressure is typically applied between the two rigid surfaces of a mould (RTM, stamping, etc.) or between a lower rigid tool and a flexible membrane (VI, diaphragm forming, etc.). In this section the pressure refers to the force applied on a textile compacted between two platens of finite area. The pressure is obtained by dividing the value of the force by the

area of the platens, assuming that the textile sample has the same dimensions. Textiles are made of yarns, which in turn are made of fibres. As it is transmitted through the textile, the externally applied force is actually split into numerous small forces that are transmitted at the numerous points of contact between individual fibres. Therefore, the concept of an average pressure that is constant over the surface of the platens is an approximation. A more detailed investigation would reveal higher pressures on the yarns and no pressure in the empty gaps separating them (Fig. 2.21). The pressure distribution on any given plane cutting through the material would reflect the geometry of the preform on that plane, with pressure levels on individual yarns being significantly higher than the average applied pressure. Here the compaction pressure is defined as the applied force divided by the area of the platens, including the yarns and the empty volumes defined between them.

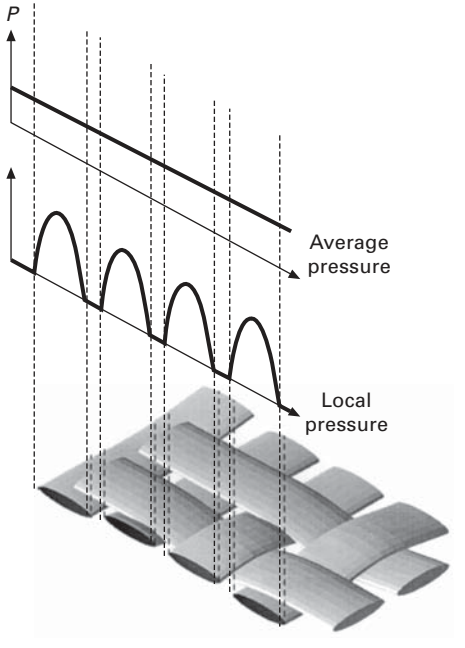

2.21 Definitions of local and average pressure during textile compaction.

The other variable recorded in a compaction test is the preform height (thickness), which is subsequently expressed as a fibre volume fraction. The reason for this is that preforms can be made of any number of textile layers. A given preform will often feature varying numbers of textile layers in different locations, as well as diverse combinations of different textiles. Using a single relationship between the applied pressure and the resulting fibre volume fraction is simpler and more general. Also, the fibre volume

fraction of a part is often more critical to designers than the thickness. However, although the concept of a fibre volume fraction applied to a single layer of textile compacted between two rigid platens is unambiguous, real preforms are generally made of more than one textile layer. In such cases the volume, or thickness, occupied by each layer is not precisely defined and individual layers typically run into each other. Fibres from a given layer can lodge themselves between fibres from another layer, and at a larger scale the peaks and valleys formed, say, by a woven textile can either fill each other or not, (Fig. 2.22). This phenomenon is known as nesting and affects the way in which the applied force is transmitted through textile layers.

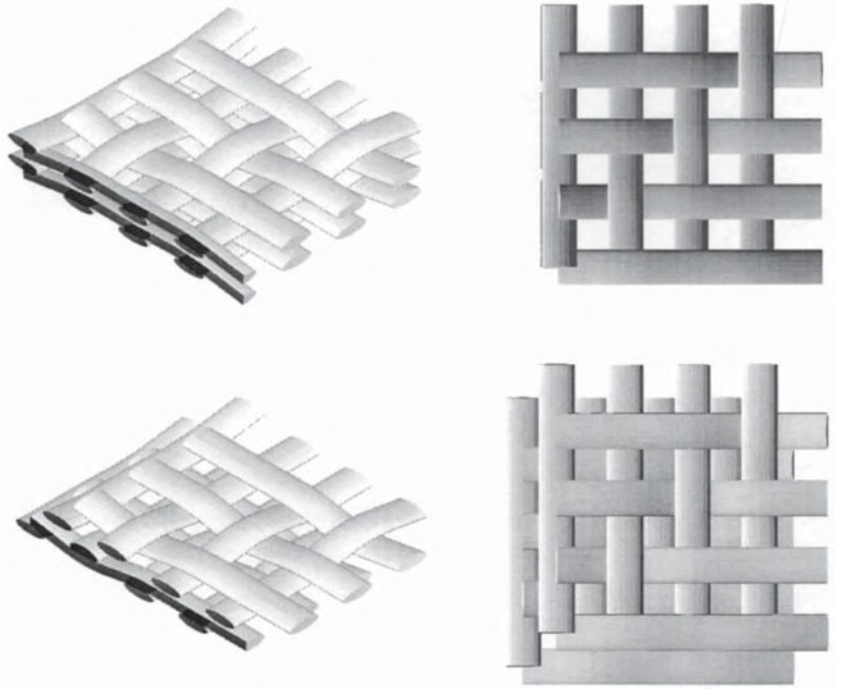

2.22 Illustration of nesting between fabric layers – no nesting (top) and maximum nesting (bottom).

Experiments have shown that the compaction behaviour of multilayer stacks of a given textile differs from that of a single layer of the same material[39]. While a single relation between P and v_f for a given textile may be used as a guideline, in simulation one should ensure that the data represent the actual lay-up envisaged for production, especially when a high-fibre volumes fraction is required. Furthermore, properties such as in-plane permeability of preforms or bending stiffness of composites depend on the relative thickness of individual textile layers. Preforms are sometimes built

with random mats located at their core or distributed through the thickness, and enclosed between layers of directional reinforcements. Such preforms will show high in-plane permeability without major reductions in their specific bending stiffness if the compaction of the random mats is controlled. The reader should note that European Standard BS EN ISO 5084:1997 'Textiles – Determination of thickness of textiles and textile products', which supersedes BS 2544, involves a static test where the textile is subjected to one nominal load only. The evolution of v_f as a function of P is not supplied by the test.

Compaction data such as those presented here are usually gathered from tests where platens are parallel and textiles are flat and normal to the compaction axis. A typical rig used to perform such tests is illustrated in Fig. 2.23[40].

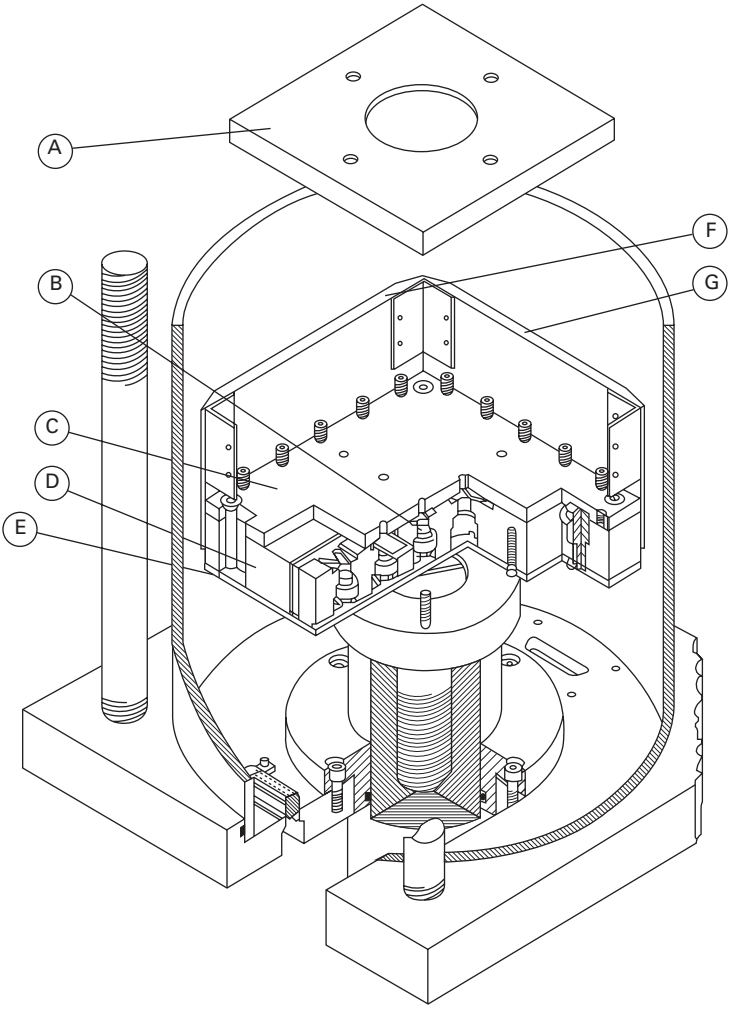

2.23 Testing fixture for reinforcement compaction[40].

Textile layers are compacted between platens A and C. Other items B to G in the figure are used to perform compaction tests on samples saturated in fluid, as discussed later in the text. The two platens are mounted to the ram and fixed traverse of a universal testing machine and the ensemble is loaded, usually at a constant displacement rate in the order of 1 mm/min. Calibration tests performed with an empty rig allow the subtraction of the deformation of the rig from the total deformation at a given force, ensuring that only the compaction of the textile layers is recorded. The sample is compacted either to a predetermined load or to a predetermined fibre volume fraction, depending on the information sought. Upon reaching this state, a number of things may happen. The displacement will be held constant to record the relaxation at a constant fibre volume fraction, or the force will be held constant to record compaction creep, or the sample will be unloaded at the same rate in order to record a compaction hysteresis.

The surfaces of production tools are rarely flat in their entirety, and they are not parallel where changes in thickness occur. Therefore at most points of the tool surfaces the compaction direction is not parallel to the axis of the press. In simulations these factors are accommodated by projecting the press displacement on the normal to the tool surface for every point of that surface, and by obtaining the corresponding pressure level. One may note that assuming that a textile compacts along the normal to the tool surfaces is not rigorously correct, as the actual relative motion of the surfaces includes a lateral component to any normal that is not parallel to the axis of the press. No published experimental data document this phenomenon, and hence it is usually neglected.

The term compaction can be used in the context of individual tows or yarns. Tow compaction happens when textiles are compacted, and is also observed when textiles are sheared (section 2.2) and submitted to tension (section 2.3). Tow compaction is discussed in more detail in Chapter 1. While it may be possible to infer tow compaction properties from experiments performed on textiles through intelligent use of textile models, the focus here is industrial production. Basic compaction cycles are described, and phenomena such as behaviour upon impregnation, relaxation and unloading are discussed. The important aspect of repeatability and statistical distribution of the data is covered, along with implications for mould design.

2.4.3 Basic compaction and relaxation curves

Figure 2.24 shows a typical compaction and unloading cycle for a stack of textile reinforcements. In this case the distance between platens was reduced at a constant rate of 0.5 mm/min, held constant for 1 min and returned to its initial value at the same rate. The curve shows the evolution of the compaction pressure P as a function of the average fibre volume fraction v_f for six layers of a woven textile; v_f varies between 0.40 and 0.60 and the maximum pressure

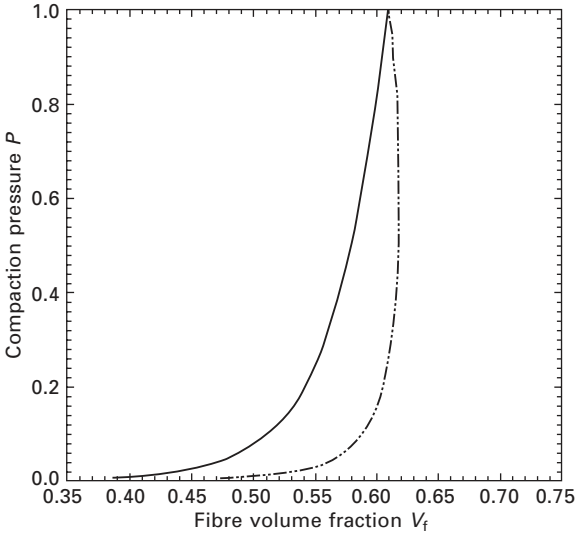

2.24 Typical compaction and unloading curves for a stack of plain weave reinforcements, tested at a constant displacement rate compaction test (pressure in MPa).

is 1.0 MPa or 10 bar; such high compaction pressures represent a practical maximum. The compaction part of the cycle can be characterised by an initial fibre volume fraction $v_{f,o}$ which relates to the unloaded textile, a representative fibre volume fraction $v_{f,r}$ read at a predetermined pressure level, and an average stiffness defined over part of the loading curve where pressure levels are significant. The curve shows that compaction pressure P builds up rapidly with v_f and that over the range of fibre volume fractions used in production parts, a small increase in v_f requires a large increase in pressure.

As one aims at maximising the fibre volume fraction in commercial parts, textiles are often compacted to levels where P increases very rapidly with v_f, making knowledge of the compaction behaviour critical in selecting a press. In processes such as RTM the press must equilibrate the compaction pressure as well as the pressure of the resin injected in the tool. Slower injection rates lead to longer production times but allow marginally higher fibre volume fractions for a given press; such aspects must be considered carefully when designing production equipment. The resistance to changes in v_f with fluctuations in P is advantageous in VI as small fluctuations in vacuum levels do not affect the reproducibility of local part thicknesses. However, it should be pointed out that v_f is more sensitive to P at the lower levels of pressure involved in that latter process. Finally, it is generally easier to control the stamping of thermoplastics when conducted under a membrane as opposed to a positive displacement press; this is important especially as

achievement of low void content requires accurate timing of heating and compaction.

The dotted line in Fig. 2.24 corresponds to the relaxation step where the distance between platens is held constant, and to load removal. The most prominent feature is that the two curves for loading and unloading do not superimpose, hence the behaviour is not elastic. A practical consequence is that if v_f is overshot, say in preform stamping, the properties of the final assembly will be altered. For example, if a RTM preform targeted at a fibre volume fraction of 50% reached a value of 55% during its production (preforming) it would produce lower compaction pressures upon closure of the actual RTM mould (constant thickness), possibly resulting in a displacement of the preform upon resin injection. However, the same phenomenon can have fortuitous consequences. In VI compaction pressure is highest when the preform is dry, and it is progressively reduced behind the flow front. Pre-compacted preforms show reduced spring back for the same compaction pressure, hence higher fibre volume fractions may be reached in the final parts. More generally, energy is absorbed when a textile is compacted, its structure is altered, and in most cases it will not return to its initial height.

Figure 2.25 illustrates a typical time relaxation curve. The curve shows the evolution of P with time t when the distance separating the platens is held constant after the initial compaction. Once a certain maximum pressure level is reached and platen travel is stopped the pressure reduces. If after a certain

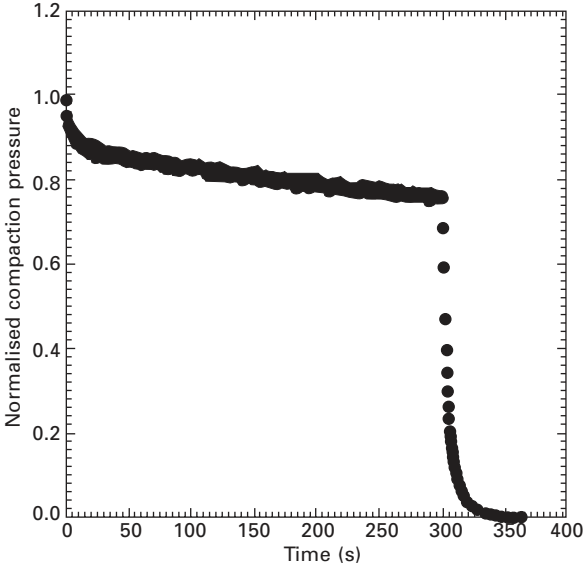

2.25 Typical pressure relaxation curve, where the pressure is measured as a function of time with the reinforcement held at a constant thickness.

time the pressure is returned to its initial maximum level the fibre volume fraction will increase further. This is why some pressure-controlled preforming presses can be observed to re-clamp at more or less regular intervals. The practical benefits of this are limited as relatively long relaxation periods lead to only small increases in v_f, especially at higher fibre volume fractions. In spite of this, relaxation is an important phenomenon as changes in relative thickness for a multilayer preform affect permeability, and reduced overall compaction pressure may render a preform more prone to movement during injection.

Figure 2.26 shows the evolution of applied load and resulting platen displacement with time for a compaction test conducted at a constant loading rate. Such tests are conducted using instrumented machines, the control of which is fairly remote to that of industrial presses. The curve is informative as its first section shows that compaction slows down as it progresses, reflecting the stiffening behaviour of compacted textiles. The second section of the curve shows the effect of an imposed constant load. The fibre volume fraction typically increases by 1–2% in 60 s, while relaxation curves typically show reductions in pressure of 15–25% in 5 min. This reinforces previous remarks stating that for fibre volume fractions representative of actual parts, time does increase v_f but only marginally. The third section corresponds to load removal and confirms previous observations. The curve features a hysteresis, hence the textile is irreversibly modified as it is compacted.

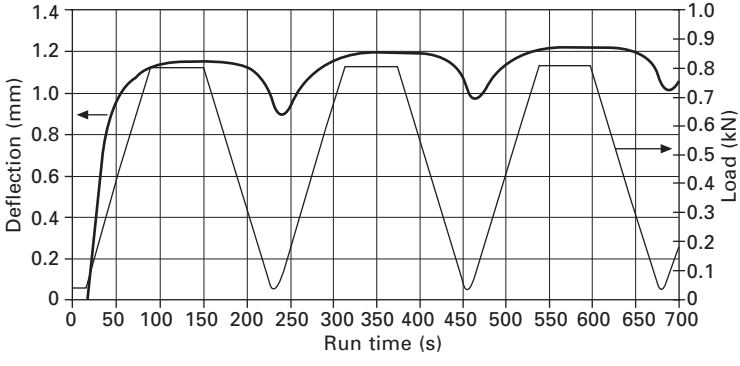

2.26 Evolution of applied load and resulting displacement (bold line) with time for a constant loading rate compaction test.

2.4.4 Effects of variable parameters

The compaction and relaxation behaviour of textile reinforcements is affected by preform construction and production parameters. For example, both compaction and relaxation are altered when the number of layers present in a preform is changed. This section documents such effects. In order to provide

a usable summary of general trends, the effect of parameters on a number of variables are considered.

For compaction the following quantities were introduced previously: the initial fibre volume fraction $v_{f,o}$ of the unloaded textile, the representative fibre volume fraction $v_{f,r}$ read at a predetermined pressure level, and the average stiffness defined over a set range of pressure levels. Another variable that will be commented upon is the rate at which the rigidity of the textile increases as the textile is compacted; this will be referred to as the stiffening index. For relaxation, a reduction in compaction pressure is observed at a constant thickness and therefore the reduction in pressure observed after a period of 5 min will be commented upon; this will be referred to as the pressure decay.

The parameters investigated for both compaction and relaxation are the number of layers (NOL) and saturation by a fluid (SAT). In the latter case, experimental observations show that the compaction behaviour of a set number of layers of reinforcement differs if the reinforcement is compacted dry or saturated with resin. Considering VI for example, this means that when the resin front reaches a given point of the preform, the compaction behaviour at that point changes, effectively becoming less stiff. This can result in a local reduction in thickness at the flow front, a phenomenon usually visible to the naked eye. Additional parameters will also be commented upon. For compaction, the effect of the number of cycles (NOC) applied to a preform will be discussed. This applies to numerous practical situations such as RTM operations where preforms are often manufactured in a separate operation to the actual moulding.

The observed effects of the NOL on compaction are as follows. Different authors have reported different trends, which may be explained by the different textiles and pressure levels used. For some textiles compacted to higher pressures, it has been shown that stacks made of a higher number of layers are more difficult to compact to a given fibre volume fraction v_f with compaction curves progressively shifting to the left (lower fibre volume fractions), mostly at higher pressures. At the onset of compaction multilayer stacks are easier to compact because of nesting; however, at higher pressures these preforms are usually more difficult to compact to a given v_f, hence fibre volume fractions are lower for a given pressure and the curve shifts to the left. While $v_{f,o}$ usually increases with NOL, $v_{f,r}$ shows the opposite trend at high pressures. Therefore both the rigidity and stiffening index tend to increase with NOL (Fig. 2.27). Other authors who have used lower compaction pressures, which are more indicative of manufacturing using VI for example, find that multilayer preforms are easier to compact to higher fibre volume fractions. Their results are not contradictory as they use different pressure levels. Besides, the effect of the number of layers on the compaction behaviour is often relatively weak and some authors have observed conflicting trends.

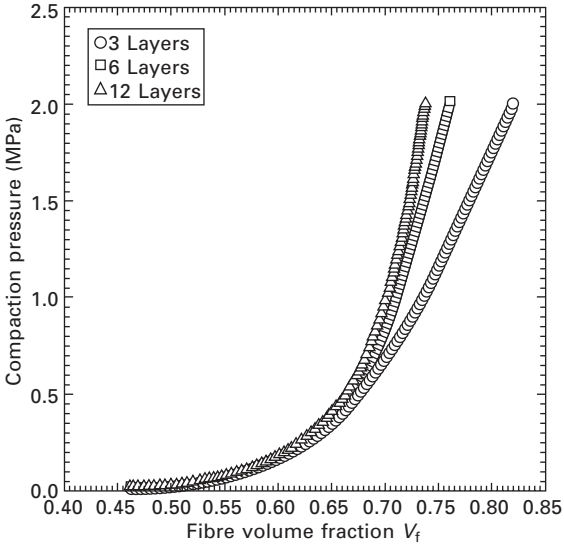

2.27 Textile compaction data for stacks with different numbers of layers for a non-crimp fabric reinforcement.

Preforms made of a higher number of layers show more relaxation in pressure at constant thickness. The pressure decay, defined as the ratio of the pressure observed after 5 mins to the maximum applied pressure, is typically reduced by up to 10% for thicker preforms.

The effects of compacting a reinforcement saturated in a fluid, say resin, are as follows. It should be noted that what is discussed here is quasi-static compaction, i.e. compaction at displacement rates that are sufficiently low to render insignificant the pressure generated by the fluid as it is squeezed out of the reinforcement stack. The phenomenon investigated in the reported experiments is the effect of saturation, and lubrication, on the individual contacts between fibres where forces are transmitted. Typical results for the effect of saturation are given in Fig. 2.28. Experiments show that saturated (v_f, P) compaction curves are generally shifted to the right, that is towards higher fibre volume fractions. The initial fibre volume fraction $v_{f,o}$ and representative fibre volume fraction $v_{f,r}$ are generally higher by a few per cent. As both values of the fibre volume fraction, the rigidity and stiffening behaviour, are generally unaffected; the compaction behaviour remains essentially identical but marginally higher values of fibre volume fraction are observed at given values of the compaction pressure. This can be observed practically for VI as the preform usually compacts to a slightly lower thickness (higher v_f) as the flow front reaches a given position. The effect cannot be observed easily for RTM; however, once enclosed in a mould it is thought that the load on a preform will progressively reduce as a result of time

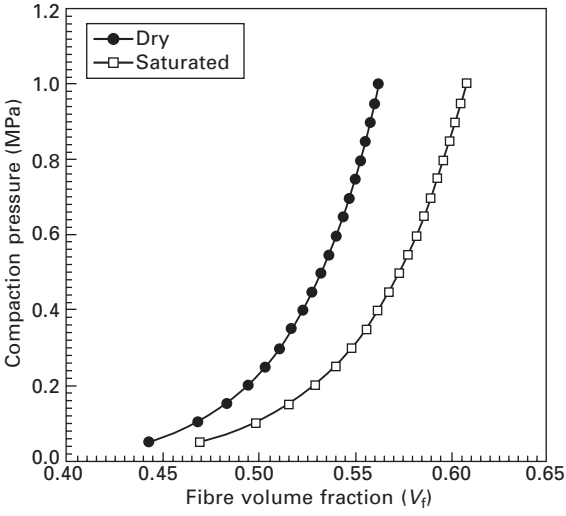

2.28 Effect of fluid saturation in textile compaction behaviour.

relaxation, and that a further reduction will be observed upon impregnation. It is therefore important to use a sufficiently thick preform that will lead to appropriate initial levels of compaction pressure, in order to ensure proper positioning of the preform in the tool throughout the process.

Saturation usually has a strong effect on the relaxation part of the cycle. Saturated stacks reach somewhat higher volume fractions when compacted, and they exhibit significantly less relaxation; after 5 mins the pressure usually remains between 75 and 90% of its initial value. It is believed that this behaviour can be explained by the lubrication of fibre-to-fibre contact points. Individual fibres will slide more easily for a saturated stack and are therefore more likely to attain a higher degree of stability for a given compaction pressure. As a result, fibres are less likely to move under pressure, exhibiting less relaxation.

The above comments are corroborated when one considers the compaction behaviour of a preform subjected to repeated compaction cycles. Figure 2.29 shows typical compaction cycles imposed on a multilayer preform; the maximum pressure level is constant at 1.0 MPa[41]. The figure clearly shows that the compaction and load release curves shift to the right on successive cycles. The shift is more marked on the first repeat and progressively diminishes on successive cycles. Both $v_{f,o}$ and $v_{f,r}$ increase, and this increase is typically more marked than those observed with saturated preforms, notably on the first cycle. The fibre volume fraction observed at higher pressures increases, but less than it does at low fibre volume fractions. Consequently, the rigidity and stiffening index also increase markedly on successive cycles. Such behaviour is observed over a number of cycles; the difference over successive

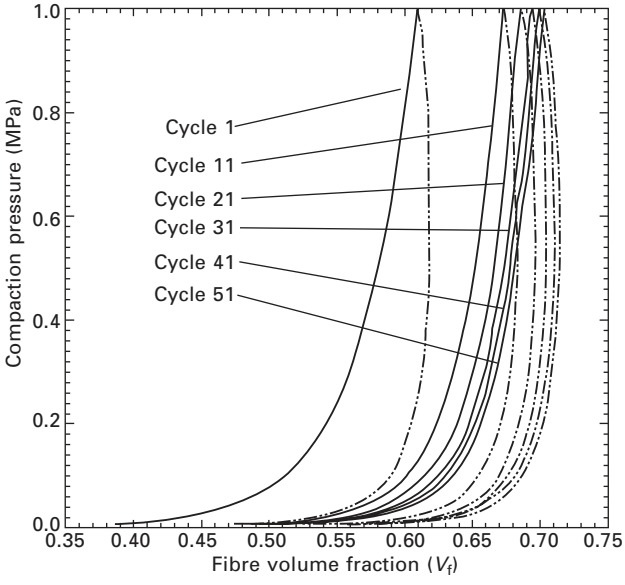

2.29 Pressure curves for successive compaction cycles applied to a multilayer plain weave preform.

cycles diminishes progressively but does not appear to stabilise, at least over 50 cycles. This, along with the fact that an important hysteresis is observed on each cycle, points to the fact that reorganisation of the fibres happens as the textile is compacted and keeps happening on successive cycles. While of little practical importance for processes such as RTM, this provides good insight on the behaviour of textile reinforcements. Furthermore, this behaviour may have consequences for VI where the preform is compacted under vacuum, unloaded upon injection and possibly reloaded during bleeding.

The above trends can be put in perspective by looking at the natural variability observed upon compaction of nominally identical stacks of textile reinforcements. Figure 2.30 shows typical data scatter for 12 identical compaction samples. Here the textile reinforcements were compacted to a lower maximum pressure of 0.1 MPa, which usually leads to more scatter for a given pressure. However, and although the trends discussed above emerge clearly from carefully conducted experiments, the amplitude of the scatter shown in Fig. 2.30 is similar to some of the weaker trends, say for example the effect of the number of layers on compaction curves. Actual production equipment is generally not selected for operation at its limit; in spite of this, variability data should be included when considering necessary forces and control accuracy.

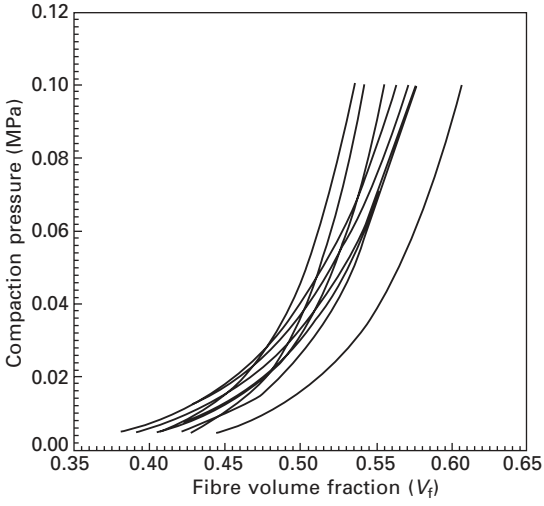

2.30 Compaction data for 12 tests conducted on samples of the same reinforcement, showing the significant data scatter that is to be expected.

2.4.5 Modelling

A number of authors have proposed models for the compaction behaviour of textiles (a thorough review of these is given by Robitaille and Gauvin[39]). Such models usually aim to fulfil one of two objectives: phenomenological models attempt to explain the behaviour from the fundamental principles of mechanics while empirical models provide a simple and usable representation of experimental data. Although both approaches were investigated for compaction, no credible explanation is available for the time relaxation of textile reinforcements and in this case a limited number of empirical models simply aim at quantifying the phenomenon.

The most widely known and used phenomenological compaction model was proposed by Cai and Gutowski[14]. The main concept behind this model is that individual fibres form arches between their contact points; as compaction progresses it is assumed that the number of contact points increases as the length of the arches is essentially proportional to the thickness of the reinforcement being compacted. Consequently, beam bending theory dictates that the arches progressively become more rigid as their number increases, resulting in a marked stiffening behaviour. The authors have proposed different equations (see equation 2.5 for an alternative example), but perhaps the most general is expressed as:

$$P_{comp} = A_s \frac{\left(\frac{v_f}{v_{fo}} - 1\right)}{\left(\frac{1}{v_f} - \frac{1}{v_{fa}}\right)^4} \qquad 2.27$$

where $v_{f,o}$ and $v_{f,a}$ are the initial and maximal fibre volume fractions, A_s is an empirical constant, and v_f and P_{comp} are the fibre volume fraction and the compaction pressure. It should be noted that owing to its nature and phenomenological origin the model uses the fibre volume fraction as the independent variable, which is not ideal; the form of the equation can make the extraction of a fibre volume fraction at a given compaction pressure awkward.

Gutowski's work provides very interesting and valuable insight into the compaction phenomenon; however, it really applies to homogeneous assemblies of parallel fibres. Results of experiments conducted on reinforcements of various architectures clearly show that the textile structure, or the way in which tows or yarns of various sizes are assembled into a planar assembly that is homogeneous and continuous at the macroscopic scale, but heterogeneous and discontinuous at the mesoscopic scale, strongly affect the behaviour. It is possible, for example, to classify compaction curves for random mats, woven textiles and stitched directional reinforcements into relatively distinct groups; this important point is discussed further in the following paragraphs. Furthermore, getting a good fit for the diverse coefficients of the models can be challenging in some cases, and values obtained for coefficients with a clear physical meaning such as $v_{f,o}$ and $v_{f,a}$ often do not match reality when the model is applied to heterogeneous textiles. The model was really developed for assemblies of aligned fibres and the lack of correspondence between the fitted and experimental values reduce its attractiveness to some extent.

The alternative consists of using empirical models. While studying changes in the values of the coefficients of such models with experimental parameters helps in identifying trends, there is no pretence at a quantitative, mechanical description of the phenomena involved in the process. However, this can be compensated by the fact that similar models can be used to describe relaxation behaviour, enabling both phenomena to be included in process simulations and treated in the same way. Empirical models of compaction and relaxation are not satisfactory in all circumstances. Numerous published works have provided remarkable phenomenological insight into compaction and other properties of fibre assemblies, as well as models that can represent real behaviour for actual fibrous structures such as ropes. Finite element analyses similar to those described in section 2.3.5 would appear to be a promising approach here, and this is expected to be an area of significant activity in the near future. At this time most of these models require very significant computational power, but work is ongoing and in the future, more efficient models that can reasonably be used to support actual production of composite parts may appear.

Most empirical models of the compaction revolve around some form of the power law. The authors and numerous others have used the following expression to fit experimental compaction data:

$$v_f = v_{fo} \cdot P_{comp}^{B} \qquad 2.28$$

where $v_{f,o}$ is the fibre volume fraction recorded under a pressure of 1 Pa and B is an empirical factor called the stiffening index. Because of the mathematical form of the equation the latter value provides a good indication of the rate of increase of the rigidity as a function of v_f; as such it is practically very useful. Here the pressure is the independent variable, and the equation is easily fitted to data.

Robitaille and Gauvin[39] proposed a similar model for time relaxation:

$$\frac{P}{P_o} = 1 - C t^{(1/D)} \qquad 2.29$$

where C is the pressure decay after 1 sec, D is the relaxation index, P_o is the initially applied pressure and P is the compaction pressure observed at time t which is the independent variable.

The above empirical formulae have allowed the formal identification of all the trends mentioned above. The compaction model was also successfully integrated into a number of process simulation models. Tables of coefficients for both equations can be found in the literature for a range of materials[39, 40] and it is very straightforward to fit experimental data to the equations. While these models do not explain the physics of compaction and relaxation and one must identify the coefficients associated to each stack of reinforcements that may be used in production, they are very useful in practice.

A recent study further extends the benefits of the compaction model when considering a number of structurally different reinforcements[42]. The curve shown in Fig. 2.31 is a compaction master curve, which presents the evolution

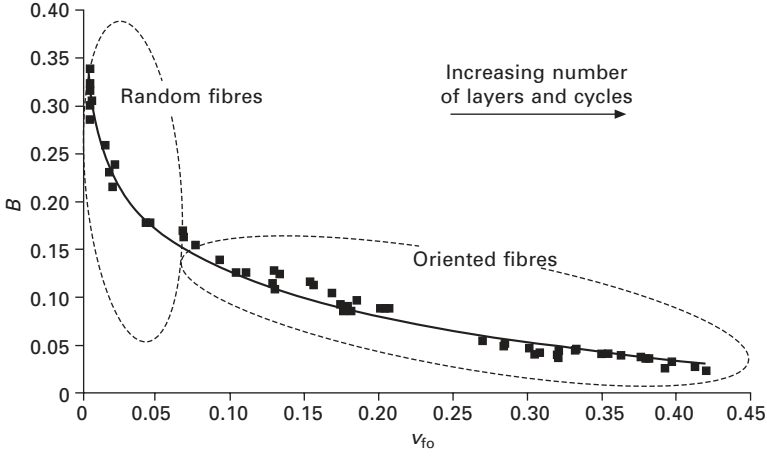

2.31 Compaction master curve, showing a relationship between stiffening index and initial fibre volume fraction values (equation 2.28) for a range of reinforcements.

of the stiffening index B as a function of the initial fibre volume fraction $v_{f,o}$ for an array of reinforcements. The curve shows a fairly clear general relationship between the two parameters. Furthermore, all random reinforcements are found on the left side of the curve, most woven fabrics occupy the centre and textiles featuring highly oriented fibres (e.g. NCFs) are found on the right. Practically this translates into the fairly simple fact that random textiles initially show low fibre volume fractions and that they stiffen relatively slowly, while crimp-free assemblies of unidirectional fibres feature high initial fibre volume fractions and stiffen very rapidly.

References

1. Blanchard P., Cao J., Chen J. and Long A.C. (co-chairs), *NSF workshop on composite sheet forming*, Lowell, MA, Sept 2001. http://www.mech.northwestern.edu/fac/cao/nsfworkshop/index.htm
2. Saville B.P., *Physical Testing of Textiles*, Cambridge, Woodhead Publishing Ltd, 1999.
3. Lomov S.V., Verpoest I., Barburski M. and Laperre J., 'Carbon composites based on multiaxial multiply stitched preforms. Part 2. KES-F characterisation of the deformability of the preforms at low loads', *Composites Part A*, 2003 **34**(4) 359–370.
4. Potter K.D., 'The influence of accurate stretch data for reinforcements on the production of complex structural mouldings', *Composites*, July 1979 161–167.
5. Skelton J., 'Fundamentals of fabric shear', *Textile Research J.*, Dec. 1976 862–869.
6. Wang J., Page R. and Paton R., 'Experimental investigation of the draping properties of reinforcement fabrics', *Composites Sci. Technol.*, 1998 **58** 229–237.
7. Canavan R.A., McGuinness G.B. and O'Braidaigh C.M., 'Experimental intraply shear testing of glass-fabric reinforced thermoplastic melts', *Proc. 4th Int. Conf. on Automated Composites*, Nottingham, Sept. 1995, 127–138.
8. Long A.C., Rudd C.D., Blagdon M. and Johnson M.S., 'Experimental analysis of fabric deformation mechanisms during preform manufacture', *Proc. 11th Int. Conf. on Composite Materials*, Gold Coast, Australia, July 1997, V: 238–248.
9. Prodromou A.G. and Chen J., 'On the relationship between shear angle and wrinkling of textile composite preforms', *Composites Part A*, 1997 **28A** 491–503.
10. Mohammad U., Lekakou C., Dong L. and Bader M.G., 'Shear deformation and micromechanics of woven fabrics', *Composites Part A*, 2000 **31** 299–308.
11. Souter B.J., Effects of fibre architecture on formability of textile preforms, PhD Thesis, University of Nottingham, 2001.
12. Kawabata S., Niwa M. and Kawai H., 'The finite-deformation theory of plain-weave fabrics Part III: The shear-deformation theory', *J. Textile Institute*, 1973 **64**(2) 61–85.
13. McBride T.M. and Chen J., 'Unit-cell geometry in plain-weave fabrics during shear deformations', *Composites Sci. Technol.*, 1997 **57** 345–351.
14. Cai Z. and Gutowski T.G., 'The 3D deformation behavior of a lubricated fiber bundle', *J. Composite Materials*, 1992 **26**(8) 1207–1237.
15. McBride T.M., The large deformation behavior of woven fabric and microstructural evolution in formed textile composites, PhD Thesis, Boston University, 1997.

16. Harrison P., Wiggers J., Long A.C. and Rudd C.D., 'A constitutive model based on meso and micro kinematics for woven and stitched dry fabrics, *Proc. 14th Int. Conf. on Composite Materials*, San Diego, July 2003.
17. Harrison P., Yu W.-R., Wiggers J. and Long A.C., 'Finite element simulation of fabric forming, incorporating predictions of a meso-mechanical energy model', *Proc. 7th Int. European Scientific Association for Material Forming Conf.*, Trondheim, Norway, April 2004, 139–142.
18. Kawabata S., Niwa M. and Kawai H., 'The finite-deformation theory of plain weave fabrics Part I: The biaxial deformation theory', *J. Textile Institute*, 1973 **64**(2) 21–46.
19. Kawabata S., 'Nonlinear mechanics of woven and knitted materials', in Chou T.W. and Ko F.K. (eds) *Textile Structural Composites*, Amsterdam, Elsevier, 1989, pp 67–116.
20. Ferron G., 'Dispositif de traction biaxiale DAX2', Document Tech-metal, Mézières-Lès-Metz, 1992 (in French).
21. Boisse P., Gasser A. and Hivet G., 'Analyses of fabric tensile behaviour. Determination of the biaxatension-strain surfaces and their use in forming simulations', *Composites Part A*, 2001 **32**(10) 1395–1414.
22. Launay J., Lahmar F., Boisse P. and Vacher P., 'Strain measurement in tests on fibre fabric by image correlation method', *Adv. Composite Lett.*, 2002, **11**(1) 7–12.
23. Dumont F., Hivet G., Rotinat R., Launay J., Boisse P. and Vacher P., 'Identification des caractéristiques mécaniques de renforts tissés à partir de mesures de déformations par corrélation d'images', *Mécanique & Industries*, in press (in French).
24. Buet-Gautier K, Analyse et simulation du comportement mécanique des renforts composites tissés, PhD Thesis, University of Orléans, 1998 (in French).
25. Buet-Gautier K. and Boisse P., 'Experimental analysis and models for biaxial mechanical behaviour of composite woven reinforcements', *Experimental Mechanics*, 2001, **41**(3), 260–269.
26. Anandjiwala R.D. and Leaf G.A.V., 'Large-scale extension and recovery of plain woven fabrics', *Textile Research J.*, 1991 **61**(11) 619–634.
27. Realff M.L., Boyce M.C. and Backer S., 'A micromechanical approach to modelling tensile behavior of woven fabrics', in Stokes V.K. (ed) *Use of Plastics and Plastic Composites: Materials And Mechanics Issues*, New York, ASME MD-Vol. 46, 1993, 285–294.
28. Dastoor P.H., Ghosh T.K., Batra S.K. and Hersh S.P., 'Computer-assisted structural design of industrial woven fabrics. Part III: Modelling of fabric uniaxial/biaxial load-deformation', *J. Textile Institute*, 1994 **85**(2) 135–157.
29. Lomov S.V., Gusakov A.V., Huysmans G., Prodromou A. and Verpoest I., 'Textile geometry preprocessor for meso-mechanical models of woven composites', *Composites Sci. Technol.*, 2000 **60** 2083–2095.
30. Grishanov S.A., Lomov S.V., Harwood R.J., Cassidy T. and Farrer C., 'The simulation of the geometry of two-component yarns. Part I: The mechanics of strand compression: simulating yarn cross-section shape', *J. Textile Institute*, 1997 **88**(2) 118–131.
31. Harwood R.J., Grishanov S.A., Lomov S.V. and Cassidy T., 'Modelling of two-component yarns. Part I: The compressibility of yarns', *J. Textile Institute*, 1997 **88**(4) 373–384.
32. Baoxing C. and Chou T.W., 'Compaction of woven-fabric preforms in liquid composite molding processes: single layer deformation', *Composite Sci. Technol.*, 1999 **59** 1519–1526.
33. Marquardt D.W., 'An algorithm for least squares estimation of nonlinear parameters', *J. Soc. Indus. Appl. Math*, 1963 **11**(2) 431–441.

34. Schnur D.S. and Zabaras N., 'An inverse method for determining elastic material properties and a material interface', *Int. J. Numerical Methods Eng.*, 1992 **33** 2039–2057.
35. Hivet G., Modélisation mesoscopique du comportement biaxial et de la mise en forme des renforts de composites tissés, PhD Thesis, University of Orléans, 1998 (in French).
36. Gasser A., Boisse P. and Hanklar S., 'Analysis of the mechanical behaviour of dry fabric reinforcements. 3D simulations versus biaxial tests', *Comp. Material Sci.*, 2000 **17** 7–20.
37. Flanagan D.P. and Belytschko T., 'A uniform strain hexahedron and quadrilateral with orthogonal hourglass control', *Int. J. Numerical Methods Eng.*, 1981 **17** 679–706.
38. Pian T.H. and Chen D., 'On the suppression of zero energy deformation modes', *Int. J. Numerical Methods Eng.*, 1983 **19** 1741–1752.
39. Robitaille F. and Gauvin R., 'Compaction of textile reinforcements for composites manufacturing. I: Review of experimental results', *Polymer Composites*, 1998 **19**(2) 198–216.
40. Robitaille F. and Gauvin R., 'Compaction of textile reinforcements for composites manufacturing. II: Compaction and relaxation of dry and H_2O-saturated woven reinforcements', *Polymer Composites*, 1998 **19**(5) 543–557.
41. Robitaille F. and Gauvin R., 'Compaction of textile reinforcements for composites manufacturing. III: Reorganization of the fiber network', *Polymer Composites*, 1999 **20**(1), 48–61.
42. Correia N., Analysis of the vacuum infusion process, PhD Thesis, University of Nottingham, 2004.